Mechanical Behavior and Its Relation to Superconducting Property of High Temperature Composite Superconductors

Jae-Kyoung SHIN

Department of Materials Science and Engineering

Kyoto University

2008

Contents

Chapter 1

General introduction

1.1 Background

Global energy demands continue to grow rapidly despite the relatively high oil and natural gas prices. World energy consumption is expected to grow by more than 50% over 2004 to 2030 according to the International Energy Outlook 2007 [1]. For the limitation of the estimated amount of the fossil fuels (petroleum, natural gas and coal), it is essential for us to use the resources most effectively. In order to achieve the sustainable development for mankind, the superconducting technologies will play a crucial role in the future society.

One of the great achievements in physics is the discovery of superconducting phenomena. Superconductor is characterized as zero electrical resistance; zero voltage across superconductor when a certain transport current passes through it. At the first time, the superconductivity was found in many pure metals such as In, Sn, Pb and Hg called type I superconductors whose critical temperature is below 4K [2]. Later, type II superconductors such as NbTi, Nb_3Sn, Nb_3Al, V_3Ga and MgB_2 [3] were discovered, but their critical temperature was low (below 30K). In these twenty years, considerable technical advances have been achieveed for the high temperature type II superconductors [4]. $Bi_2Sr_2CaCu_3O_x$ (Bi2223), $REBa_2Cu_3O_x$ (REBCO or RE123, RE: Y, Dy, Gd, Sm, Nd), and $Bi_2Sr_2CaCu_2O_x$ (Bi2212) exhibit the superconducting behavior at the temperature below 110, 92 and 85K, respectively and could be operated at the simple cooling system in liquid nitrogen (77K).

Many researches were conducted for applications of zero resistance conductors cooled with an inexpensive cryogen. However, there have been the limited realities of these new materials such as brittleness for manufacturing long flexible conductors, requirement of near-perfect crystalline for high current density, rapidly performance

drops in a magnetic field. In addition, one of the significant obstacles in the application of the superconductivity technologies is the substantially higher manufacturing cost. The price of the superconductor is usually expressed as dollars per meter length and ampere of the critical current ($/kA-m). For the comparison in the price of the copper as an engineered conductor 10$/kA-m, the price of Bi2223 is still 5 to 10 times higher than copper (excluding the cooling cost), due to the use of silver and the complexity of manufacture process. Further innovation and development will be needed to achieve for commercial availability as low as $10-30/kA-m and can be fabricated in practical application.

Despite these obstacles, a few kilometers of high temperature superconducting tapes have now been manufactured for power cables, linear motors and other electrical power components. As the question is remained whether the advantages of superconducting materials can be realized in industrial application or not, the remaining works are to search and investigate the fundamentals for further improvements of these wonderful and difficult materials.

1.2 Features of crystal structure of Bi2223

The general chemical formula of the Bi-system superconductors is given by $Bi_2Sr_2Ca_{n-1}Cu_nO_x$ (x=2n+4+δ). The critical temperature (T_C) increases from 10K for single-layered (n=1) $Bi_2Sr_2Cu_1O_6$ (Bi2201) to 85K for bi-layered (n=2) $Bi_2Sr_2Ca_1Cu_2O_8$ (Bi2212) and further to 110K for tri-layered (n=3) $Bi_2Sr_2Ca_2Cu_3O_{10}$ (Bi2223). However, when $n \geq 4$, the reduction of T_C takes place. Among them, the Bi2223 or Bi2212 superconductor composite material has been one of the most promising superconductors that are commercially applicable materials in long length and high current density. Strictly speaking, since the critical temperature of Bi2212 (85K) is close to liquid nitrogen temperature (77K), the application of Bi2212 is actually limited. Thus, the temperature margin of Bi2212 at 77K is so small that only Bi2223 has the possibility to design at 77K among Bi-system high temperature superconductors. Figure 1.1 shows the schematic illustration of the crystal structure of Bi2223 [5]. However, due to the difficulty of obtaining the single phase Bi2223 by sintering of precursors, the Bi is partially substituted by Pb in order to raise the volume fraction of Bi2223 [6]. In this dissertation, Bi2223 is an abbreviation for $Bi(Pb)_2Sr_2Ca_2Cu_3O_{10+\delta}$. Bi2223 has a tetragonal, layered, orthorhombic perovskite structure composed of two

charge-reservoir layers (Bi(Pb)-O, Sr-O) sandwiching three CuO_2 planes of strong superconductivity. In Bi2223, the charge-reservoir layer consists of a double (Bi,Pb)-O and its neighbouring Sr-O layers, the superconducting layers being a stack of three CuO_2 layers interleaved by two Ca layers [7].

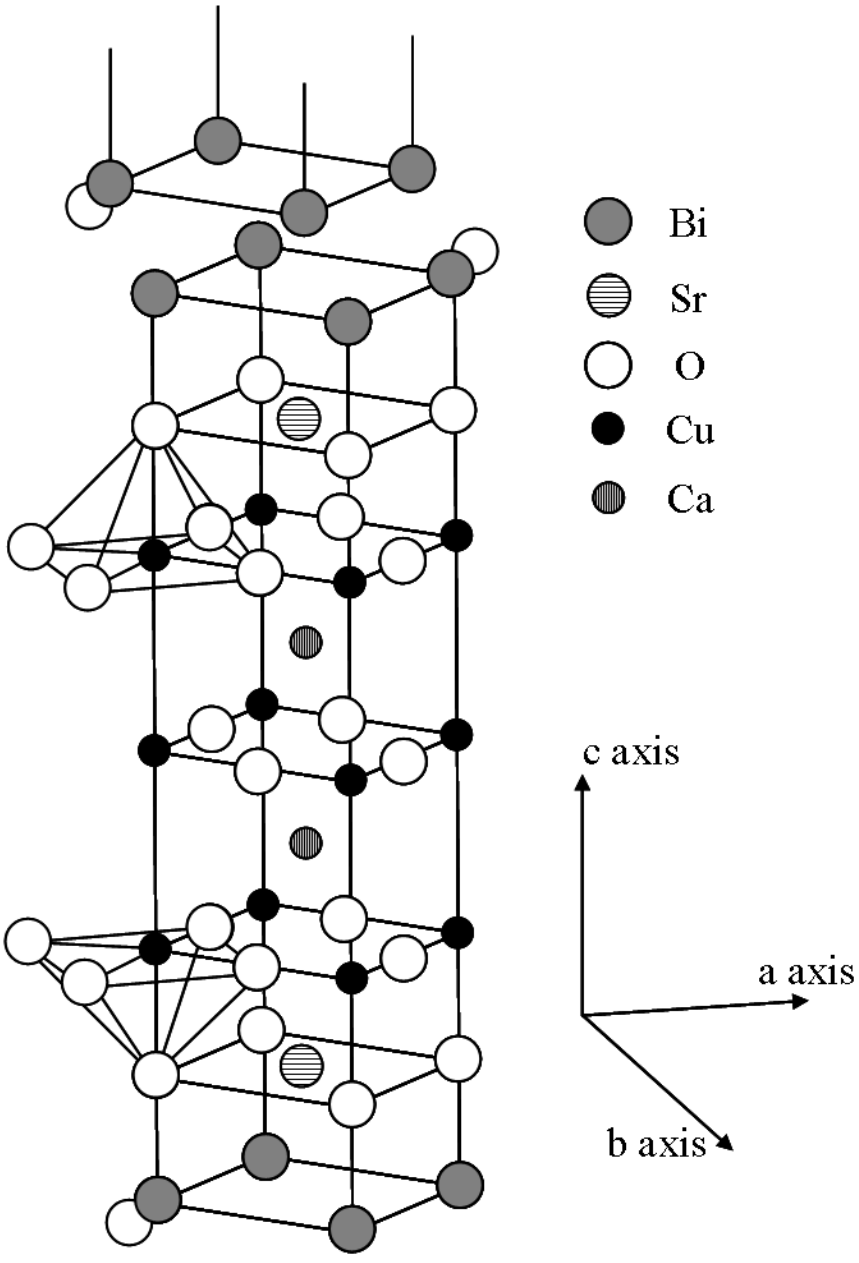

Figure 1.1 Crystal structure of Bi2223 [5].

Bi2223 consists of thin plate-shaped grains perpendicular to c-axis as shown in figure 1.2. The grains are easily cleaved perpendicular to c-axis. From the structural feature of Bi2223, the super-currents preferentially flow along the a-b plane [7]. The anisotropy of Bi2223 is so large that irreversible field (B_{irr}) at 77K is only 0.2~0.3T [8], restricting 77K applications

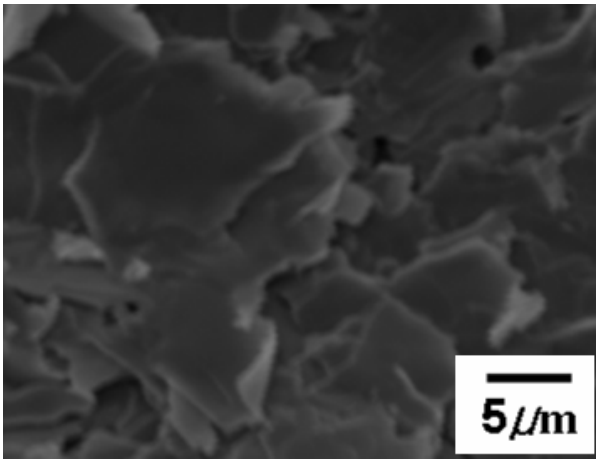

Figure 1.2. A scanning electron microscopy image of the Bi2223 grains perpendicular to c-axis.

1.3 Fabrications of high temperature superconductor materials

1.3.1 Bi-Sr-Ca-Cu-O

Up to now, Bi-system conductors have been fabricated by power-in-tube (PIT) method [9]. Figure 1.3 shows the schematic illustration of the power-in-tube process for Bi2223 or Bi2212 composite tape or wire [10]. Firstly, a precursor is made in the form of the powder which contains the compounds that become superconducting materials under heat treatment. The powder is packed into metal tube typically silver. Ag is less reactive with the superconducting core materials during thermal processing in the fabrication process and forms a template upon which the high temperature superconductor (HTS) material can grow. Typically, the tube is filled with HTS powder, then extruded or drawn to a suitable diameter about 1~2 mm. For multifilamentary conductor, the wire is organized by a stack of for example, 7, 19, 37, 55, 61, 85, or

higher numbers of filaments. This stack is then inserted in another tube, and the composite is extruded or drawn. The wires are required to have sufficient mechanical strength withstanding the mechanical and electromagnetic stresses. The use of Ag alloy as a sheath is effective for improving the mechanical strength of composite tape or wire [11]. The final step consists of one or more heat treatments so that the powder reacts and forms the desired HTS material within each filament. The volume fraction of the superconducting phase is typically 30~40%. Figure 1.4 shows the example of the transverse cross-sections of the multi-filamentary Bi2223 tape and Bi2212 wire.

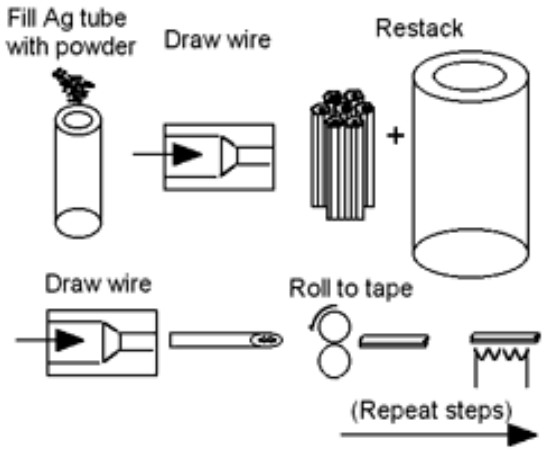

Figure 1.3. Schematic illustration of the power-in-tube process
for Bi2223 or Bi2212 composite tape or wire [10].

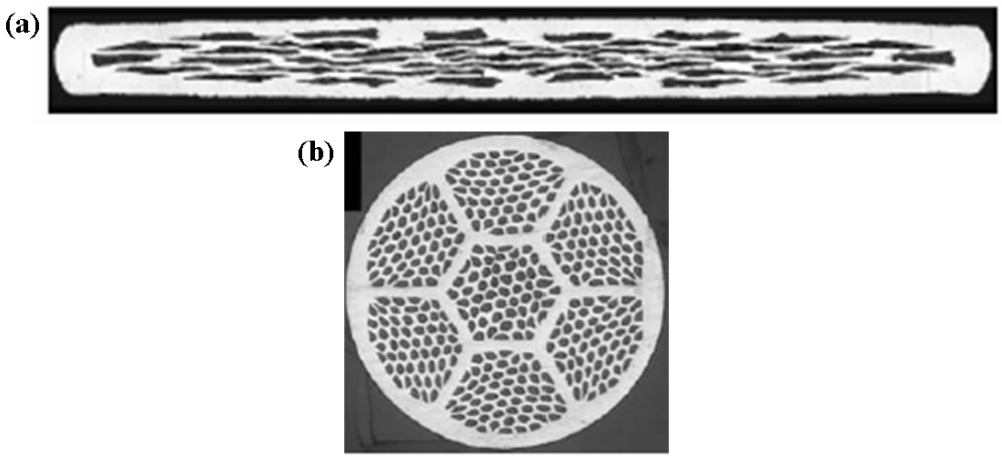

Figure 1.4. Transverse cross-section of the multi-filamentary
(a) Bi2223 tape and (b) Bi2212 wire.

1.3.2 Coated conductors

The significant improvements for fabrication of high critical current density and long length superconductors have been achieved in rare earth RE-Ba_2-Cu_3-O_X (REBCO) (RE: Y, Dy, Nd, Sm, Eu or Gd) coated conductors. Coated conductors optimize the excellent alignment of the superconducting conductor layer for high critical current. The REBCO compounds exhibit essentially high critical current properties in high magnetic due to their relatively low electromagnetic anisotropy. Tremendous efforts have been made for developing practical long conductors using metal substrates after discovery of bi-axial alignment technique. Figure 1.5 shows the example of the schematic illustration of YBCO coated conductor, which is characterized by Au/YBCO/buffer layer/Ni based Hastelloy substrate. Depositing a superconductor film epitaxially onto a textured buffer layer or textured substrate so as to achieve biaxial texture is the process used to fabricate superconductors. The textures are achieved by two different route either RABiTS (Rolling Assisted and Biaxially Textured Substrate) [12], or depositing an aligned buffer layer on the nontextured metal such as IBAD (Ion Beam Assisted Deposition) [13] and ISD (Inclined Substrate Deposition) [14]. The deposited biaxially textured ceramic buffer layers (CeO_2/YSZ or MgO) are deposited on the polycrystalline, randomly oriented, Hastelloy substrates and the thin cap layer is grown on the thick buffer layer. The cap layer serves to decrease the gap between the buffer layer columns and improve the surface quality for subsequent coating of superconducting materials. The REBCO films are formed by co-evaporation in the rotation turntable system for YBCO and SMBCO or deposited by an electron gun using a winder to fabricate the long length coated conductors [15]. Finally, a protective layer of Ag or Au was deposited on the top.

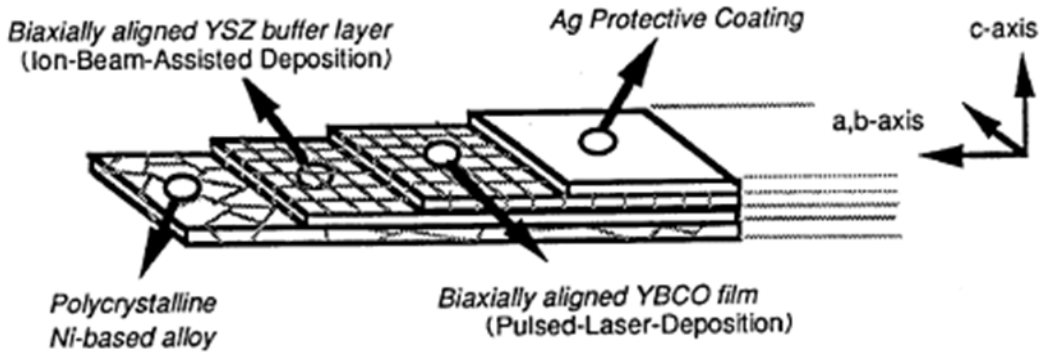

Figure 1.5. Schematic illustration of YBCO coated conductor [13].

Recently, several research groups successfully produced Bi2223 composite tape (or wire) of the 1000m long length with critical current (I_C) values of higher than 150A at 77K in a self field [16,17]. Also in Bi2212 systems, the composites with I_C above 1000A at 4.2K in a self field have been developed [18]. The Bi-system composites have several disadvantages such as a low critical current density (J_C) under magnetic fields, which limits their usage only below 20 K [19]. On the other hand, the J_C value of the coated conductor system does not drop so critically under high magnetic fields [20], coated conductor has more advantages in cost, mechanical strength and losses in AC applications. Various national projects have been conducted by DOE national program in America, NEDO in Japan and DARPAS in Korea with the goals of 500m long lengths with a high I_C values over 300A at 77 K in self field. Based on the recent achievements, the performance projection of the Bi2223, Bi2212 tapes (or wires) and YBCO coated conductors is summarized in Table 1.1.

Table. 1.1. Performance projections in critical current and long length of HTS [21].

	2003	2007	2010	2015	2020
Bi2223/Ag tape (500m long, 0.24x4mm²) I_c at 77K/self field	100A (J_c=3·10⁴A/cm²)	→ 150 (5·10⁴)	→ 200 (6·10⁴)	→ ~250 (~8·10⁴)	
Bi2212/Ag wire (500m long, ϕ1mm) I_c at 4.2K/self field	1000A (Ag/SC=3, J_c=5·10⁵A/cm²)		→ 1500A (2, 5·10⁵)		
YBCO coated conductor I_c at 77K/self field	38A/cm (100m long)	→ 100~300 (500)	→ 300 (500)	→ 300~500 (500)	→ 300~500 (500~1000)

comments J_c : Critical current dencity in superconductor

1.4 Application of superconductors

Several research efforts have made the progress in high temperature superconductors with the goal of low cost, large scale application coupled with high electrical and mechanical performances. With the inspiration of the zero resistance, the major application of high temperature superconductors is the power transmission cables with low loss of high critical current density as shown in figure 1.6(a) [22]. With the increase of the demand of electric power, HTS cables will offer significant benefits over

conventional overhead transmission lines and copper cables. The major features of HTS cables are the capacity power up more than 10 times in comparison with the conventional Cu based cables, helping to reduce grid congestion and installation by means of the underground HTS cables. Actually, many HTS cables have been developed and installed around world [23-25]. The Ultera has installed a single 200m long HTS 3-phase cable at America Electric Power (AEP) Bixby substation in Columbus, Ohio which has the parameters such as 13.2kV, 69MVAand 3000Arms [23]. The Albany Project has also installed a HTS cables with a 350m length in 34.5kV and 800Arms [24] and in-grid operation was started on July in 2006.

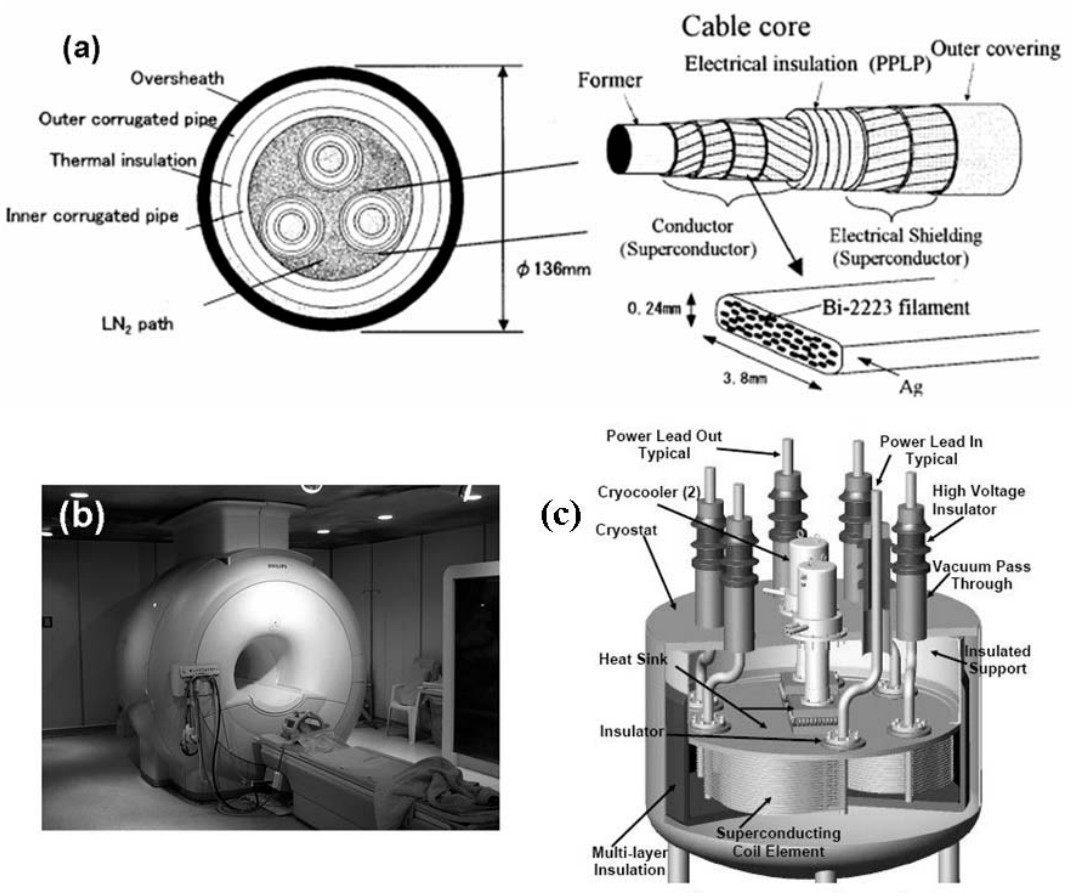

Figure 1.6. (a) Illustration of the structure of HTS cable [22], (b) Magnetic Resonance Imaging (MRI) [26] and (c) Superconducting fault current limiter [26].

Due to the higher magnetic field creation, superconducting materials has been applied in the field of the medical diagnostics for many years. By impinging a derived strong magnetic field into the body in the extremely uniform field, the energy as a frequency is detected and displayed graphically (Magnetic Resonance Imaging (MRI) as shown in figure 1.6(b)) [26]. Thus, MRI is a noninvasive method for seeing inside the body without using ionizing radiation. The technique now has widespread use in hospitals in diagnosing injuries to joints and bones, detecting tumors, and in general detecting diseases that change human anatomy. In the MRI systems, low temperature superconductors such as Nb-based superconductor has been used with liquid helium bath cooling, which serves well by their low cost, coupled with their ability to be fabricated as strong, round wires with distinct filament structures, high current density and a high superconductor fill factor. However, in order to build and supply the smaller, less complicated (liquid helium free), lower cost superconducting MRI systems, the magnets that can operate at higher temperatures (higher than 4.2 K) and deliver the greater stability and reduce the coil noise is required. Thus, with the combination of lower wire price, higher operating temperature, and lower cooling costs, the high temperature superconductors will be able to be applied to MRI manufacturers to build systems that require no liquid helium and have lower initial system costs and lower operating costs.

Besides, superconducting Magnetic Energy Storage (SMES) systems store energy in the magnetic field created by the flow of direct current in a superconducting coil which has been cryogenically cooled to a temperature below its superconducting critical temperature. HTS can be applied in the field of the lossless energy storage device in a power system for load leveling, back-up, supply to the loads sensitive to momentary voltage disturbances or power interruptions and damping synchronous generators oscillations. In addition, the feasibility of application in HTS is to apply for electrical power devices such as (i) transformers, generators and motors, fault-current limiters as shown in figure 1.6(c) [26], and (ii) magnetic separators which need the ability to selectively separate certain materials.

1.5 Critical transport current in Bi2223

Figure 1.7 shows a typical voltage (V)-current (I) characteristic in superconductors. The relation of voltage (V) and current (I) near the critical point was

approximately by the power-law function given as

$$V=\mathrm{A}\cdot I^{\mathrm{n}} \tag{1.1}$$

where A and n are fitting constants. The critical current was estimated with a criterion of $1\mu V$/cm. The n value refers to the sharpness of the transition from superconductivity to normal conducting state. Many researches have studied the inhomogeneous current distribution of the Bi-system. Bi2223 has anisotropic current transport properties and super-currents flow preferentially in the a-b plane. By theoretical approaches, the brick-wall (BW) model [27], railway-switch (RS) model [28] and freeway model [29] were proposed to be the mechanism of the current limiting factors. The critical current density (J_C) is generally understood to be limited by the grain-to-grain connectivity. Although PIT processing of Bi2223 produces only a strong uniaxial texture, long-range percolative paths of low energy grain boundaries are developed which permit the strongly linked current flow. In addition, sausaging, voids, microcracks, different orientation angles at grain boundaries and dispersion of non superconducting phases from the microstructural viewpoint are the inhomogeneities as weak link [29], resulting in determining the current flowing and the generation of voltage over the sample. In the micrographic studies, the current percolates through a polycrystalline network containing many weak links are exhibited. Performances of HTS conductors with the grain structure are studied with magneto-optical imaging (MOI) of visualizing non-uniformities of current flow in polycrystalline conductors as shown in figure 1.8 [7]. The image of the Bi-system conductors allows a direct determination of the spatial distribution of the current flow and the total amount of current shunted into silver.

From the mechanical viewpoint, the brittleness of the superconducting filaments makes them very susceptible to strain induced cracks. It is well known that the critical current (I_C) of HTS is reduced due to the damage evolution when applied strain exceeds the irreversible strain limit (ε_{irr}) [30]. Indeed, in the textured Bi2223 filament, constituting of thin plate-shaped grains whose c-plane is parallel to the longitudinal direction, the transverse (perpendicular to the c-plane) fracture and longitudinal (parallel to the c-plane) fracture of the grain occur. Mostly, the fracture of the filaments was accompanied by a zigzag fracture process in a form of alternative occurrence of transverse and longitudinal fractures observed in scanning electron microscopy (SEM). [31].

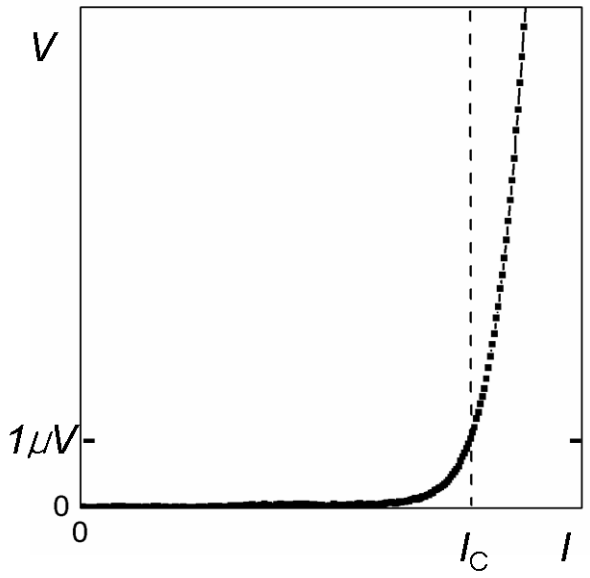

Figure 1.7. Typical *V-I* characteristic of high temperature superconductor.

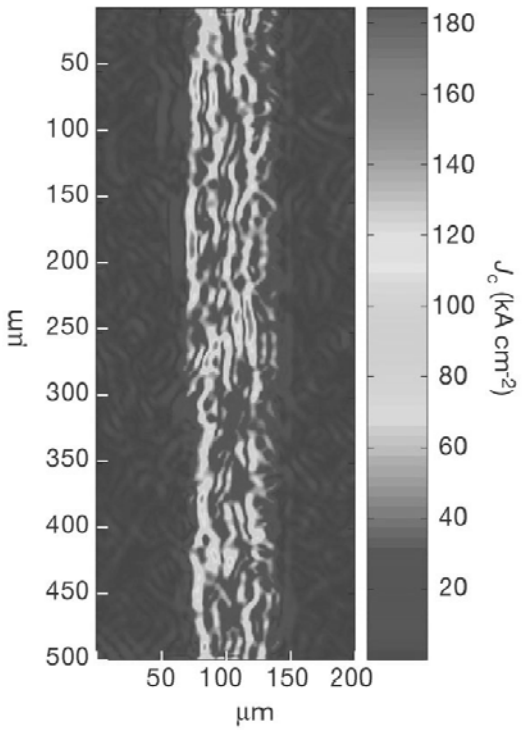

Figure 1.8. Distribution of the local critical current density with magneto-optical imaging (MOI) [7].

1.6 Purpose of the present work

Mechanical and electromagnetic stresses are exerted on superconducting composite materials during fabrication and service operation, which change the strain state and cause damage. Accordingly, the superconducting property varies when the superconducting materials (tape or wire) are stressed. It has been reported that the intrinsic tensile fracture strain of Bi2223 filaments is around 0.1% [31-33]. It means that the superconducting current-transporting Bi2223 filaments are damaged with such a low fracture strain (at low stress), resulting in loss of the superconductivity. Due to the difference in coefficient of thermal expansion among Bi2223 filaments, Ag and Ag alloy, the thermally induced residual strain is exerted during cooling/heating process. It is known that the tensile strain tolerance of the critical current of Bi2223 composite superconductors is improved when the compressive residual strain of Bi2223 filaments in the current transport direction (sample length direction) is enhanced. The understanding of the fracture behavior of the HTS composite tapes (or wires) under applied strain and its influence on critical current is an important research subject. Thus, the aim of the present work is to clarify the mechanical behavior and its relation to superconducting property of Bi2223 composite tape and Bi2212 composite wire. The present thesis consists of the following contents.

In chapters 2, 3 and 4, the stress-strain curves of the composite at room temperature and 77K measured by tensile test, the residual strain of filaments at room temperature measured by the X-ray diffraction method, the critical current-applied tensile strain relation at 77K and thermal expansion curves of the composite and Ag measured by the thermo-mechanical test were analyzed. It was attempted to reveal the residual strain change with temperature in the cooling and heating process by experiment and modeling analysis.

In chapter 5, the critical current determining parameter "fracture strain (ε_f) – residual strain (ε_r)" of the local elements and overall sample was estimated for the tensile- and bending-strained samples. It was attempted to correlate the local critical current distribution to overall critical current.

In chapter 6, a special devices for simultaneous measurement of strains of plural local elements and overall sample was developed to study the sample location dependence of critical current I_C-applied tensile strain relation at 77K of Bi2223 composite tape. With the present approach, the difference in critical current I_C-tensile strain relation among the local elements under a common applied stress was clearly detected.

In chapter 7, spatial distribution of voltage and current caused by the cracking of Bi2223 filament under applied tensile strain was studied. Due to the cracking of Bi2223 filament, voltage generation along the interface between filament and Ag takes place, and the critical current is reduced consequently. It was attempted to reveal the influence of filament cracking on critical current, and the effect of the partial cracking of filament on the voltage-current relation, and to describe the change of critical current as a function of applied tensile strain in a quantitative manner.

References

[1] International Energy Outlook 2007 (published by the Energy Information Agency of the US Department of Energy; http://www.eia.doe.gov/oiaf/ieo/pdf/highlights.pdf).

[2] H. Kamerlingh Onnes, Leiden Comm. 122b (1911) pp.3-5, pp.13-15, pp.21-25.

[3] J. Nagamatsu, N. Nakagawa, T. Muranaka, Y. Zentani, A. Akimitsu, Nature, **410** (2001) 63.

[4] J. G. Bednorz, K. A. Mülle, Z. Phys., **B64** (1986) 189.

[5] J. M. Tarascon, Y. Le Page, P. Barboux, B. G. Bagley, L. H. Greene, W. R. McKinnon, G. W. Hull, M. Giroud, D. M. Hwang, Phys. Rev. B, **37** (1988) 9382.

[6] M. Takano, J. Takada, K. Oda, H. Kitaguchi, Y. Miura, Y. Ikeda, Y. Tomii, H. Mazaki, Jpn, J. Appl. Phys., **27** (1988) L1041.

[7] D. C. Larbalestier, A. Gurevich, D. M. Feldmann, A. Polyanskii, Nature, **414** (2001) 368.

[8] L. A. Schwartzkopf, J. Jiang, X. Y. Cai, D. Apodaca, D. C. Larbalestier, Appl. Phys. Lett., **75** (1999) 3168.

[9] J. Tenbrink, K. Heine, H. Krauth, Cryogenics, **30** (1990) 422.

[10] H. Kitaguchi, H. Kumakura, MRS Bulletin, **26** (2001) 121.

[11] R. Navarro, Supercond. Sci. Technol., **13** (2000) R147.

[12] A. Goal, D. P. Norton, J. D. Christen, Q. He, B. Staffian, F. A. List, D. F. Lee, P. M. Martin, C. E. Klabundle, E. Hatfield, V. K. Sikka, Appl. Phys. Lett., **69** (1996) 1795.

[13] Y. Iijima, M. Hosaka, N. Tanabe, N. Sadakata, T. Saitoh, O. Kohno, and J. Yoshitomi, Adv. Supercond., **VIII** (1996) 659.

[14] M. Bauer, R. Semerad, H. Kinder, IEEE Trans. Appl. Supercond., **9** (1999) 1502.

[15] W. Prusseit, G. Sigl, R. Nemetschek, C. Hoffmann, J. Handke, A. Lümkemann, H. Kinder, IEEE Trans. Appl. Supercond., **15** (2005) 2608.

[16] M. Kikuchi, T. Kato, K. Ohkura, N. Ayai, J. Fujikami, K. Fujino, S. Kobayashi, E. Ueno, K. Yamazaki, S. Yamade, K. Hayashi, K. Sato, T. Nagai, Y. Matsui, Physica C, **445-448** (2006) 717.

[17] S. Yamade, N. Ayai, J. Fujikami, S. Kobayashi, E. Ueno, K. Yamazaki, M. Kikuchi, T. Kato, K. Hayashi, K. Sato, H. Kitaguchi, J. Shimoyama, Physica C, **463-465** (2007) 821.

[18] H. Maeda, P. V. P. S. S. Sastry, U. P. Trociewitz, J. Schwartz, K. Ohya, M. Sato, W. P. Chen, K. Watanabe, M. Motokawa, Physica C, **386** (2003) 115.

[19] D. Dimos, P. Chaudhari, J. Mannhart, Phys. Rev. B, **41** (1990) 4038.

[20] M. Inoue, T. Kiss, T. Kuga, M. Ishimaru, M. Takao, T. Matsushita, Y. Iijima, K. Kakimoto, T. Saitoh, S. Awji, K. Watanabe, Y. Shiohara, Physica C, **392–396** (2003) 1078.

[21] O. Tsukamoto, Cryogenics, **45** (2005) 3.

[22] T. Masuda, T. Kato, H. Yumura, M. Watanabe, Y. Ashibe, K. Ohkura, C. Suzawa, M. Hirose, S. Isojima, K. Matsuo, S. Honjo, T. Mimura, T. Kuramochi, Y. Takahashi, H. Suzuki, T. Okamoto, Physica C, **378-381** (2002) 1174.

[23] J. A. Demko, I. Sauers, D. R. James, M. J. Gouge, D. Lindsay, M. Roden, J. Tolbert, D. Willén, C. Taeholt, C.T. Nielsen, IEEE. Trans. Appl. Supercond., **17** (2007) 2047.

[24] T. Masuda, H. Yumura, M. Watanabe, H. Takigawa, Y. Ashibe, C. Suzawa, H. Ito, M. Hirose, K. Sato, S. Isojima, C. Weber, R. Lee, J. Moscovic, IEEE. Trans. Appl. Supercond., **17** (2007) 1648.

[25] J. Y. Yoon, S. R. Lee, J. Y. Kim, IEEE. Trans. Appl. Supercond., **17** (2007) 1656.

[26] Superconductivity, http://www.conectus.org/xxtechnology.html

[27] L. Bulaevskii, J. R. Clem, L. I. Glazman, A. P. Malozemoff, Phys. Rev. B, **45** (1992) 2545.

[28] B. Hensel, J. C. Grrivel, A. Jeremie, A. Perin, A. Pollini, R. Flükiger, Physica C, **205** (1993) 329.

[29] G. N. Riley, A. P. Malozemoff, Q. Li, S. Fleshler, T. G. Holesinger, JOM, **49** (1997) 24.

[30] J. W. Ekin, D. K. Finnemore, Q. Li, J. Tenbrink, W. Carter, Appl. Phys. Lett., **61** (1992) 858.

[31] S. Ochiai, T. Ishida, D. Doko, K. Morishita, H. Okuda, S. S. Oh, D. W. Ha, M. Hojo, M. Tanaka, M. Sugano, K. Osamura, Supercond. Sci. Technol., **18** (2005) S232.

[32] S. Ochiai, K. Hayashi, K. Osamura, Cryogenics, **33** (1993) 976.

[33] M. Suenaga, Y. Fukumoto, P. Haldar, T.R. Thurston, U. Wildgruber, Appl. Phys. Lett., **67** (1995) 3025.

Chapter 2

Analysis of residual strain change of Bi2212, Ag alloy and Ag during heating and cooling process in Bi2212/Ag/Ag alloy composite wire

Nomenclatures

T_H: Heat-treatment temperature
T_0: Strain accumulation start temperature
T_1: Temperature which Ag comes to be yielded in tension
T_2: Temperature which Ag comes to be yielded in compression
ΔT: Temperature difference
θ_{comp}: Bragg Peak angle of Bi2212 filaments in the composite
θ_0: Bragg Peak angle of extracted Bi2212 filaments
E_{Bi}: Young's modulus of Bi2212 filaments
E_{Ag}: Young's modulus of Ag
E_{Alloy}: Young's modulus of Ag alloy
V_{Bi}: Volume fraction of Bi2212 filaments
V_{Ag}: Volume fraction of Ag
V_{Alloy}: Volume fraction of Ag alloy
$\varepsilon_{c,I\rightarrow II}$: Transition strain from stage I to stage II
$\varepsilon_{c,II\rightarrow III}$: Transition strain from stage II to stage III
$\varepsilon_{c,III\rightarrow IV}$: Transition strain from stage III to stage IV

$\varepsilon_{y,Ag}$: Yield strain of Ag
$\varepsilon_{y,Alloy}$: Yield strain of Ag alloy
$\varepsilon_{r,Bi,RT}$: Residual strain of Bi2212 filaments in the composite wire at room temperature
$\varepsilon_{r,Bi,77K}$: Residual strain of Bi2212 filaments in the composite wire at 77K
$\varepsilon_{r,Alloy,RT}$: Residual strain of Ag alloy in the composite wire at room temperature
$\varepsilon_{r,Alloy,77K}$: Residual strain of Ag alloy in the composite wire at 77K
$\varepsilon_{r,Bi}$: Elastic component of residual strain of Bi2212 filaments
$\varepsilon_{r,Ag}$: Elastic component of residual strain of Ag
$\varepsilon_{r,Alloy}$: Elastic component of residual strain of Ag Alloy
$\Delta\varepsilon$: Residual strain difference for temperature difference ΔT
$\varepsilon_{f,Bi}$: Intrinsic fracture strain of Bi2212 filaments
$\sigma_{y,Ag}$: Yield stress of Ag
α_c: Coefficient of thermal expansion (CTE) of the composite wire
α_{Bi}: CTE of Bi2212 filaments
α_{Ag}: CTE of Ag
α_{Alloy}: CTE of Ag alloy

2.1 Introduction

The long and high critical current density - multi-filamentary $Bi_2Sr_2Ca_1Cu_2O_{8+x}$ (Bi2212) superconductor composite wires have been developed [1,2]. In these composite wires, the thermally induced residual strains are considered to be accumulated during fabrication and application, as well as in Bi2223 composite tapes [3-5], which will affect on the superconducting property. The present work attempted to reveal the residual strain change with temperature in the cooling and heating process by experiment and modeling analysis.

The thermally induced residual strain of the Bi2212 filaments is compressive and represents the negative value in the current transportation direction, due to the difference in coefficient of thermal expansion among constituents (Bi2212[6], Ag and Ag alloy [7,8]). In cooling process from the annealing temperature, it is deduced that the creep behavior of Ag and Ag alloy at high temperatures releases the residual strain, and therefore the residual strain starts to be accumulated below such a temperature [9] and is accumulated with decreasing temperature. The residual strain is highest at cryogenic temperatures such as 77 and 4.2 K. When the sample is heated from such cryogenic

temperatures, for instance to room temperature, the residual strain is released. The present work was carried out to reveal such a change of residual strain with temperature during cooling and heating process by the following procedure. (1) Estimation of the residual strain of Bi2212 filaments at room temperature by the X-ray diffraction method whose procedure has been shown in our preceding work [9-11]. (2) Estimation of the property values such as Young's modulus and coefficient of thermal expansion of the constituents and yield strain of Ag, which are needed for analysis. (3) Estimation of the temperature at which residual strain starts to be accumulated and the change of residual strain with temperature by modeling analysis using the rule of mixtures, in which the property- values estimated in (1) and (2) were substituted.

2.2 Experimental procedure

2.2.1 Samples and their thermal history

Figure 2.1 shows the cross-section of Bi2212 composite wire used in the present work. From the image analysis of the cross-section, the volume fractions of the Bi2212 filaments, Ag and Ag alloy were estimated to be 0.32, 0.49 and 0.19, respectively. The overall diameter was 0.93mm. The present samples had the following thermal history, as schematically shown in figure 2.2. (i) They were cooled from the heat-treatment temperature (T_H) to room temperature RT(1). (ii) They were cooled from RT(1) to 77K(1) for pre-check of the critical current. (iii) They were heated from 77K(1) to room temperature RT(2).

The samples with such a thermally history were sent from KERI to Kyoto University (KU). At RT(2) and 77K(2), the stress-strain curve and residual strain were measured at KU. Also the thermal expansion measurement was carried out between RT(2) and 600K at KU for such samples.

As Ag is soft, Ag behaves in a following manner in each stage (i, ii and iii), as similarly as the Ag in the Bi2223/Ag/Ag alloy tape [9].

In stage (i) (cooling from the temperature T_H to RT(1)), the strain accumulation starts at T_0 (RT(1) < T_0 <T_H). During cooling from T_0 to RT(1), tensile strain is accumulated in Ag since the coefficient of thermal expansion of Ag (and Ag alloy) is higher than Bi2212.

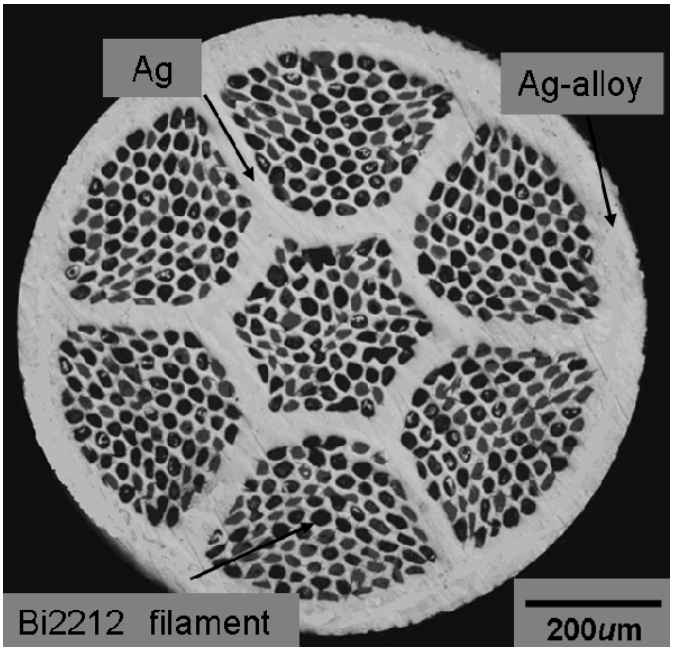

Figure 2.1. Polished cross-section of Bi2212 superconductor composite wire.

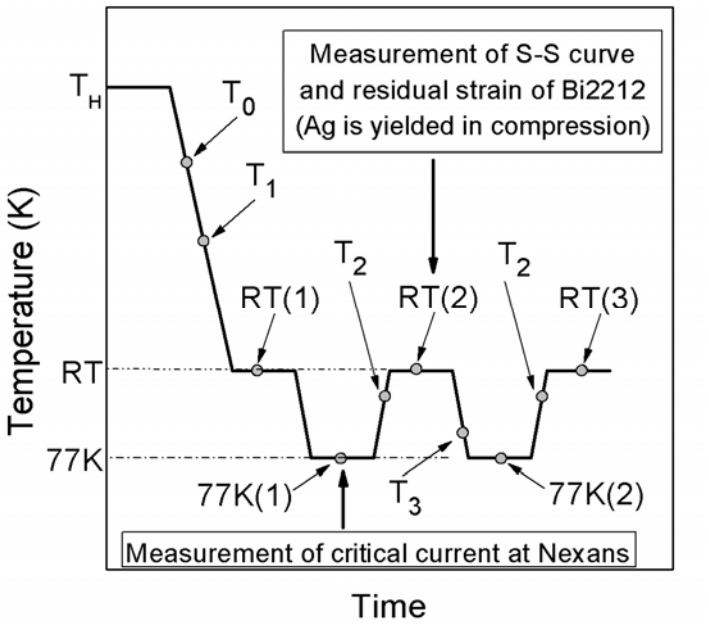

Figure 2.2. Thermal history of the sample.

Accordingly, Ag deforms first elastically until Ag comes to be yielded in tension at T_1 ($RT(1) < T_1 < T_0$), and Ag deforms plastically in tension below T_1. In stage (ii) (cooling from RT(1) to 77K), Ag deforms plastically as well as in $RT(1)<T<T_1$. In stage (iii) (heating from 77K to RT(2)), compressive strain is added in Ag. Ag comes to be yielded in compression at T_2 ($77K < T_2 < RT(2)$). Accordingly Ag behaves elastically in $77K<T<T_2$ and plastically in $T_2<T<RT(2)$. The samples are cooled again from RT(2) to 77K.

2.2.2 Measurement of residual strain of Bi2212 in composite at room temperature

To estimate the residual strain of Bi2212 filaments at RT(2), the in situ strain measurements with Bi2212 composite wires were carried out at the beamline 46XU of the synchrotron radiation facility, SPring 8, Japan. The residual strain was estimated by extrapolation of the measured relation of Bi2212 strain to the applied tensile strain on composite to zero applied strain by regression analysis, as in our former works [9-11]. As the stress-free reference sample, the Bi2212 filaments, extracted from the same composite wire by dissolving Ag and Ag alloy with a NH_4OH/H_2O_2 solution, were used. The Bragg peaks of Bi2212 filaments as well as that of the strain-free extracted Bi2212 filaments were measured for (200) plane.

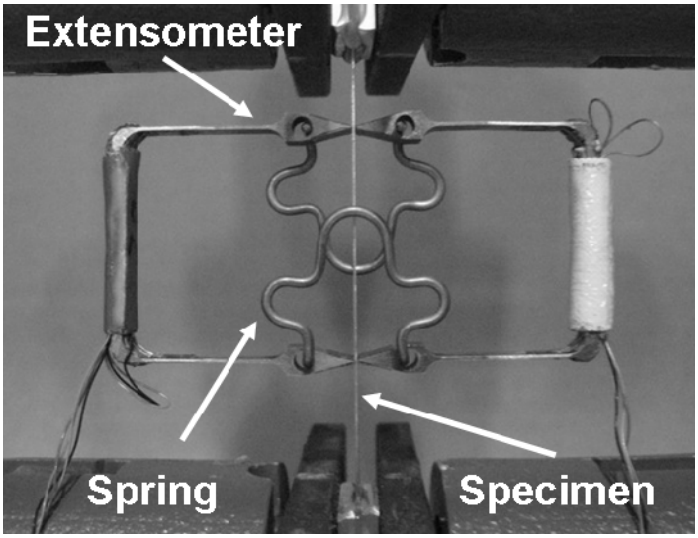

Figure 2.3. Nyilas type extensometer for measurement of the strain in tensile test.

2.2.3 Measurement of stress-strain curve of the composite wire at room temperature and 77K

Tensile test was carried out using a universal testing machine (autograph AG-50kNG, Shimadzu, Japan) at a strain rate of $2*10^{-4}s^{-1}$ at room temperature (RT(2)) and 77K(2), whose result will be used to estimate the Young's modulus of all constituents and yield strain of Ag and Ag alloy in 2.3.2. For measurement of the strain, a couple of very light Nyilas type extensometers [12] was attached directly to the sample with a 25mm gauge length as shown in figure 2.3.

2.2.4 Measurement of thermal expansion of the composite wire and Ag between room temperature and 600K

A TMA (Thermomechanical Analysis) apparatus (TMA8140, Rigaku, Japan) was used for the measurement of the thermal expansion between RT(2) (300K) and 600K. The linear coefficient of thermal expansion in the temperature range 300-400K where Ag deforms plastically (details will be shown in 2.3.3) was estimated by $\Delta L/(L_0\Delta T)$, where ΔL is the change in length of the sample during heating and L_0 is the sample length at room temperature.

2.3 Results and discussion

2.3.1 Residual strain of Bi2212 at room temperature

Figure 2.4 shows the change of Bragg peaks with increasing applied strain. It is clearly seen that the peak position shifts to the lower angle with increasing applied tensile strain. From the Bragg peak shift under applied tensile strain due to change for the lattice parameter, the Bi2212 filaments strain was obtained. From the Bragg peak angle of the Bi2212 filaments in the composite (θ_{comp}) and that of the extracted filaments (θ_0), the strain of Bi2212 filaments in the composite was estimated by,

$$\Delta a / a = \varepsilon_{Bi} = \{(1 / \sin(\theta_0) - 1 / \sin(\theta_{comp})) / (1 / \sin(\theta_0))\}. \quad (2.1)$$

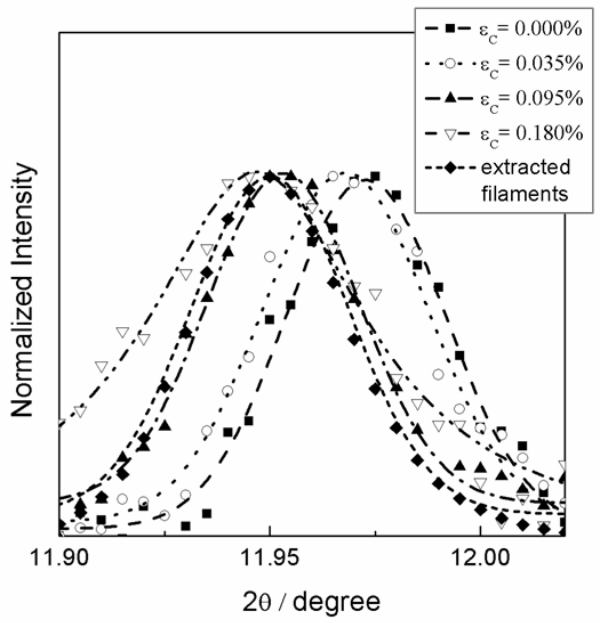

Figure 2.4. Change of the Bragg peaks with increasing applied strain.

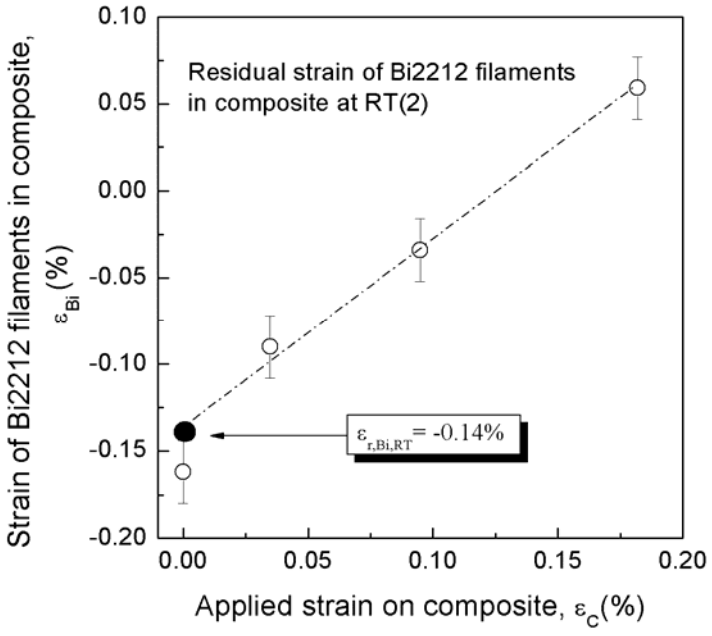

Figure 2.5. Change of Bi2212 filaments strain with increasing applied tensile strain on the composite.

Figure 2.5 shows the change of Bi2212 filaments strain with increasing applied tensile strain on the composite. For estimation of the residual strain of Bi2212 filaments at zero applied strain, the relation between the filaments strain and composite strain was extrapolated linearly to the value at zero applied tensile strain. The residual strain of Bi2212 filaments in composite at room temperature was estimated to be -0.140%.

2.3.2 Estimation of mechanical properties of the constituents (Bi2212, Ag and Ag alloy) from the measured stress-strain curve of the composite

Figure 2.6 and 2.7 show the measured tensile stress-strain curve of the Bi2212 composite wire at RT(2) and 77K(2), respectively. It is noted that Ag has been yielded in compression since it had been cooled down to 77K(1) and then warmed to room temperature (RT(2)) as shown in figure 2.2. Thus, Ag deforms elastically upon loading. The residual strain of Ag alloy was tensile but was lower than the yield strain as shown later. The residual strain of Bi2212 filaments was compressive. Accordingly, all constituents (Ag, Ag alloy and Bi2212 filaments) deform elastically in the early stage of deformation. With increasing applied strain on composite, Ag comes to be yielded when the strain of Ag reaches the tensile yield strain. With further loading, Ag alloy comes to be yielded. In the late stage, the Bi2212 filaments come to be fractured.

The mechanical property values such as Young's modulus of all constituents, yield strain of Ag and Ag alloy and fracture strain of Bi2212 filaments are needed for analysis of residual strain accumulation process. These mechanical property values were estimated from the stress-strain curves, as follows. The tensile stress-strain curve in figure 2.6 was composed of the four stages I, II, III and IV depending on the elastic and plastic behavior of Ag and Ag alloy and fracture of Bi2212 filaments. Each stage is characterized as follows.

In stage I, all constituents (Bi2212 filaments, Ag and Ag alloy) deform elastically. At the end of stage I, Ag comes to be yielded since it is soft as shown later.

In stage II, Ag has been yielded while Bi2212 filaments and Ag alloy deform elastically. At the end of stage II, Ag alloy comes to be yielded.

In stage III, Ag and Ag alloy have been yielded while Bi2212 filaments deform elastically. At the end of stage III, the fracture of the Bi2212 filaments starts.

In stage IV, the Bi2212 filaments are fractured more and more (multiple fracture) since the stress is transferred even to the once fractured filaments [13-15]. In the multiple fracture stage, the fracture-induced reduction in stress carrying capacity of the

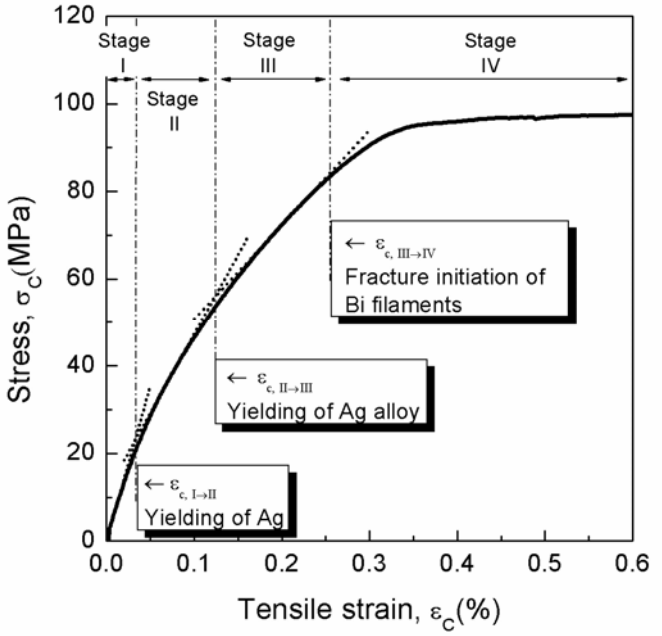

Figure 2.6. Measured stress-strain curve of the Bi2212 composite wire at room temperature (RT(2)).

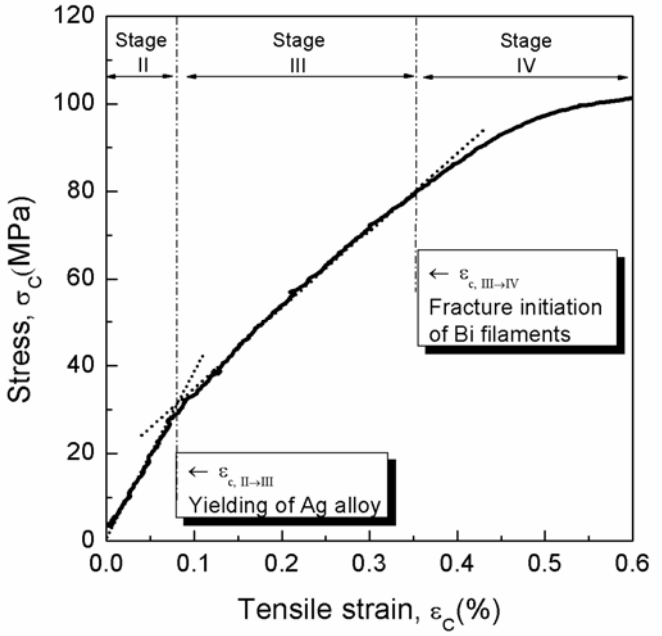

Figure 2.7. Measured stress-strain curve of the Bi2212 composite wire at 77K(2).

filaments is balanced with the strain hardening-induced increase in stress carrying capacity of the Ag and Ag alloy, leading to the nearly constant stress of the composite [16]. Figure 2.8 shows the polished longitudinal section of the damaged portion after applying tensile strain up to 1.0%. Actually, the originally continuous filaments show the multiple fractures.

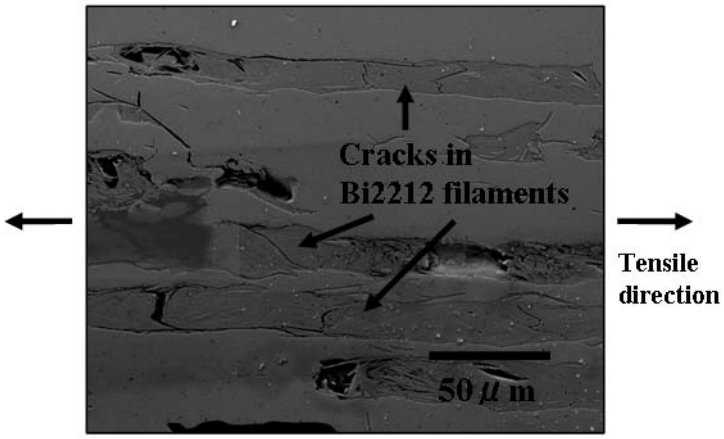

Figure 2.8. Polished longitudinal section of the damaged portion of the composite wire strained in tension by 1.0%.

From the slope in each stage in figure 2.6, the Young's modulus (E) values, $E_{c,I}$, $E_{c,II}$ and $E_{c,III}$ were read to be 71.6, 36.6 and 21.2, respectively, where the subscripts I, II and III refer to stages I, II and III, respectively. The Young's modulus of the composite wire in each stage is approximately given by the rule of mixture based on the volume fraction V [9].

Stage I: $E_{c,I} = E_{Bi}V_{Bi} + E_{Ag}V_{Ag} + E_{Alloy}V_{Alloy}$ (2.2)

Stage II: $E_{c,II} = E_{Bi}V_{Bi} + E_{Alloy}V_{Alloy}$ (2.3)

Stage III: $E_{c,III} = E_{Bi}V_{Bi.}$ (2.4)

where the subscripts Bi, Ag and Alloy refer to Bi2223 filaments, Ag and Ag alloy, respectively. By substituting the measured values of $E_{c,I}$, $E_{c,II}$, $E_{c,III}$, V_{Bi}, V_{Ag} and V_{Alloy} aforementioned above into equations (2.2) to (2.4), the Young's moduli of the Bi2212

filaments (E_{Bi}), Ag alloy (E_{Alloy}) and Ag (E_{Ag}) were estimated to be 66.3, 81.1 and 71.4GPa, respectively.

During cooling from annealing temperature to room temperature and then 77K, Ag is yielded in tension below T_1 (Figure 2.2) and undergoes plastic deformation, because the coefficient of thermal expansion of Ag and Ag alloy ($20*10^{-6}K^{-1}$, shown later in 3.3) are larger than that of Bi2212 filament ($11.5*10^{-6}K^{-1}$, shown later in 3.3). The sample used in this work had been cooled to 77K(1) for measurement of critical current. At 77K(1), Ag has been yielded in tension. When it is warmed to room temperature (RT(2)), compressive strain is added to Ag and Ag alloy and tensile one to Bi2212. In the present sample, Ag has been yielded in compression at RT(2). The initial stage of stress-strain curve in this study corresponded to the elastic deformation region of Ag. Therefore, the strain ($\varepsilon_{c,I\rightarrow II}$) at the deviation from stage I to stage II corresponds to the strain change of Ag from compressive to tensile yielding, which is given by the two times of the yield strain $\varepsilon_{Ag,\,y}$ of Ag ($\varepsilon_{c,I\rightarrow II} = 2\varepsilon_{y,Ag}$). The $\varepsilon_{c,I\rightarrow II}$ in figure 2.6 is read to be 0.038%. Thus $\varepsilon_{y,Ag}$ is estimated to be 0.019%, which corresponds to the yield stress of 13.6MPa ($=\varepsilon_{y,Ag}E_{Ag}$). In the literature [17], the yield stress of annealed Ag has been reported to be 54MPa. In this case, the heat-treatment temperature is, however, around 700K. On the contrary, the present samples were heat-treated at 1163K. Such a high temperature heat-treatment makes Ag very soft. Actually, the yield stress of Ag annealed at 1073K has been measured to be 11.2MPa [18] and 10.9MPa [19], which were close to the present result. In the present work, the yield strain is defined at stage I to stage II as shown in figure 2.6. On this point, the present yield strain is lower than that defined at 0.2% offset strain. However, as Ag is very soft, the ratio (w) of strain hardening rate ($d\sigma/d\varepsilon$) to Young's modulus (E) is reported to be 0.008 [18], due to which we approximated Ag as the elastic-perfect plastic body. If we incorporate the strain hardening, the yield stress of Ag is given by $\sigma = \sigma_{y,Ag} + wE_{Ag}(\varepsilon-\varepsilon_{y,Ag})$ [18]. In this case, the yield stress at 0.2% offset strain is calculated to be 14.6MPa. If we use such a 0.2% offset yield stress, the yield strain of Ag ($\varepsilon_{y,Ag}$) is calculated to be 0.0204% ($=\sigma_{y,0.2\%\ offset}/E_{Ag}$), which is close to the present yield strain 0.019%. The result analyzed by the present yield stress 13.6MPa will be compared with the 0.2% off set strain (14.6MPa) and it will be shown that the results are almost the same in 3.3. At the transition from stage II to stage III, the strain ($\varepsilon_{c,II\rightarrow III}$ = 0.130%) corresponds the yielding of Ag alloy in composite wire. The yield strain of Ag alloy ($\varepsilon_{y,Alloy}$) is expressed by $\varepsilon_{y,Alloy} = \varepsilon_{c,II\rightarrow III} + \varepsilon_{r,Alloy,RT}$, where $\varepsilon_{r,Alloy,RT}$ is the residual strain of Ag alloy in the composite wire at room temperature, which was 0.240% as substituting yield stress of Ag (13.6MPa), residual stress of Bi2212 filaments ($\varepsilon_{r,Bi,RT}E_{Bi}$ = -92.8MPa) and volume fracture of each constituent into equation (2.5) (will be shown in 3.3). Accordingly, the

yield strain of Ag alloy ($\varepsilon_{y,Alloy}$) was estimated to be 0.370%. The transition from state III to stage IV corresponds to the fracture of the Bi2223 filaments. The fracture strain of Bi2212 filaments ($\varepsilon_{c,III\rightarrow IV}$= 0.250~0.270%) is given by ($\varepsilon_{f,Bi}-\varepsilon_{r,Bi,RT}$). As the residual strain of Bi2212 filaments in composite wire was estimated to be -0.140%, The intrinsic fracture strain of Bi2212 filaments ($\varepsilon_{f,Bi}$) was evaluated to be 0.110~0.130%.

On the other hand, the stage I did not appear the stress-strain curve at 77K as shown in figure 2.7. Since the tensile strain was exerted on Ag during cooling RT to 77K, Ag was yielded on the way. Stage II appeared in the initial deformation region. At the transition from stage II to stage III, the strain ($\varepsilon_{c,II\rightarrow III}$ = 0.072%) corresponds the yielding of Ag alloy in composite wire. Likewise the calculation method at RT, the yield strain of Ag alloy at 77K ($\varepsilon_{y,Alloy,77K}$) is expressed by $\varepsilon_{y,Alloy,77K} = \varepsilon_{c,II\rightarrow III} + \varepsilon_{r,Alloy,77K}$, where $\varepsilon_{r,Alloy,77K}$ is the residual strain of Ag alloy in the composite wire at 77K. The increment in tensile residual strain of Ag alloy in composite due to cooling from RT(2) to 77K(2) was calculated to 0.075% by equations (2.12) and (2.14) (shown later in 3.4). Accordingly, the residual strain of Ag alloy at 77K, $\varepsilon_{r,Alloy,77K}$, was estimated to be 0.315%. Also the yield strain of Ag alloy at 77K, $\varepsilon_{y,Alloy,77K}$ was estimated to be 0.387%. With further applied strain on the composite wire, the fracture of Bi2212 filaments initiated at the strain of 0.350~0.370%, which corresponds to $\varepsilon_{f,Bi}-\varepsilon_{r,Bi,77K}$, where $\varepsilon_{r,Bi,77K}$ is the residual strain of Bi2212 filaments in the composite at 77K. Under the approximation that the intrinsic fracture strain of Bi2212 filaments, $\varepsilon_{f,Bi}$, is not changed with temperature in the range between RT and 77K, the residual strain of Bi2212 filaments in composite wire at 77K, $\varepsilon_{r,Bi,77K}$, was estimated to be -0.24%.

2.3.3 Estimation of the coefficient of thermal expansion of Bi2212 filaments by means of TMA

Figure 2.9 shows the thermal expansion curves of Bi2212 composite wire between 300 and 600K, together with the curve of Ag alone. The coefficient of thermal expansion (CTE) of Ag between 300 and 400K was estimated to be $20*10^{-6}K^{-1}$.

As stated in 2 (as shown in figure 2.2), Bi2212 composite wire experienced the thermal history from cooling heat-treatment temperature (T_H) to RT(1), then further cooled down to 77K(1) and up to RT(2). In this situation at RT(2), Ag is already yielded in compression. During heating from 300 to 600K to measure the thermal expansion of Bi2212 composite wire, further compressive strain is exerted due to the higher CTE of Ag and Ag alloy than that of Bi2212. Ag is treated as the perfect elastic-plastic body and the CTE of Ag alloy was taken to be same as that of Ag. Under no application of

external stress, the total residual stress is zero, which is expressed by,

$$-\sigma_{y,Ag}V_{Ag} + \varepsilon_{r,Bi,RT}E_{Bi}V_{Bi} + \varepsilon_{r,Alloy,RT}E_{Alloy}V_{Alloy} = 0 \quad (2.5)$$

where $\varepsilon_{r,Bi,RT}$ and $\varepsilon_{r,Alloy,RT}$ are residual strains of Bi2212 filaments and Ag alloy in the composite at room temperature, respectively. Also, the total residual stress is zero at any temperature. Noting the temperature difference between room temperature and arbitrary one as ΔT, equation (2.6) is hold.

$$-\sigma_{y,Ag}V_{Ag} + [\ (\alpha_{c,II}^{-} - \alpha_{Bi}^{-})E_{Bi}\Delta T + \varepsilon_{r,Bi,RT}E_{Bi}\ ]V_{Bi} + [\ (\alpha_{c,II}^{-} - \alpha_{Alloy})E_{Alloy}\Delta T + \varepsilon_{r,Alloy,RT}E_{Alloy}\ ]V_{Alloy} = 0 \quad (2.6)$$

where $\alpha_{c,II}^{-}$ and α_{Bi}^{-} are the CTE of the composite and Bi2212 filaments, respectively, and the superscript –(minus) refers to the compressively yielded state of Ag. Substituting equation (2.5) into equation (2.6), we have

$$\alpha_{c,II}^{-} = (\alpha_{Bi}^{-}E_{Bi}V_{Bi} + \alpha_{Alloy}E_{Alloy}V_{Alloy}) / (E_{Bi}V_{Bi} + E_{Alloy}V_{Alloy}). \quad (2.7)$$

The $\alpha_{c,II}^{-}$ was estimated to be $15.1*10^{-6}K^{-1}$ from the slope of the measured thermal expansion-temperature relation in figure 2.9. Substituting the values of $\alpha_{c,II}^{-}$, α_{Alloy} (same as α_{Ag}), $E_{Bi}V_{Bi}$, $E_{Alloy}V_{Alloy}$ into equation (2.3), we have $\alpha_{Bi}^{-}=11.5*10^{-6}K^{-1}$.

For the temperature range where Ag deforms elastically, the CTE of the composite wire ($\alpha_{c,I}$) is given by,

$$\alpha_{c,I}= (\alpha_{Bi}E_{Bi}V_{Bi} + \alpha_{Ag}E_{Ag}V_{Ag} + \alpha_{Alloy}E_{Alloy}V_{Alloy}) / (E_{Bi}V_{Bi} + E_{Ag}V_{Ag}+ E_{Alloy}V_{Alloy}) \quad (2.8)$$

The $\alpha_{c,I}$ was calculated to be $17.4*10^{-6}K^{-1}$. In the case where Ag has been yielded in compression due to warming, Ag behaves elastically from the compressively yielded state to tensile yielding state when the composite is cooled. Also, in the case where Ag has been yielded in tension due to cooling, Ag behaves elastically from the tensile yielded state to compressive yielding state when the composite is warmed. Noting the temperature difference to cause such cases as $\Delta T'$,

$$2\varepsilon_{y,Ag} = (\alpha_{c,I} - \alpha_{Ag})\Delta T' \quad (2.9)$$

is satisfied. Substituting the values of $\varepsilon_{y,Ag}$, $\alpha_{c,I}$ and α_{Ag} estimated above, $\Delta T'$ is calculated to be 146K. This value will be used in 3.4 and 3.5 for analysis of change of

residual stress with temperature during cooling and warming process. If we use the 0.2% offset yield stress (14.6MPa), which corresponds to $\varepsilon_{y,Ag}$=0.0204%, the temperature difference ΔT to cause compressive to tensile yielding vise and versa is calculated to be 155K which is very close to ΔT=146K calculated with the present yield stress 13.6MPa. In this way, the estimated change of residual strain of Bi2212 filaments with temperature is practically the same as that estimated for 0.2% offset yield stress. In practice, it is difficult to estimate 0.2% offset yield stress of Ag from the stress-strain curve of the composite. The method employed in the present work to estimate the yield-stress from the stress-strain curve is very simple and useful in practice.

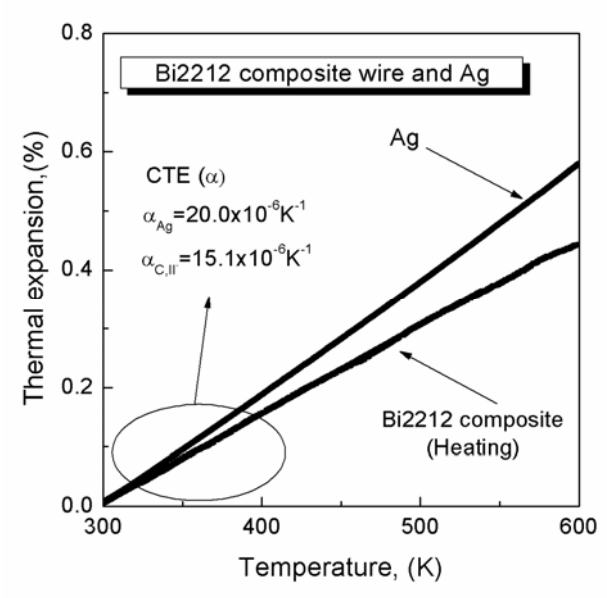

Figure 2.9. Measured thermal expansion curves of Bi2212 composite wire and Ag during heating and cooling between 300 and 600K.

2.3.4 Estimation of strain accumulation temperature in the Bi2212 composite

As shown in 3.3, the coefficient of thermal expansion (CTE) of Bi2212 filaments, Ag and Ag alloy between 300 and 400K was estimated to be α_{Bi}=11.5*10^{-6}K^{-1} and α_{Ag}=α_{Alloy}=20*10^{-6}K^{-1}, as well as that of composite $\alpha_{c,I}$ (Ag elastic region) and $\alpha_{c,II}$ (Ag plastic region) was estimated to be 17.4*10^{-6}K^{-1} and 15.1*10^{-6}K^{-1}, respectively.

In the range where Ag deforms elastically, the change of residual strain $\Delta\varepsilon$ of each constituent for the temperature difference is expressed as follows,

$$\Delta\varepsilon_{Bi} = (\alpha_{c,I} - \alpha_{Bi})\,\Delta T \quad (2.10)$$

$$\Delta\varepsilon_{Ag} = (\alpha_{c,I} - \alpha_{Ag})\,\Delta T \quad (2.11)$$

$$\Delta\varepsilon_{Alloy} = (\alpha_{c,I} - \alpha_{Alloy})\,\Delta T. \quad (2.12)$$

As Ag undergoes plastic deformation, the change of residual strain of Bi2212 and Ag alloy is expressed as follows,

$$\Delta\varepsilon_{Bi} = (\alpha_{c,II} - \alpha_{Bi})\,\Delta T \quad (2.13)$$

$$\Delta\varepsilon_{Alloy} = (\alpha_{c,\,II} - \alpha_{Alloy})\,\Delta T. \quad (2.14)$$

As stated already, the stress-strain curve of Bi2212 composite wire and the residual strain of Bi2212 in composite wire were measured at RT(2) where Ag is yielded in compression. According to the estimated yield strain of Ag ($\varepsilon_{y,Ag}$=0.019%), the temperature difference necessary to cause yielding from the zero strain state was estimated to be -73K ($=\varepsilon_{y,Ag}/(\alpha_{c,I}-\alpha_{Ag})$). As has been shown in 3.3, the temperature difference to cause compressive to tensile vise and versa was 146K ($=2\varepsilon_{y,Ag}/(\alpha_{c,I}-\alpha_{Ag})$).

During cooling from the heat-treatment temperature to RT(1), there exists the temperature (T_0) where the strain accumulation starts (Figure 2.2). During cooling from T_0 to RT(1), Ag deforms elastically until Ag comes to be yielded in tension at T_1 ($RT < T_1 < T_0$) before the temperature reaches RT since the temperature difference $|RT - T_0|$ is larger than 73K. T_1 is the temperature at which Ag is yielded in tension. The difference between T_0 and T_1, ($T_1 - T_0$) is -73K as stated above. Below T_1, Ag deforms plastically during cooling process to RT(1) and then 77K(1). When the Bi2212 composite wire is warmed up from 77K(1), the compressive strain is induced to Ag. When the Bi2212 composite is heated from 77K(1) to RT(2), compressive strain is accumulated in Ag, due to which Ag deforms first elastically and at T_2 ($77K(1) < T_2 < RT(2)$), Ag comes to be yielded in compression before the temperature reaches RT(2), since the temperature difference $|RT - 77K|$ is larger than 146K. Contrary to the cooling process, as the temperature increases, Ag turns to be yielded in compression at the temperature (T_2). Namely, the state of deformation of Ag changes from elastic deformation in the temperature range between 77K(1) and T_2, to plastic deformation in compression between T_2 and RT(2). As $(\alpha_{c,I} - \alpha_{Ag})(T_2 - 77K) = 2\varepsilon_{y,Ag}$ holds owing to the change of Ag-strain from tensile to compressive yielding, T_2 is calculated to be 223K.

The residual strain of Bi2212 in composite wire measured with X-ray at RT_2 (-0.140%) is the essential parameter to solve the unknown values of T_0 and T_1. The strain of Bi2212 filaments ($\varepsilon_{r,Bi}$) which had undergone the whole thermal history is expressed as follows,

$$\varepsilon_{r,Bi}(T_0 \rightarrow T_1 \rightarrow RT(1) \rightarrow 77K(1) \rightarrow T_2 \rightarrow RT(2)) = \Delta\varepsilon_{Bi}(T_0 \rightarrow T_1) + \Delta\varepsilon_{Bi}(T_1 \rightarrow RT(1)) + \Delta\varepsilon_{Bi}(RT(1) \rightarrow 77K(1)) + \Delta\varepsilon_{Bi}(77K(1) \rightarrow T_2) + \Delta\varepsilon_{Bi}(T_2 \rightarrow RT(2)) \quad (2.15)$$

Substituting $T_1 - T_0$=-73K and T_2=223K into equation (2.10) and (2.13) depending on the deformation behavior of Ag, we had $\Delta\varepsilon_{Bi}(T_0 \rightarrow T_1)$=-0.046%, $\Delta\varepsilon_{Bi}(RT(1) \rightarrow 77K(1))$ = -0.082%, $\Delta\varepsilon_{Bi}(77K(1) \rightarrow T_2)$ = 0.092% and $\Delta\varepsilon_{Bi}(T_2 \rightarrow RT(2))$ = 0.028%, respectively. Substituting these calculated strain changes of Bi2212 filaments and $\varepsilon_{r,Bi,RT}$=-0.14% into equation (2.12), T_1 was estimated to be 655K. From the relation of $T_1 - T_0$=-73K, T_0 was revealed to be 728K.

2.3.5 Estimation of change of the residual strain of Ag and Bi2212 filaments with temperature

Using the estimated values of T_0 and T_1, the change of residual strain of constituents in the composite between RT and 77K can be calculated in a similar manner. The calculation results of the change of residual elastic strain of Ag, Ag alloy and Bi2223 filaments are presented in figure 2.10, 2.11 and 2.12.

In Ag (Figure 2.10), the thermally induced strain starts to be accumulated at T_0. Until T_1, Ag deforms elastically and the strain reaches to be 0.019% ($+\varepsilon_{y,Ag}$, yielded strain of Ag). Then Ag deforms plastically in tension, keeping the constant elastic strain ($+\varepsilon_{y,Ag}$) to 77K(1) through RT(1). When the composite wire is heated from 77K(1), Ag deforms elastically up to T_2 (223K). With further heating to RT(2), Ag deforms plastically in compression, keeping the constant elastic strain ($-\varepsilon_{y,Ag}$). When it is cooled again to 77K(2), Ag deforms elastically until the temperature reaches T_3 (152K). Then, Ag deforms plastically in tension, keeping the constant elastic strain ($+\varepsilon_{y,Ag}$). Such a situation continues from T_3 to 77K(2). In this way, Ag undergoes the elastic and plastic deformation in tension and in compression, during the cooling and heating process.

In Ag alloy (Figure 2.11), the tensile strain stats to be accumulated at T_0 and increases with decreasing temperature as well as that in Ag. At T_1 (Ag comes to be yielded in tension), the strain of the Ag alloy becomes 0.019%. With further cooling, it reaches 0.194% at RT(1). When the composite wire is further cooled to 77K(1), the tensile

strain of Ag alloy increases to 0.302%. When the composite wire is heated from 77K(1), compressive strain is added. At RT(2), the strain of Ag alloy becomes 0.227%. When the composite wire is cooled again from RT(2) to 77K(2), the strain at 77K(2) becomes again 0.302%. Accordingly, during the thermal cycle between RT and 77K, the strain of Ag alloy changes as follows; 0.227% at RT → 0.265% at 152K → 0.302% at 77K → 0.264% at 223K → 0.227% at RT.

In Bi2212 filaments (Figure 2.12), the compressive strain starts to be accumulated at T_0 and increases with decreasing temperature, while tensile strain is accumulated in Ag and Ag alloy. At T_1, the strain of the Bi2212 filaments becomes -0.046%. With further cooling, it reaches -0.178% at RT(1). When the composite wire is further cooled to 77K(1), the compressive strain of Bi2212 filaments increases to -0.260%. When the composite wire is heated from 77K(1), tensile strain is added. At RT(2), the strain of Bi2212 filaments becomes -0.140%, as measured by the x-ray diffraction method. When the composite wire is cooled again from RT(2) to 77K(2), the strain at 77K(2) becomes again -0.26%. Accordingly, during the thermal cycle between RT and 77K, the strain of Bi22122 filaments changes as follows; -0.140% at RT → -0.232% at 152K → -0.260% at 77K → -0.168% at 223K → -0.140% at RT. As stated in 3.2, the residual strain of Bi2212 filaments in composite was estimated to be -0.240% from the stress-strain curve at 77K. The present calculated value (-0.260 %) from the thermal history was close to -0.240 %. This result suggests that the present method is a useful tool for description of the residual strain changes as a function of temperature between the onset temperature of strain accumulation and 77K.

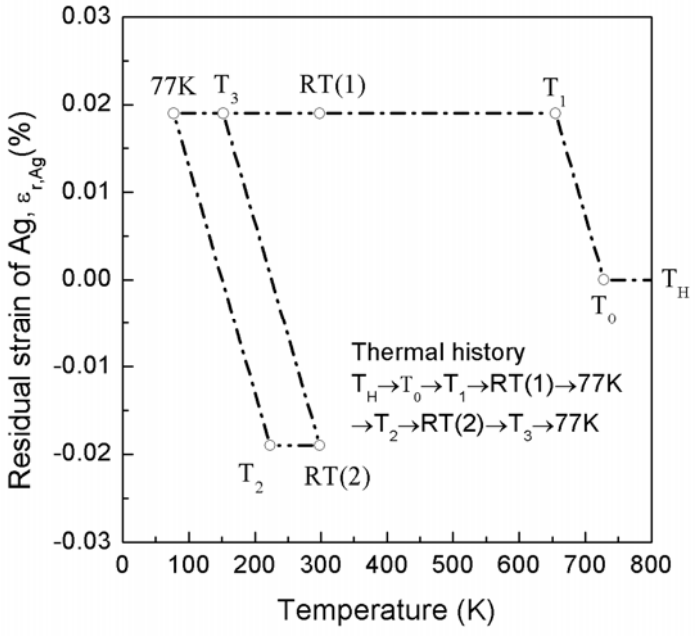

Figure 2.10. Change of the residual elastic strain of Ag in the composite wire with temperature.

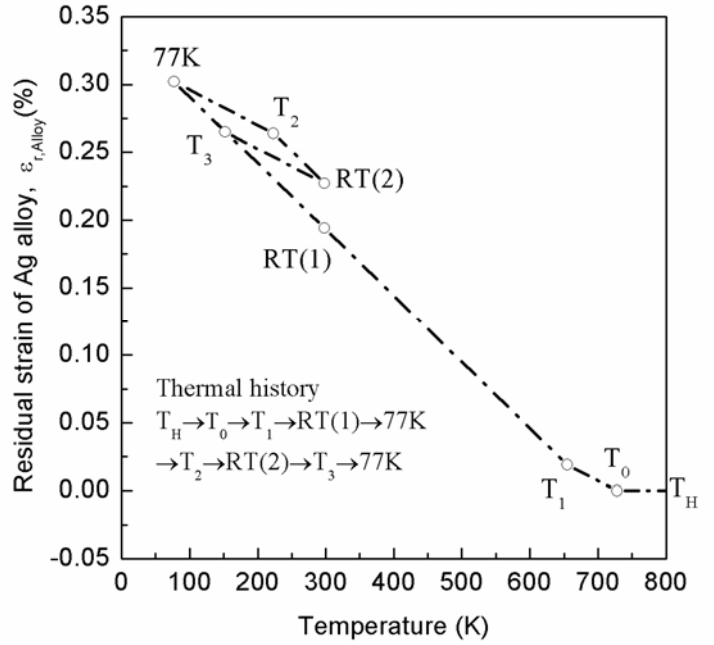

Figure 2.11. Change of the residual strain of Ag alloy in the composite wire with temperature.

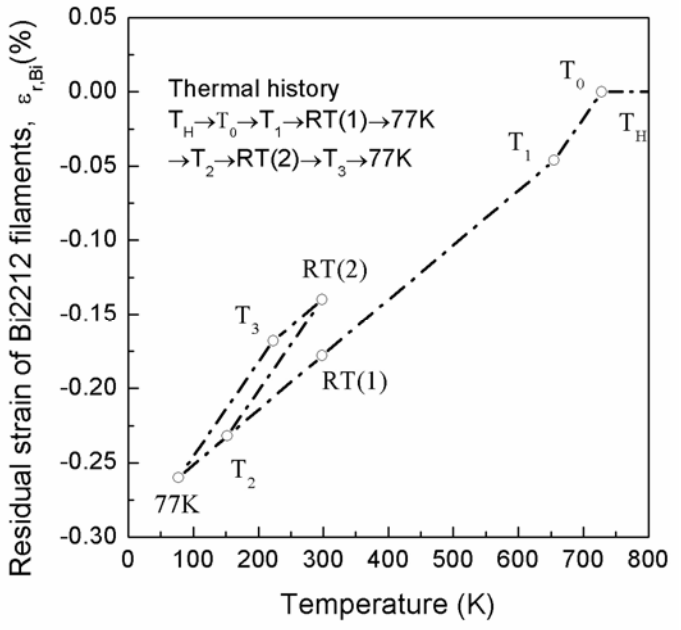

Figure 2.12. Change of the residual strain of Bi2212 filaments in the composite wire with temperature.

2.4 Conclusions

To reveal the residual strain change of the constituents (Bi2212, Ag alloy and Ag) during cooling and heating process in the Bi2212/Ag/Ag alloy composite superconductor, the stress-strain curves of the composite at room temperature and 77K measured by tensile test, the residual strain of Bi2212 filaments at room temperature measured by the X-ray diffraction method, and thermal expansion curves of the composite and Ag measured by the thermo-mechanical test were analyzed. It was found that, during cooling from the heat treatment temperature to 77K, the residual strain of Bi2212 filaments along the length varies as; compressive strain starts to be accumulated at 728K → -0.046% at 655K → -0.178% at room temperature → -0.260% at 77K. When the compote wire is heated from 77K up to room temperature and then is cooled down to 77K again, the residual strain varies as; -0.260% at 77K → -0.168% at 223K → -0.140% at room temperature → -0.232% at 152K → -0.260% at 77K. The variations of residual strain of Ag and Ag alloy were also revealed as a function of temperature in a similar manner.

References

[1] H. Miao, H. Kitaguchi, H. Kumakura, K. Togano, T. Hasegawa, T. Koizumi, Physica C, **303** (1998) 81.

[2] Y. Aoki, T. Koizumi, N. Ohtani, T. Hasegawa, L. Motowidlo, R. D. Sokolowski, R. M. Scanlan, S. Nagaya S, Physica C, **335** (2000) 1.

[3] H. Kitaguchi, K. Itoh, H. Kumakura, T. Takeuchi, K. Togano, H. Wada, IEEE Trans. Appl. Supercond., **11** (2001) 3058.

[4] J. W. Ekin, D. K. Finnermore, Q. Li, J. Tenbrink, W. Carter W Appl. Phys. Lett., **61** (1992) 858.

[5] A. Otto, L. J. Masur, J. Gannon, E. Podtburg, D. Daly, G. J. Yurek, A. P. Malozemoff, IEEE Trans. Appl. Supercond., **3** (1993) 915.

[6] J. Tenbrink, H. Krauth, Supercond. Sci. Technol., **7** (1994) 754.

[7] N. Yamada, K. Nara, M. Okaji, T. Hikata, T. Kanebo, N. Sadakata, Cryogenics, **38** (1998) 397.

[8] M. Sugano, K. Itoh, A. Nyilas, T. Kiyoshi, Physica C, **445-448** (2006) 751.

[9] S. Ochiai, H. Rokkaku, K. Morishita, J. K. Shin, S. Iwamoto, H. Okuda, M. Hojo, K. Osamura, M. Sato, A. Otto, E. Harley, A. Malozemoff, Supercond. Sci. Technol., **20** (2007) 202.

[10] H. Okuda, K. Morishita, S. Ochiai, D. Doko, M. Matsui, H. Fujimoto, M. Sato, Physica C, **411** (2004) 114.

[11] H. Okuda, H. Rokkaku, K. Morishita, J. K. Shin, S. Iwamoto, S. Ochiai, M. Sato, K. Osamura, A. Otto, E. J. Harley, A. Malozemoff, Scripta Mater., **55** (2006) 691.

[12] A. Nyilas, K. Osamura, M. Sugano, Supercond. Sci. Technol., **16** (2003) 1036.

[13] S. Ochiai, 1993 Mechanical Properties of Metallic Composites (Marcel Dekker Inc, New York) p473-510.

[14] A. Kelly, W. R. Tyson, J. Mech. Phys. Solids, **13** (1965) 329.

[15] S. Ochiai, T. Sawada, M. Hojo, J. Sci. Eng. Comp. Mater., **6** (1997) 63.

[16] S. Ochiai, T. Nagai, H. Okuda, S. S. Oh, M. Hojo, M. Tanaka, M. Sugano, K. Osamura, Supercond. Sci. Technol., **16** (2003) 988.

[17] ASM Handbook vol 2 Properties and Selection: Nonferrous Alloys and Special-Purpose Materials 1990 (Cleverland, OH: ASM International) p699.

[18] S. Ochiai, K. Hayashi, K. Osamura, J. Mater. Sci., **25** (1990) 3467.

[19] M. Sugano, Doctor Thesis Kyoto University (2003) p28.

Chapter 3

Thermally induced residual strain accumulation in Bi2223/Ag/Ag alloy composite superconductor

3.1 Introduction

Bi2223 superconducting composite tapes are subjected to mechanical and electromagnetic stresses during fabrication/ winding and operation [1–3]. Under the applied strain, the critical current is reduced with increasing applied strain beyond the irreversible strain due to the damage evolution [1–23]. In the case where tensile strain is applied to samples, the irreversible strain is given by the 'fracture strain–residual strain' of the Bi2223 filaments [4, 5, 15]. The residual strain of the Bi2223 filaments, arising during cooling of samples due to the difference in the coefficients of thermal expansion among the constituents (Bi2223, Ag and Ag alloy sheath), is compressive in the current transportation direction and therefore negative [4, 5, 7, 13, 15, 21, 23]. As the fracture strain of the Bi2223 filaments is not necessary high (around 0.1% [4, 5, 7, 12, 13, 15, 20–22]), the residual strain contributes largely to the strain tolerance of critical current of the composite tape.

In the residual strain accumulation process, it is deduced that the Ag and Ag alloy in the composite tape, more or less, creep at high temperatures, which may act to release the residual strain. In order to describe the change of residual strain of Bi2223 filaments with temperature, it is first needed to estimate the temperature at which the residual strain practically starts to be accumulated during cooling and then to estimate the influence of the successive thermal history on the residual strain. It is noted that the

change of residual strain of Bi2223 filaments with temperature is affected by factors such as the cooling rate and volume fraction of each constituent. These factors are different among the different fabrication route samples [3, 5, 12, 22, 24–26]. The aim of the present work is to develop a comprehensive estimation method of the residual strain change of all constituents of Bi2223 filaments, Ag and Ag alloy as a function of temperature, applicable to any fabrication route samples.

The first feature of the present method is to prepare the different stress state samples A (Ag is yielded in compression in the current transportation direction) and B (Ag is yielded in tension by additional heat treatment to sample A), and to estimate the product (E_iV_i) of Young's modulus (E_i) and volume fraction (V_i) of the constituents (i = Bi2223, Ag and Ag alloy) from the slope of the stress–strain curves. With this method, even when the Young's modulus and volume fraction of the constituents are unknown individually, the values of (E_iV_i) necessary for estimation of the residual strain of Bi2223 filaments can be obtained directly for any fabrication route samples.

The second feature is to combine these estimated parameters with the residual strain of Bi2223 at room temperature, measured with the x-ray diffraction method, for estimation of the residual strain change of all constituents with temperature. The estimated residual strain of the Bi2223 at 77 K will be examined by the experimentally measured strain tolerance of the critical current of the composite tape at 77 K and the aforementioned reported fracture strain of Bi2223 (0.1%).

3.2 Experimental procedure

3.2.1 Samples

The high critical current type composite tape (HTS high current density wire®), fabricated by American Superconductor Corporation (AMSC), was used as the experimental sample. The cross section of the sample is shown in figure 3.1. It contained 55 Bi2223 filaments. The width and thickness of the tape were 4.1 and 0.22 mm, respectively. The overall cross-sectional area was 0.89mm^2.

The as-supplied sample is noted as sample A in this work. This sample had been cooled down from the heat-treatment temperature (T_H) to 77 K for pre-checking of the critical current at AMSC and had then been heated to room temperature, as schematically shown in figure 2(a). In this sample, Ag had been yielded in compression

at room temperature, as will be shown later in sections 3.1 and 3.2.

In order to prepare the different stress state samples for tensile test, sample A was additionally heat-treated at 573 K for 600 s and was then cooled down to room temperature, as shown in figure 2(b). In this sample, Ag was yielded in tension at room temperature, as will be shown later in sections 3.1 and 3.2. Such an additionally heat-treated sample is noted as sample B.

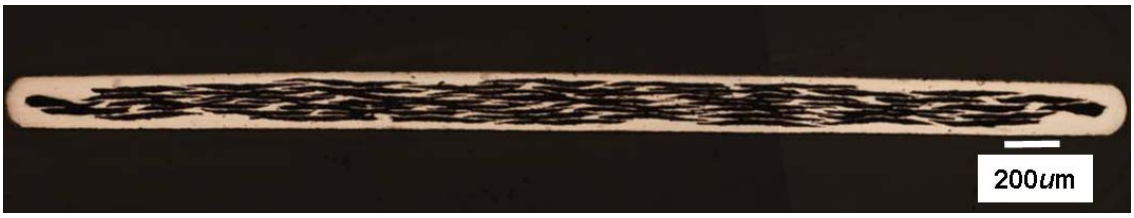

Figure 3.1. Cross section of the sample.

3.2.2 Tensile test

The tensile test was carried out using a universal testing machine (autograph AG-50kNG, Shimadzu, Japan) at a strain rate of $2\times10^{-4}s^{-1}$ at room temperature for a gauge length 25mm. Tensile strain was applied in the longitudinal direction (current transportation direction). The strain of the composite tape was measured with a very lightweight extensometer developed by Nyilas [18, 27].

3.2.3 Measurement of residual strain of Bi2223 filament in the composite tape by x-ray diffraction method

In situ strain measurement of Bi2223 filaments in the composite tape (sample A) at room temperature under the applied tensile strain ε_C of 0–0.09% was carried out at the beamline 46XU of the synchrotron radiation facility, SPring 8, Japan, under the proposal number 2005B0149. From the result, the residual strain of Bi2223 filaments was obtained by the procedure shown below. The experiment was carried out in a similar manner to our former work [28] with a slight modification. The key points of the procedure are briefly summarized as follows.

(1) A small tensile test machine was mounted on a Huber 512.1 Eulerian cradle on a multi-axis diffractometer.

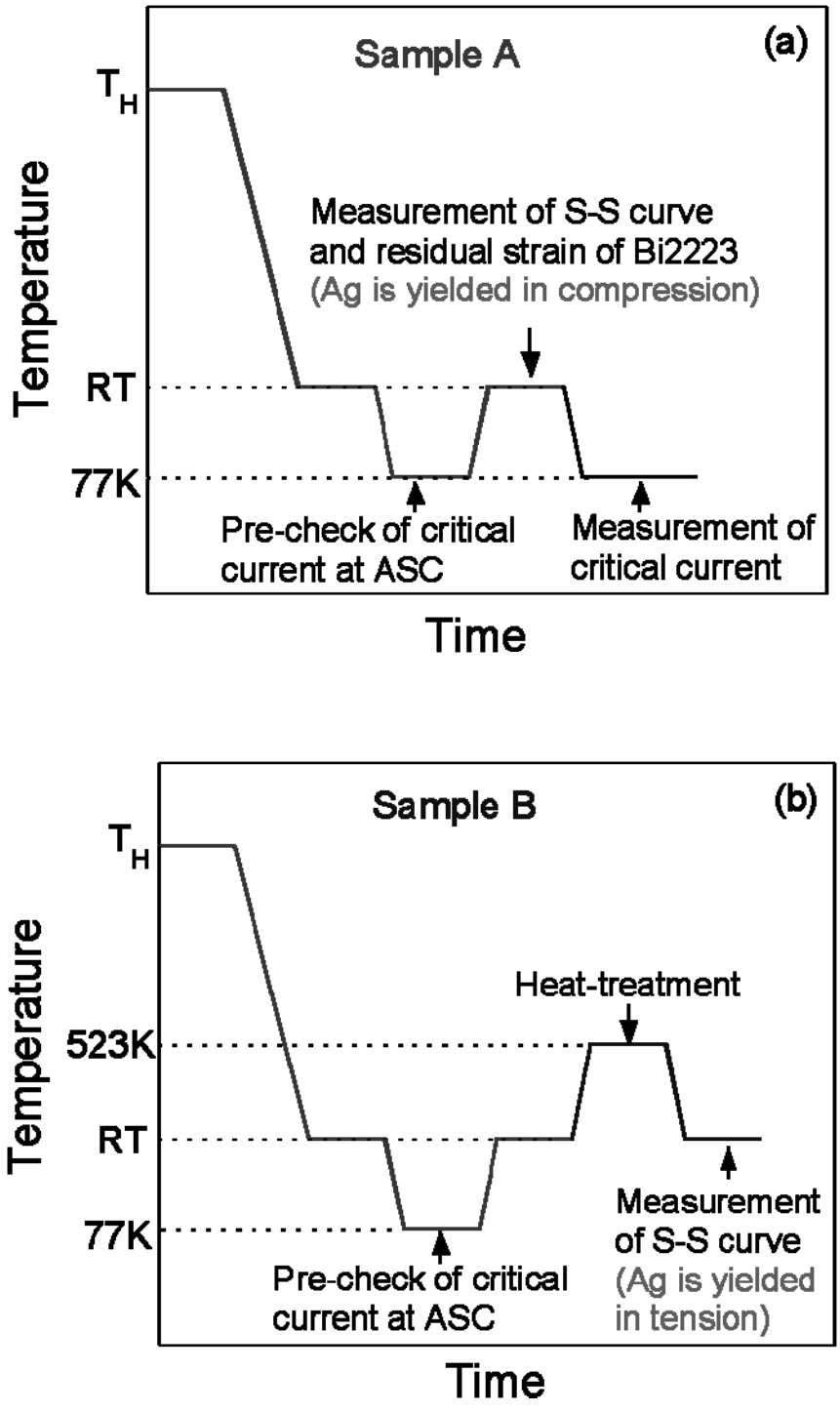

Figure 3.2. Thermal history of samples A and B.

(2) The position of the sample was monitored by two charge coupled device (CCD) telescopes.
(3) Sample A was used for the test, on which the tensile strain εc was applied in the range from 0 to 0.09% in steps of around 0.015% in order to measure the change of strain of the Bi2223 filaments in the composite. As a reference specimen, the strain-free bare Bi2223 filaments, which were extracted from the composite tape by etching away the Ag and Ag alloy with a NH4OH/H2O2 solution, was used. No strain was applied on this specimen. The Bragg peaks of the strained Bi2223 filaments in the composite and strain-free Bi2223 filaments alone were measured from the former and latter specimens, respectively.
(4) A strong x-ray from an undulator was monochromatized into a beam of 22keV and introduced to the specimen position.
(5) The beam size was taken to be $0.5\times1.0\text{mm}^2$ in the present work, which was made larger than the former measurement [28] of $0.1\times0.5\text{mm}^2$ to obtain an averaged strain from a wider area.
(6) The peak positions of the (200) and (220) planes were measured for the strained Bi2223 filaments in the composite as well as for the strain-free extracted Bi2223 ones. From the difference in the peak position between the strained and strain-free Bi2223, the strain of Bi2223 filaments in the composite was obtained for each plane and the results were averaged. Such a procedure was repeated for each applied strain ε_C. In this way, the change of the strain ε_{Bi} of Bi2223 in the composite with increasing applied strain on composite εc was measured.
(7) The residual strain of Bi2223 filaments $\varepsilon_{r,Bi,RT}$ corresponding to εc = 0%, was estimated by applying the least square method to the measured relation between the strain of Bi2223 filaments in the composite and applied strain on composite εc.

3.2.4 Critical current measurement as a function of applied strain

The change of critical current I_C of the composite tape with increasing applied tensile strain εc was measured by the ordinary four-probe method at 77 K with a criterion of $1\mu V\text{cm}^{-1}$ in a self-magnetic field. The distance between the voltage taps was 20mm. The strain of the composite samples at 77 K was measured with the Nyilas type extensometers [18, 27] as well as that at room temperature.

3.3 Results and discussion

3.3.1 Estimation of the mechanical parameters (Young's modulus × volume fraction) of the constituents and yield strain of Ag from the stress–strain curves of samples A and B

As shown later in section 3.3.2, many parameters are needed for estimation of the residual strain of each constituent (Bi2223, Ag and Ag alloy). Among them, the yield strain of Ag ($\varepsilon_{y,Ag}$), $E_{Bi}V_{Bi}$, $E_{Ag}V_{Ag}$ and $E_{Alloy}V_{Alloy}$ were estimated in the following manner from the stress–strain curves at room temperature of samples A and B with different residual stress states, where E and V are the Young's modulus and volume fraction, respectively, and the subscripts Bi, Ag and Alloy refer to the Bi2223, Ag and Ag alloy, respectively.

Figures 3.3 and 3.4 show the early stage portions of the stress–strain curves of samples A and B, respectively. The stress–strain curves in figures 3.3 and 3.4 are characterized by the following three regions.

Region I: Bi2223, Ag and Ag alloy deform elastically.

Region II: Bi2223 and Ag alloy deform elastically, while Ag deforms plastically.

Region III: Bi2223 deforms elastically, while Ag and Ag alloy deform plastically.

As the strain hardening coefficient ($d\sigma/d\varepsilon$, where σ is the stress and ε is the strain in plastic deformation stage) of metal is, in general, far lower than the Young's modulus E, the Young's modulus of the composite tape is expressed by

$$\text{Region I: } E_{c,I} = E_{Bi}V_{Bi} + E_{Ag}V_{Ag} + E_{Alloy}V_{Alloy} \quad (3.1)$$

$$\text{Region II: } E_{c,II} = E_{Bi}V_{Bi} + E_{Alloy}V_{Alloy} \quad (3.2)$$

$$\text{Region III: } E_{c,II} = E_{Bi}V_{Bi}. \quad (3.3)$$

As has been shown in figure 3.2(a), sample A had been cooled down from the heat-treatment temperature to 77K and had then been heated to room temperature. As the coefficient of thermal expansion of Bi2223 is lower than that of Ag and Ag alloy (table 3.1), Ag is yielded in tension at 77 K. Upon heating from 77 K to room temperature (293 K), compressive stress is exerted on Ag. The increment in temperature 216 K (293–77 K) is large enough to cause compressive yielding of Ag, as shown later in detail in section 3.3.2.2. Thus, at room temperature, Ag is yielded in compression.

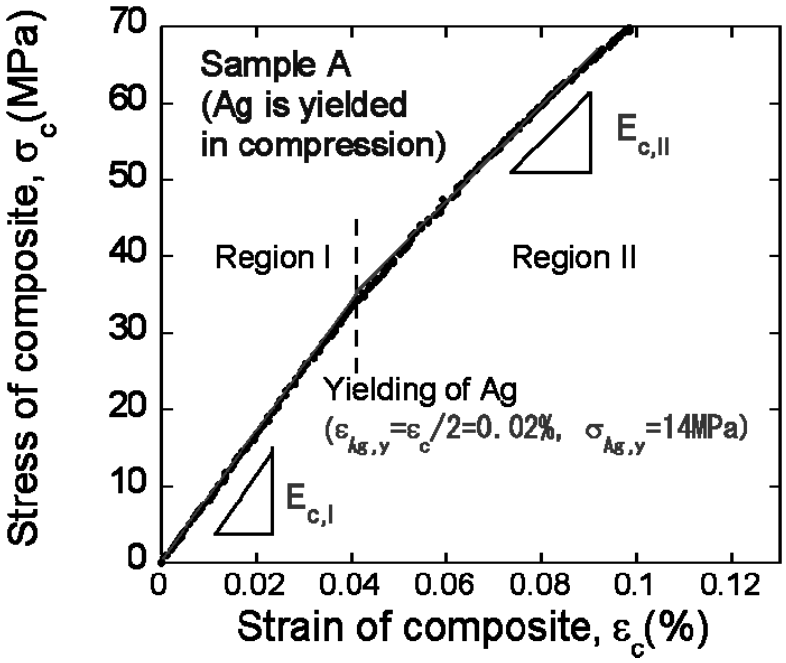

Figure 3.3. Tensile stress-strain curve of sample A in the early stage of deformation at room temperature.

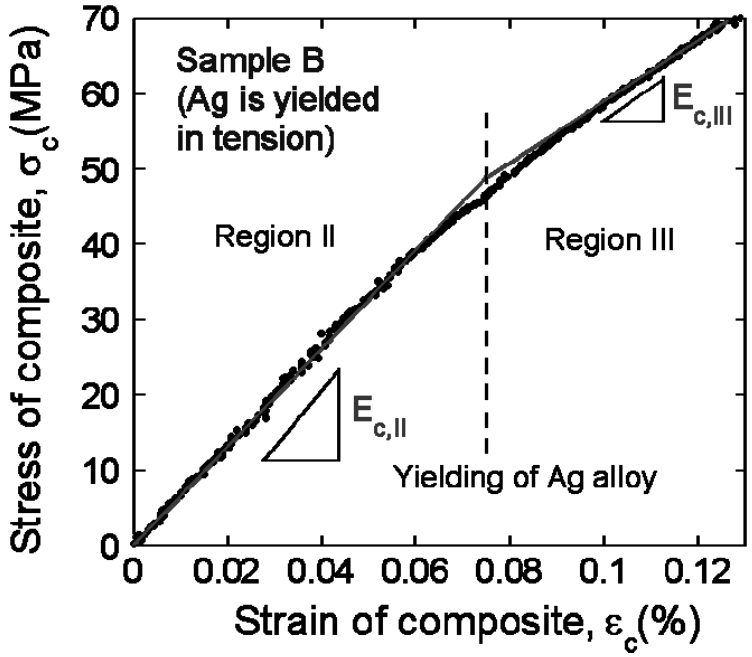

Figure 3.4. Tensile stress-strain curve of sample B in the early stage of deformation at room temperature.

Table. 3.1. Input values for stress analysis.

Overall cross-sectional area (mm^2)		0.89
Young's modulus x volume fraction of constituents, E_iV_i (i = Ag, Ag alloy and Bi2223) (GPa)	$E_{Ag}V_{Ag}$	22.9
	$E_{Alloy}V_{Alloy}$	22.1
	$E_{Bi}V_{Bi}$	40.7
Young's modulus of composite (GPa)	Region I ($E_{c,I}$)	85.7
	Region II ($E_{c,II}$)	62.8
	Region III ($E_{c,III}$)	40.7
Yield strain (%)	Ag ($\varepsilon_{Ag,y}$)	0.02
	Ag alloy	(Elastic)
	Bi2223	(Elastic)
Coefficient of thermal expansion of constituents (10^{-6} K^{-1})	Ag (α_{Ag})	17.1
	Ag alloy (α_{Alloy})	17.1
	Bi2223 (α_{Bi})	11.0
Coefficient of thermal expansion of composite tape (10^{-6} K^{-1})	Ag-elastic region ($\alpha_{c,I}$)	14.2
	Ag-plastic region ($\alpha_{c,II}$)	13.1

When such a composite tape is pulled in tension, Ag deforms elastically from the yielded state in compression to that in tension. Noting the yield stress and strain of Ag as $\sigma_{y,Ag}$ and $\varepsilon_{y,Ag}$, respectively, Ag deforms elastically in the applied strain range from zero to $2\sigma_{y,Ag}/E_{Ag}$ ($=2\varepsilon_{y,Ag}$). Thus, the strain at the transition from region I to II in the stress–strain curve in figure 3.3 corresponds to $2\varepsilon_{y,Ag}$. Beyond region I, region II, where Bi2223 and Ag alloy deform elastically and Ag is yielded, appears, as shown in figure 3.3. As $2\varepsilon_{y,Ag}$ is read to be 0.04%, $\varepsilon_{y,Ag}$ is estimated to be 0.02%. The yield stress of Ag in this sample is given by $\varepsilon_{y,Ag}E_{Ag}$=14 MPa (E_{Ag}=71GPa [29]). This result shows that Ag is very soft. The yield stress of Ag at room temperature has been reported to be 54MPa when annealed at around 700K [29]. However, such a value is too high for the present Bi2223 composite tapes which have been heat-treated at around 1100K. Actually, the yield stress of Ag annealed at 1073K has been reported to be very low (around 11MPa (11.2MPa [30], 10.9MPa [31])). The present result is near to such reported values. The $E_{c,I}$ and $E_{c,II}$ values correspond to the slopes in regions I and II in the stress–strain curve in figure 3.3, respectively.

On the other hand, sample B was prepared by heating sample A to 573K from room temperature and subsequently cooling it from 573K to room temperature (figure 2(b)). Thus, tensile stress was exerted on Ag during cooling. Since the temperature difference in cooling, −230K (=293–523K), is large enough to cause tensile yielding of Ag, as shown later in section 3.2.2, Ag is yielded. Thus, no region I appears. Region II appears

in the initial deformation region. With further increasing applied strain, Ag alloy comes to be yielded and region III appears. The $E_{c,II}$ and $E_{c,III}$ values in the stress–strain curve in figure 3.4 correspond to the slopes of regions II and III, respectively. The $E_{c,I}$, $E_{c,II}$ and $E_{c,III}$ values, measured from the slopes in regions I, II and III in figures 3.3 and 3.4, were 85.7, 62.8 and 40.7GPa, respectively, on an average of three test specimens. Substituting the measured $E_{c,I}$, $E_{c,II}$ and $E_{c,III}$ values into equations (3.1)–(3.3), we had 40.7, 22.9 and 22.1GPa for $E_{Bi}V_{Bi}$, $E_{Ag}V_{Ag}$ and $E_{Alloy}V_{Alloy}$, respectively. These parameters, together with the estimated yield strain value (0.02%) of Ag mentioned above, are tabulated in table 3.1. They will be used in section 3.3.2 below for estimation of strain accumulation of the constituents (Bi2223, Ag and Ag alloy) with temperature.

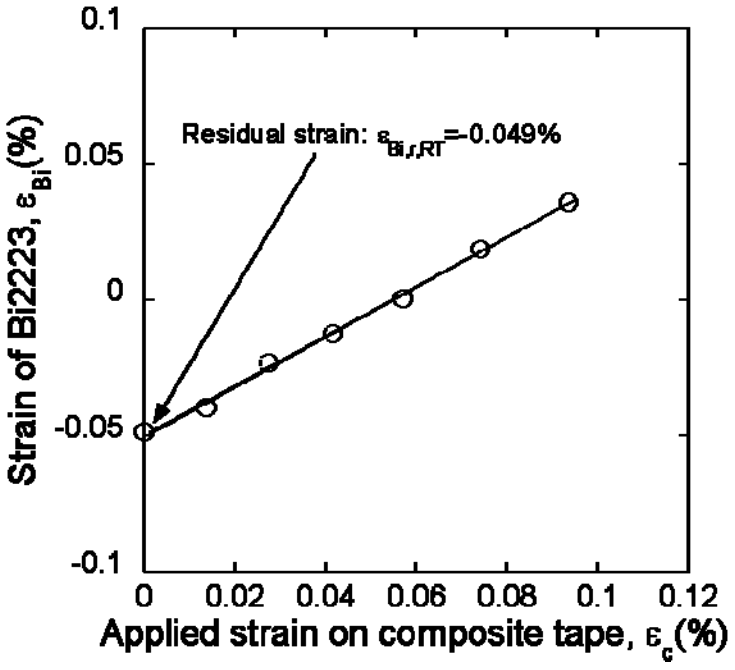

Figure 3.5. Change of strain ε_{Bi} of Bi2223 filaments in sample A with increasing applied strain ε_C on composite, measured by the X-ray diffraction method.

3.3.2 Strain accumulation in the constituents (Bi2223, Ag and Ag alloy) in composite (sample A) with temperature

Figure 3.5 shows the change of strain ε_{Bi} of Bi2223 filaments in sample A with increasing applied strain ε_C on composite, measured by the x-ray diffraction method.

From this result, the residual strain $\varepsilon_{r,Bi,RT}$ of Bi2223 at room temperature, corresponding to εc = 0%, was revealed to be −0.049%.

During cooling from the heat-treatment temperature (T_H), the residual strain is accumulated in each constituent due to the difference in thermal expansion coefficient among the constituents. In this process, it is deduced that the creep behavior of Ag and Ag alloy at high temperatures releases the residual strain, and therefore the residual strain starts to be accumulated below such high temperatures. We define the effective temperature at which the thermally induced strain starts to be accumulated as T_0. The value of T_0 will be determined later in 3.3.2.3 by combining the residual strain value of Bi2223 (−0.049%) at room temperature mentioned above with the calculation result using the following equations.

3.3.2.1 Equations used for calculation of thermally induced strain accumulation in Bi2223, Ag, and Ag alloy

In the present analysis of the thermally induced residual strain accumulation in the constituents (Bi2223, Ag and Ag alloy) below the temperature T_0, the Ag alloy and Bi2223 are treated as elastic bodies and the Ag is treated as the elastic–perfect plastic body. Within the range where Ag deforms elastically, the coefficient of thermal expansion of the composite $\alpha_{c,I}$ is given by [4, 5, 12, 15, 20, 22, 23, 26, 30–32],

$$\alpha_{c,I} = (\alpha_{Bi}E_{Bi}V_{Bi} + \alpha_{Ag}E_{Ag}V_{Ag} + \alpha_{Alloy}E_{Alloy}V_{Alloy}) / E_{c,I} \quad (3.4)$$

where α, E and V are the coefficient of thermal expansion, Young's modulus and volume fraction, respectively, and $E_{c,I}$ is the Young's modulus of the composite tape, given by equation (3.1). The measured values of $E_{Bi}V_{Bi}$, $E_{Ag}V_{Ag}$, $E_{Alloy}V_{Alloy}$ and $E_{c,I}$ in table 3.1 can be used directly for calculation of equation (3.4). In the range where Ag deforms elastically, the change in residual strain $\Delta\varepsilon_i$ (i= Bi2223, Ag and Ag alloy) of each constituent for the temperature difference ΔT is given by [15, 23, 25, 31, 32],

$$\Delta\varepsilon_{Ag} = (\alpha_{c,I} - \alpha_{Ag})\,\Delta T \quad (3.5)$$

$$\Delta\varepsilon_{Alloy} = (\alpha_{c,I} - \alpha_{Alloy})\,\Delta T \quad (3.6)$$

$$\Delta\varepsilon_{Bi} = (\alpha_{c,I} - \alpha_{Bi})\,\Delta T. \quad (3.7)$$

The coefficient of thermal expansion of Bi2223, Ag and Ag alloy in the relevant temperature range is approximately given by $\alpha_{Bi}=11.0\times10^{-6}K^{-1}$ and $\alpha_{Ag}=\alpha_{Alloy}=17.1\times10^{-6}K^{-1}$ [31], which are also tabulated in table 3.1. Substituting the values of $E_{Bi}V_{Bi}$, $E_{Ag}V_{Ag}$, $E_{Alloy}V_{Alloy}$, $E_{c,II}$, α_{Bi}, α_{Ag} and α_{Alloy} listed in table 3.1 into equation (3.4), we have $\alpha_{c,I}= 14.2\times10^{-6}K^{-1}$. Within the range where Ag deforms plastically, the coefficient of thermal expansion of the composite $\alpha_{c,II}$ is approximately given by [4, 5, 31, 32],

$$\alpha_{c,II} = (\alpha_{Bi}E_{Bi}V_{Bi} + \alpha_{Alloy}E_{Alloy}V_{Alloy}) / E_{c,II} \quad (3.8)$$

where $E_{c,II}$ is the Young's modulus of the composite tape in Region II where Ag deforms plastically, which has been measured from the stress–strain curve. Substituting the values of $E_{Bi}V_{Bi}$, $E_{Alloy}V_{Alloy}$, α_{Bi}, α_{Alloy} and $E_{c,II}$ listed in table 3.1 into equation (3.8), we have $\alpha_{c,II}=13.1\times10^{-6}K^{-1}$. In the range where Ag deforms plastically, the change in residual strain of the Ag alloy and Bi2223 for the temperature difference ΔT is given by

$$\Delta\varepsilon_{Alloy} = (\alpha_{c,II} - \alpha_{Alloy})\,\Delta T \quad (3.9)$$

$$\Delta\varepsilon_{Bi} = (\alpha_{c,II} - \alpha_{Bi})\,\Delta T. \quad (3.10)$$

The total strain of Ag under plastic deformation is the sum of the elastic strain $\varepsilon_{Ag,elastic}$ and the plastic one $\varepsilon_{Ag,plastic}$. Under the approximation of Ag as an elastic–perfect plastic body, only the elastic component $\varepsilon_{Ag,elastic}$ in the total strain is concerned with the stress carrying capacity of Ag. Thus the stress of Ag, σ_{Ag}, is given by $\varepsilon_{Ag,elastic}E_{Ag}$. The elastic component of residual strain of Ag, $\varepsilon_{Ag,elastic}$, under plastic deformation is given by

$\varepsilon_{Ag,elastic} = +\varepsilon_{y,Ag}$ when Ag deforms plastically is tension (3.11)

$\varepsilon_{Ag,elastic} = -\varepsilon_{y,Ag}$ when Ag deforms plastically is compression. (3.12)

In this way, the change of thermally induced residual strain of the constituents in the composite tape is calculated by using equations (3.4) to (3.12).

It is noted that the calculation method of the residual strain presented in this work for multi-filamentary composite is applicable also to mono-filamentary composite, since the primary factor to determine the residual stress is the volume fraction of the constituents, as indicated by equations (3.4) to (3.10).

3.3.2.2 Key temperatures for calculation of the change in strain of Bi2223, Ag alloy and Ag with temperature

As Ag and Ag alloy have higher coefficient of thermal expansion than Bi2223, tensile strain is induced in Ag and Ag alloy during cooling and compressive strain in Bi2223, while compressive strain is induced in Ag and Ag alloy and tensile strain in Bi2223 during heating. As Ag has low yield strain (0.02%, as has been shown in 3.3.1), it comes to be yielded in tension and in compression during cooling and heating, respectively, when the exerted strain on Ag reaches the yield strain. The change of strain of Ag from zero to tensile (and compressive) yielding state is caused by the temperature difference 69K ($= |\varepsilon_{y,Ag}/(\alpha_{c,I} - \alpha_{Ag})|$) and the change of strain from tensile to compressive (and vice versa) yielding by the temperature difference 138 K ($=2|\varepsilon_{y,Ag}/(\alpha_{c,I} - \alpha_{Ag})|$). Accordingly, the behavior of Ag varies during cooling and heating, which affects the change of residual strains of Bi2223 and Ag alloy. The key temperatures of the behavior of Ag are schematically shown in figure 3.6. It is noted that (i) sample A was cooled down to room temperature RT (=293K: marked as RT(1) in figure 3.6) and then to 77K (marked as 77K(1)) for the pre-check of the critical current and then heated up to room temperature RT(2), (ii) the stress–stain curve (figure 3.3) of this sample and the residual strain of Bi2223 in the composite tape (figure 3.5) were measured at RT(2), and (iii) the strain tolerance of the critical current of this sample (the result will be shown later in 3.3.3) was measured at 77 K (77K(2) in figure 3.6).

In such a thermal history, Ag behaves in the following manner. In the cooling process from the heat-treatment temperature T_H to RT(1), the strain accumulation actually starts at T_0 ($RT < T_0 < T_H$). (The T_0 value will be estimated to be 563 K later in 3.3.2.3.) During cooling from T_0 to RT(1), Ag deforms elastically until Ag comes to be yielded in tension at T_1 ($RT < T_1 < T_0$) before the temperature reaches RT since the temperature difference $|RT - T_0|$ is larger than 69 K. The values of T_0 and T_1 are unknown at this stage, but the difference between them, $T_1 - T_0$, is known to be −69K ($=\varepsilon_{y,Ag}/(\alpha_{c,I} - \alpha_{Ag})$). Thus Ag deforms elastically in the temperature range of T_0 to T_1 and then plastically in the temperature range of T_1 to RT(1). At RT(1), Ag is yielded in tension. Such a tensile-yielded state of Ag continues during cooling from the room temperature RT(1) to 77K(1). Namely, Ag deforms plastically in the temperature range from RT(1) to 77K(1). Thus at 77K(1), Ag is yielded in tension.

When the composite tape is heated from 77K(1) to room temperature RT(2), the compressive strain is accumulated in Ag, due to which Ag deforms first elastically and, at T_2 ($77K < T_2 < RT$), Ag comes to be yielded in compression before the temperature reaches RT, since the temperature difference $|RT - 77K|$ is larger than 138K.

(The value of T_2, which satisfies $(\alpha_{c,I}-\alpha_{Ag})(T_2-77)=-\varepsilon_{y,Ag}$, is calculated to be 77+138 = 215 K.) Accordingly, Ag deforms elastically in the temperature range from 77K(1) to T_2 and plastically in compression in the temperature range from T_2 to RT(2). Thus at RT(2), Ag is yielded in compression. Such a compressively yielded state of Ag at RT(2), realized by heating from 77K to RT(2), is in contrast to the tensile-yielded state of Ag at RT(1), realized by cooling from T_0 to RT(1).

When the composite tape is again cooled to 77K(2) from the room temperature RT(2), tensile strain accumulated in Ag during cooling, due to which Ag deforms elastically until it comes to be yielded in tension at T_3, which is given by RT−138 =155K. The tensile-yielded state of Ag continues during further cooling from T_3 to 77 K(2). Thus Ag is tensile-yielded at 77K(2). During heating from 77K(2) to room temperature RT(3), the compressive strain exerting on Ag causes yielding of Ag at T_4, which is the same as T_2 (215K) since the strain situation at 77K(2) is the same as that at 77K(1).

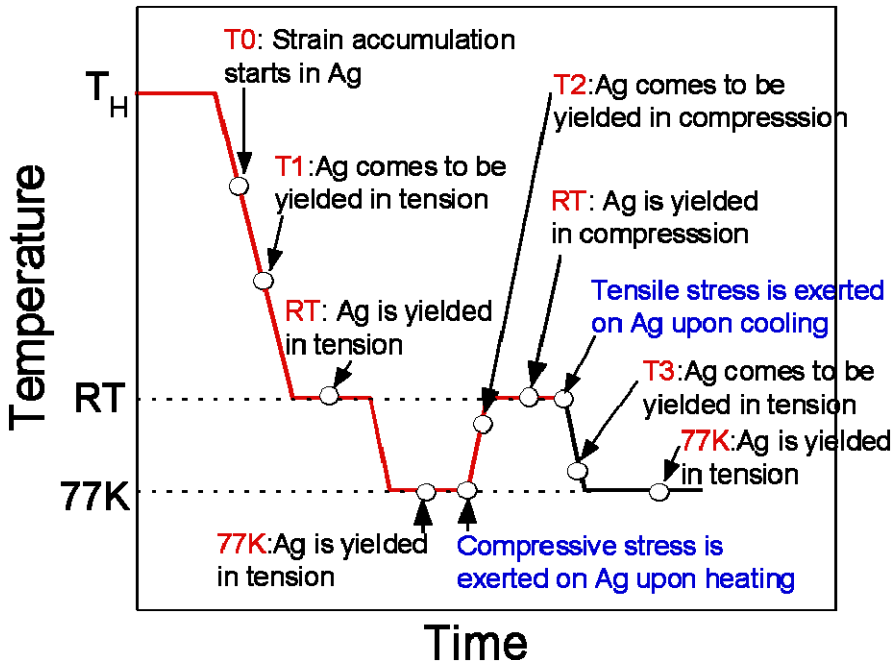

Figure 3.6. Behavior of Ag in the thermal history (sample A).

As stated above, Ag deforms elastically and plastically during cooling and heating. The strain change $\Delta\varepsilon_i$ of each constituent (i = Bi2223, Ag and Ag alloy) for the temperature difference between the successive key temperatures (figure 3.6) can be

calculated by equations (3.4) to (3.7) for the temperature range where Ag deforms elastically and by equations (3.8) to (3.12) for the temperature range where Ag deforms plastically.

The definite equations used for calculation are tabulated in table 3.2. $T_2(=T_4)$ and T_3 correspond to 215 and 155K, respectively, as shown above. At this stage, the temperatures T_0 and T_1 were unknown, but the difference T_1-T_0 was −69K, as shown above. Thus once either is known, the other is calculated. They were determined by combining the calculated strain change in Bi2223 between the key temperatures with the x-ray result (figure 3.5), as follows.

Table 3.2. Changes in residual elastic strain of Ag ($\Delta\varepsilon_{Ag}$), Ag alloy ($\Delta\varepsilon_{Alloy}$) and Bi2223 ($\Delta\varepsilon_{Bi}$) due to the temperature change indicated in the left column. –(*) and –(**) for $\Delta\varepsilon_{Ag}$ refer to plastic deformation in tension and in compression, respectively.

Temperature change	$\Delta\varepsilon_{Ag}$	$\Delta\varepsilon_{Alloy}$	$\Delta\varepsilon_{Bi}$
$T0 \rightarrow T1$	$(\alpha_{c,I}-\alpha_{Ag})\,(T1-T0)$	$(\alpha_{c,I}-\alpha_{Alloy})\,(T1-T0)$	$(\alpha_{c,I}-\alpha_{Bi})\,(T1-T0)$
$T1 \rightarrow$ RT(1)	$-(*)$	$(\alpha_{c,II}-\alpha_{Alloy})\,(RT-T1)$	$(\alpha_{c,II}-\alpha_{Bi})\,(RT-T1)$
RT(1) $\rightarrow$ 77 K(1)	$-(*)$	$(\alpha_{c,II}-\alpha_{Alloy})\,(77-RT)$	$(\alpha_{c,II}-\alpha_{Bi})\,(77-RT)$
77 K(1) $\rightarrow T2$	$(\alpha_{c,I}-\alpha_{Ag})\,(T2-77)$	$(\alpha_{c,I}-\alpha_{Alloy})\,(T2-77)$	$(\alpha_{c,I}-\alpha_{Bi})\,(T2-77)$
$T2 \rightarrow$ RT(2)	$-(**)$	$(\alpha_{c,II}-\alpha_{Alloy})\,(RT-T2)$	$(\alpha_{c,II}-\alpha_{Bi})\,(RT-T2)$
RT(2) $\rightarrow T3$	$(\alpha_{c,I}-\alpha_{Ag})\,(T3-RT)$	$(\alpha_{c,I}-\alpha_{Alloy})\,(T3-RT)$	$(\alpha_{c,I}-\alpha_{Bi})\,(T3-RT)$
$T3 \rightarrow$ 77 K(2)	$-(*)$	$(\alpha_{c,II}-\alpha_{Alloy})\,(77-T3)$	$(\alpha_{c,II}-\alpha_{Bi})\,(77-T3)$
77 K(2) $\rightarrow T4(=T2)$	$(\alpha_{c,I}-\alpha_{Ag})\,(T4-77)$	$(\alpha_{c,I}-\alpha_{Alloy})\,(T4-77)$	$(\alpha_{c,I}-\alpha_{Bi})\,(T4-77)$
$T4(=T2) \rightarrow$ RT(3)	$-(**)$	$(\alpha_{c,II}-\alpha_{Alloy})\,(RT-T4)$	$(\alpha_{c,II}-\alpha_{Bi})\,(RT-T4)$

3.3.2.3 Estimation of T_0 and T_1

The residual strain of Bi2223 in the composite was measured with x-rays at room temperature RT(2). Namely the composite tape had the thermal history $T_0 \rightarrow T_1 \rightarrow$ RT(1) $\rightarrow$ 77K(1) $\rightarrow T_2 \rightarrow$ RT(2). The strain of Bi2223 with such a thermal history, $\varepsilon_{r,Bi}(T_0 \rightarrow T_1 \rightarrow RT(1) \rightarrow 77K(1) \rightarrow T_2 \rightarrow RT(2))$, is given by

$$\varepsilon_{r,Bi}(T_0 \rightarrow T_1 \rightarrow RT(1) \rightarrow 77K(1) \rightarrow T_2 \rightarrow RT(2)) = \Delta\varepsilon_{Bi}(T_0 \rightarrow T_1) + \Delta\varepsilon_{Bi}(T_1 \rightarrow RT(1)) + \Delta\varepsilon_{Bi}(RT(1) \rightarrow 77\,K(1)) + \Delta\varepsilon_{Bi}(77\,K(1) \rightarrow T_2) + \Delta\varepsilon_{Bi}(T_2 \rightarrow RT(2)). \quad (3.13)$$

Substituting the values listed in table 3.1, and $T_0 - T_1 = 69$ K and $T_2 = 215$ K obtained in (B), into the equations in table 3.2, we had $\Delta\varepsilon_{Bi}(T_0 \rightarrow T_1) = -0.022\%$, $\Delta\varepsilon_{Bi}(RT \rightarrow 77\ K) = -0.045\%$, $\Delta\varepsilon_{Bi}(77K \rightarrow T_2) = +0.044\%$, and $\Delta\varepsilon_{Bi}(T_2 \rightarrow RT) = +0.016\%$. Then substituting these calculated values and $\varepsilon_{r,Bi}(T_0 \rightarrow T_1 \rightarrow RT(1) \rightarrow 77K(1) \rightarrow T_2 \rightarrow RT(2)) = -0.049\%$ ($\varepsilon_{r,Bi,RT}$ value measured by x-ray diffraction method) into equation (3.13), we had $\Delta\varepsilon_{Bi}(T_1 \rightarrow RT(1)) = -0.042\%$ and then $T_1 = 494$ K. As $T_1 - T_0$ was -69 K, T_0 was determined to be 563 K. It is noted that $T_0 = 563$ K was estimated by using the property values in the relevant temperature range (77–600 K). In practice, the Young's modulus and yield stress of Ag decreases with increasing temperature. Thus, it is speculated that the residual strain starts to be accumulated at higher temperatures than 563 K in practice. It is, however, emphasized that the estimated T_0 value is a useful and convenient parameter for analysis of the strain change of the constituents for the relevant temperature range, as shown below.

3.3.2.4 Change of elastic component of strain of Ag and elastic strain of Ag alloy and Bi2223 with temperature

Substituting the temperatures T_0, T_1, T_2, T_3 and T_4 ($=T_2$) estimated in 3.3.2.2 and 3.3.2.3 into the equations listed in table 3.2, the strain change $\Delta\varepsilon_i$ (i = Ag, Ag alloy and Bi2223) between the subsequent key temperatures was calculated. Then, by adding the $\Delta\varepsilon_i$ values one after another in the thermal history, the variations of the elastic component of the residual strain of Ag ($\varepsilon_{r,Ag}$) and the elastic residual strain of Ag alloy ($\varepsilon_{r,Alloy}$) and Bi2223 ($\varepsilon_{r,Bi}$) were calculated as a function of temperature. The calculation results for $\varepsilon_{r,Ag}$, $\varepsilon_{r,Alloy}$ and $\varepsilon_{r,Bi}$ are presented in figures 3.7, 3.8 and 3.9, respectively.

Concerning the behavior of Ag (figure 3.7), first Ag deforms elastically from zero strain at T_0 (563K) to the strain $+\varepsilon_{y,Ag}$ at T_1 (494K). Then it deforms plastically, keeping the constant elastic component of $+\varepsilon_{y,Ag}$, in the temperature range from T_1 to 77K through RT. Upon heating of the composite tape from 77K, Ag deforms elastically up to T_2 (215K). At T_2, Ag is yielded in compression and its strain reaches $-\varepsilon_{y,Ag}$. With further heating to RT, it deforms plastically in compression, keeping the elastic component of $-\varepsilon_{y,Ag}$. Thus at RT, it has been yielded in compression. When it is cooled again to 77K, it deforms elastically from RT to T_3 (155K) at which it is yielded in tension and the elastic strain reaches $+\varepsilon_{y,Ag}$, and then it deforms plastically in tension from T_3 to 77K, keeping the elastic component of the strain $+\varepsilon_{y,Ag}$. In this way, Ag exhibits elastic deformation, tensile plastic deformation and compressive plastic deformation, depending on the cooling and heating process.

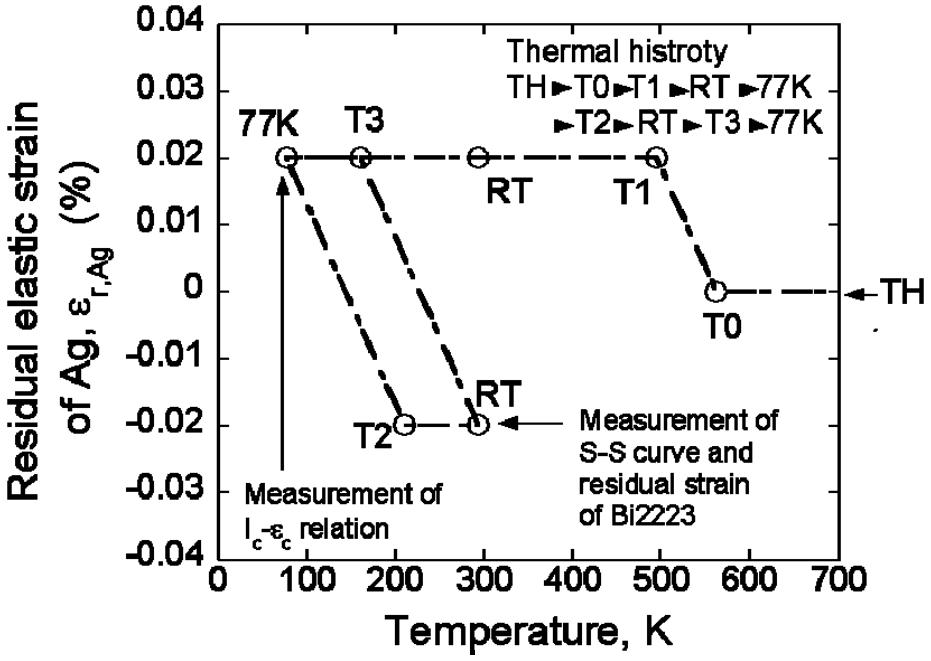

Figure 3.7. Change of elastic component of residual strain of Ag in sample A with temperature.

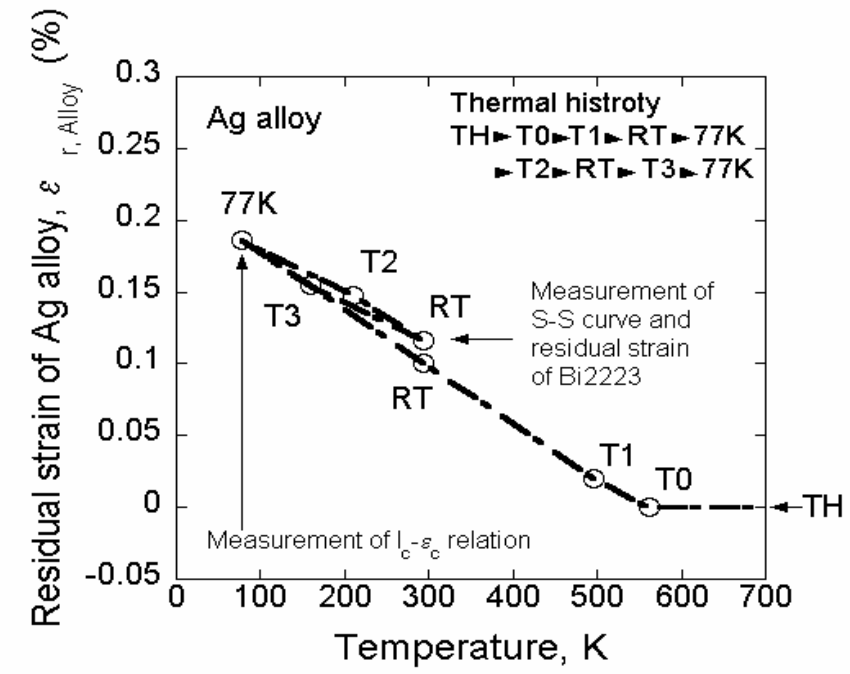

Figure 3.8. Change of elastic component of residual strain of Ag alloy in sample A with temperature.

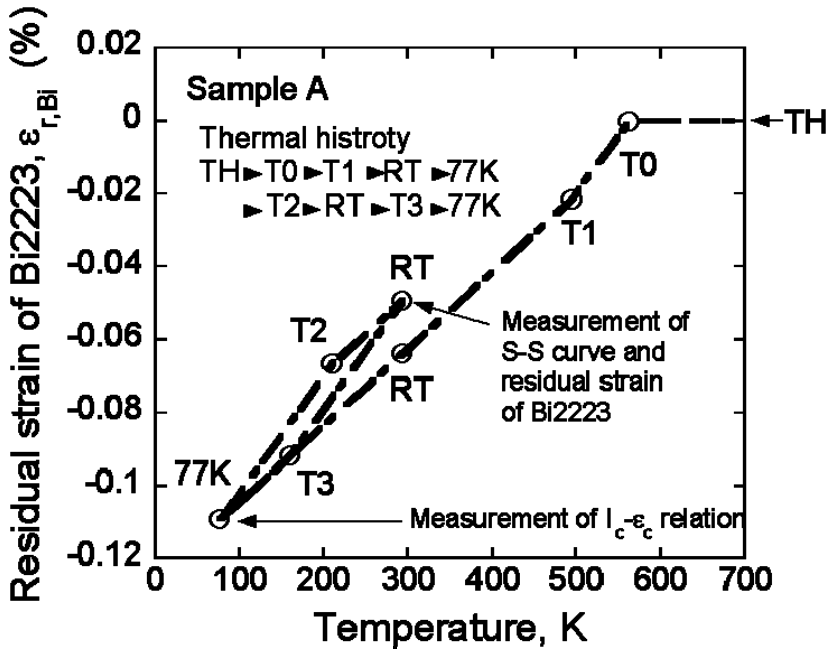

Figure 3.9. Change of elastic component of residual strain of Bi in sample A with temperature.

It is noted that, when the composite tape is thermally cycled between RT and 77K, the elastic component of the strain of Ag is cycled along RT($-\varepsilon_{y,Ag}$) → T_3($+\varepsilon_{y,Ag}$) → 77K($+\varepsilon_{y,Ag}$) → T_2($-\varepsilon_{y,Ag}$) → RT($-\varepsilon_{y,Ag}$), as shown in figure 3.7. The elastic component strain at RT is $-\varepsilon_{y,Ag}$. On the other hand, in the case where the tape is simply cooled from the heat-treatment temperature (T_H) to RT, the elastic component strain of Ag is $+\varepsilon_{y,Ag}$ at RT. In this way, the elastic component strain of Ag is different even at the same temperature, being dependent on the thermal history. Accordingly, the strain of Bi2223 (and Ag alloy) is also dependent on the thermal history, as shown later.

As indicated in 3.3.2.3, the temperature difference necessary to cause the change of strain of Ag from $+\varepsilon_{y,Ag}$ to $-\varepsilon_{y,Ag}$ upon heating is 138 K. This indicates that, if sample A, in which Ag is yielded in compression ($\varepsilon_{Ag,elastic} = -\varepsilon_{y,Ag}$), is heated by more than 138K from RT and then cooled to RT, Ag is yielded in tension ($\varepsilon_{Ag,elastic} = +\varepsilon_{y,Ag}$) at RT, corresponding to Ag's elastic strain state of $\varepsilon_{Ag,elastic} = +\varepsilon_{y,Ag}$ in sample B. Thus, sample A shows region I in the stress–strain curve (figure 3.3) but not sample B (figure 3.4) in which region II appears in the initial deformation stage.

As shown in figure 3.8, the tensile strain is accumulated in Ag alloy practically below the temperature T_0 due to the higher coefficient of thermal expansion than

Bi2223. Then the tensile strain increases with decreasing temperature. At room temperature, the strain of Ag alloy becomes 0.100% when cooled from the heat-treatment temperature. When the tape is further cooled to 77K and then heated to room temperature, the strain of Ag alloy becomes 0.116% at room temperature. Such a difference is attributed to the difference of the state in Ag (yielded in tension and compression for the former and latter cases, respectively). While Ag alloys deforms elastically, once the sample has been cooled down to 77K, the strain hysteresis of Ag alloy between 77K and RT is cyclic (77K → T_2 → RT → T_3 → 77K) (figure 3.8), due to the compressive and tensile yielding of Ag at T_2 and T_3, respectively (figure 3.7).

As shown in figure 3.9, the compressive strain of Bi2223 is practically accumulated below the temperature T_0 due to the lower coefficient of thermal expansion than Ag and Ag alloy. Then the compressive strain increases with decreasing temperature. At room temperature, the strain of Bi2223 becomes −0.064%. When the tape is further cooled to 77K, it becomes −0.110%. When the tape is heated from 77K, it becomes −0.049% at RT, which is the value estimated by the x-ray method. When it is cooled again from RT to 77K, it becomes again −0.110% at 77K. During the thermal cycling between RT and 77K, the strain cycle of Bi2223 is expressed as −0.049% at RT→ −0.093% at T_3 (155 K) → −0.110% at 77K→ −0.065% at T_2 (215 K) → −0.049% at RT.

In this way, the strain of Bi2223 varies in accordance with thermal history; in the case of simple cooling from T_0 to RT, the strain of Bi2223 at RT is −0.064%, but, when additional thermal history RT → 77K → RT is given to the composite tape, it becomes −0.049%. It is also noted that the strain of Bi2223 at 77K is −0.110% for both thermal histories of T_0 → 77K and T_0 → 77K → RT → 77K, since the temperature difference between RT and 77K is larger than 138K (necessary temperature difference to change the elastic strain of Ag by $2\varepsilon_{y,Ag}$), leading to $\varepsilon_{Ag,elastic} = +\varepsilon_{y,Ag}$ at 77K regardless of the thermal history. Thus the strain of Bi2223 is always −0.110%.

3.3.3 Critical current-applied strain relation at 77K and estimation of intrinsic fracture strain of Bi2223 filaments in the present composite tape

As stated in 3.3.2, the residual strain of Bi2223 filaments at 77K is −0.11%. The fracture strain of Bi2223 filaments has been reported to be nearly 0.1% [4, 5, 7, 12, 13, 15, 20–22]. Thus the strain tolerance of critical current at 77K of the present sample A is expected to be nearly 0.21%. In order to check whether such an expected strain

tolerance value is actually found in the present sample or not, the change of the critical current I_C was measured at 77K as a function of applied strain εc, from which the strain tolerance value was estimated. Figure 3.10 shows the result, in which the critical current I_C is normalized with respect to that of the sample under no applied strain, I_{C0}. The serious reduction in I_C/I_{C0} occurred at εc = 0.21%, agreeing well with the expected value. This result implies that the present method is useful for description of the residual strain accumulation as a function of temperature below T_0.

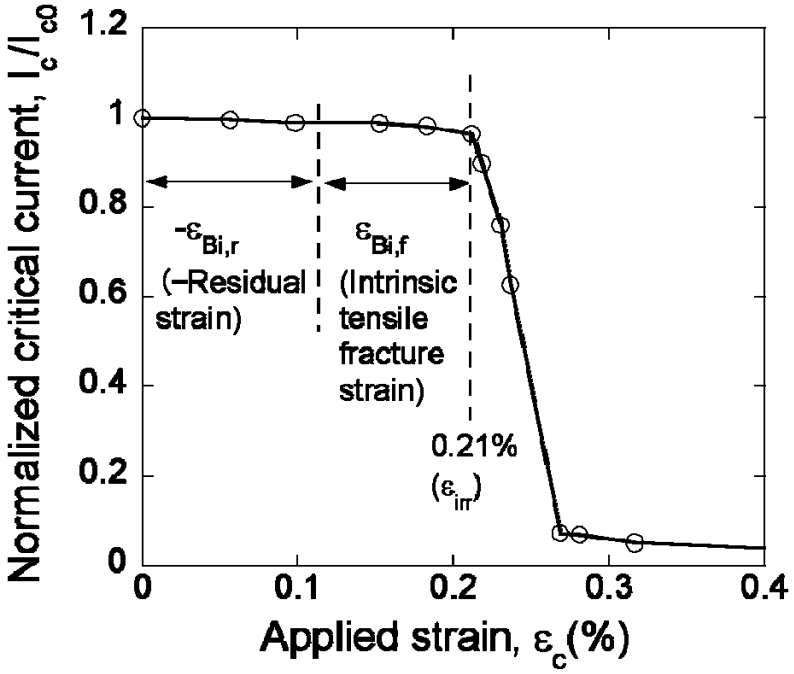

Figure 3.10. Change of normalized critical current I_C/I_{C0} of sample A at 77K with increasing applied tensile strain εc.

3.4 Conclusions

(1) A method to estimate the thermally induced residual strain accumulation under varying temperatures in Bi2223/Ag/Ag alloy was presented, in which the mechanical property values measured from the stress–strain curves of the samples with different residual strain states, the residual strain value of Bi2223 filaments in the composite tape at room temperature measured by x-ray diffraction and the reported coefficients of

thermal expansion of the constituents in the relevant temperature range (77–600K) were incorporated.

(2) The presented method was applied to the high critical current type composite tape fabricated by American Superconductor Corporation. The following results were obtained for this composite. (i) The temperature, at which the residual strain starts to be accumulated effectively, was found to be 563K in terms of the property values of the constituents in the relevant temperature range. (ii) The accumulation of the thermally induced strain of all constituents (Bi2223, Ag and Ag alloy) was estimated as a function of temperature. (iii) The estimated residual strain value at 77K (−0.11%) and the reported fracture strain of Bi2223 filaments (0.1%) accounted well for the measured strain tolerance of the critical current at 77K (0.21%).

References

[1] N. Savvides, J. Herrmann, D. Reilly, K- H. Muller, F. Darmann, G. McCaughey, R. Zhao, M Apperly, Physica C, **306** (1998) 129.

[2] H. J. N van Eck, K. Vargast, B. ten Haken, H. H. J ten Kate, Supercond. Sci. Technol., **15** (2002) 1213.

[3] H. Kitaguchi, K. Itoh, H. Kumakura, T. Takeuchi, K. Togano, W. Wada, IEEE Trans. Appl. Supercond., **11** (2001) 3058.

[4] S. Ochiai, K. Hayashi, K. Osamura, Cryogenics, **33** (1993) 976.

[5] S. Ochiai, K. Hayashi, K. Osamura, Cryogenics, **32** (1992) 799.

[6] L. Gherardi, P. Caracino, G. Coletta, Cryogenics, **34** (1994) 781.

[7] W. R. Blumenthal, R. A. Moore, J. Y. Coulter, J. F. Bingert, K. V. Salazar, J. Electron. Mater., **24** (1995) 1805.

[8] R. Welshe, A. M. Fuchs, K. Jakob, G. Pasztor, Cryogenics, **36** (1996) 419.

[9] B. ten Haken, A. Godeke, H-J. Schluver, H. ten Kate, Adv. Cryog. Eng., **42** (1997) 651.

[10] B. ten Haken, A. Beuink, H. ten Kate, IEEE Trans. Appl. Supercond., **7** (1999) 2043.

[11] R. T. Aloysius, A. Sobha, P. Guruswamy, U. Samaprasad, Supercond. Sci. Technol., **14** (2001) 85.

[12] R. Passerini, M. Dhallé, E. Giannini, G. Witz, B. Seeber, R. Flükiger, Physica C, **371** (2002) 173.

[13] K. Osamura, M. Sugano, K. Matsumoto, Supercond. Sci. Technol., **16** (2003) 971.

[14] S. J. Sun, W. Liu, X. P. Chen, M. Y. Li, Z. Han, Supercond. Sci. Technol., **16** (2003) 984.

[15] S. Ochiai, T. Nagai, H. Okuda, S. S. Oh, M. Hojo, M. Tanaka, M. Sugano, K. Osamura, Supercond. Sci. Technol., **16** (2003) 988.

[16] K. Katagiri, H. S. Shin, K. Kasaba, T. Tsukinokizawa, K. Hiroi, T. Kuroda, K. Itoh, H. Wada, Supercond. Sci. Technol., **16** (2003) 995.

[17] H. S. Shin, K. Katagiri, Supercond. Sci. Technol., **16** (2003) 1012.

[18] A. Nyilas, K. Osamura, M. Sugano, Supercond. Sci. Technol., **16** (2003) 1036.

[19] H. J. N. van Eck, D. C. van der Laan, M. Dhallé, B. ten Haken, H. H. J. ten Kate, Supercond. Sci. Technol., **16** (2003) 1026.

[20] M. Hojo, M. Nakamura, T. Matsuoka, M. Tanaka, S. Ochiai, M. Sugano, K. Osamura, Supercond. Sci. Technol., **16** (2003) 1043.

[21] S. Ochiai et al., Supercond. Sci. Technol., **18** (2005) S232.

[22] M. Hojo, M. Nakamura, M. Tanaka, T. Adachi, M. Sugano, S. Ochiai, K. Osamura, Supercond. Sci. Technol., **18** (2005) S356.

[23] A.Otto, E. J. Harley, R. Marson, Supercond. Sci. Technol., **18** (2005) S308.

[24] O. O. Oduleys, S. J. Pen, N. McN. Alford, Supercond. Sci. Technol., **11** (1998) 858.

[25] R. Passerini, M. Dhalle, B. Seeber, R. Flükiger, Supercond. Sci. Technol., **15** (2002) 1507.

[26] H. M. Ledbetter, S. A. Kim, R. B. Goldfarb, Phys. Rev. B, **39** (1989) 9689.

[27] A. Nyilas, Supercond. Sci. Technol., **18** (2005) S409.

[28] H. Okuda, K. Morishita, S. Ochiai, D. Doko, M. Matsui, H. Fujimoto, M. Sato, Physica C, **411** (2004) 114.

[29] ASM Handbook vol 2 Properties and Selection: Nonferrous Alloys and Special-Purpose Materials 1990 (Cleveland, OH: ASM International) p699.

[30] S. Ochiai, K. Hayashi, K. Osamura, J. Mater. Sci., **25** (1990) 3467.

[31] M. Sugano, (2003) Doctor Thesis Kyoto University, p28.

[32] D. K. Hale, J. Mater. Sci., **11** (1976) 2105.

Chapter 4

Thermally and mechanically induced residual strain and strain tolerance of critical current in stainless steel-laminated Bi2223/Ag/Ag alloy composite superconductor

List of strain variables

$\Delta\varepsilon_{1,IT}$, $\Delta\varepsilon_{1,SS}$: Increment of strain of insert tape (IT) and stainless steel (SS) due to pre-load for lamination.

$\Delta\varepsilon_{2,IT}$, $\Delta\varepsilon_{2,SS}$: Change of elastic strain of insert tape (IT) and stainless steel (SS) in the strain range from elastic state to compressive yielding of Ag in the stress relaxation process after lamination.

$\Delta\varepsilon_{3,IT}$, $\Delta\varepsilon_{3,SS}$: Change of strain of insert tape (IT) and stainless steel (SS) in the stress relaxation process from the onset of the compressive yielding of Ag to the final stress state.

$\Delta\varepsilon_{T,77K,Ic95\%}$: Increase in tensile strain tolerance by lamination at critical current reduction by 5% from the original value.

$\Delta\varepsilon_{w95\%Ic}$: Strain tolerance window defined as the axial strain range from compressive through tensile in which the critical current remains above 95% of its original level.

$\varepsilon_{Ag,IT,elastic}$, $\varepsilon_{Ag,LT,elastic}$: Elastic component of residual strain of yielded Ag in insert tape (IT) and laminated one (LT).

ε_{Bi}: Strain of Bi2223 filaments in the laminated composite tape at room temperature under applied tensile strain on the composite tape, measured by X ray diffraction.

$\varepsilon_{Bi,f,C,77K,IT}$, $\varepsilon_{Bi,f,C,77K,LT}$: Compressive fracture strain of Bi2223 filaments in insert tape (IT) and laminated one (LT) at critical current reduction by 5% from the original value.

$\varepsilon_{Bi,f,T,77K,IT}$, $\varepsilon_{Bi,f,T,77K,LT}$:Tensile fracture strain of Bi2223 filaments in insert tape (IT) and laminated one (LT) at critical current reduction by 5% from the original value.

$\varepsilon_{Bi,M}$: Mechanically induced residual strain in Bi2223 filaments by lamination.

$\varepsilon_{Bi,T}$(RT): Thermally induced residual strain in Bi2223 at room temperature

$\varepsilon_{Bi,r}$(RT):Total residual strain in Bi2223 filaments in laminated tape at room temperature

$\varepsilon_{Bi,r,77K,IT}$, $\varepsilon_{Bi,r,77K,LT}$: Residual strain of Bi2223 filaments in insert tape (IT) and laminated one (LT) at 77K.

$\varepsilon_{c,T}$: Applied tensile strain on composite tape

$\varepsilon_{IT,M}$, $\varepsilon_{SS,M}$□: Mechanically induced residual strain in insert tape (IT) and stainless steel (SS) by lamination, followed by stress relaxation.

$\varepsilon_{T,77K,Ic95\%,IT}$, $\varepsilon_{T,77K,Ic95\%,LT}$: Applied tensile strains of insert tape (IT) and laminated one (LT) at critical current reduction by 5% from the original value.

4. 1 Introduction

When a Bi2223/Ag/Ag alloy composite tape is cooled from the heat-treatment temperature to the cryogenic one, the compressive residual strain is accumulated in Bi2223 filaments in the current transporting direction due to the difference in coefficient of thermal expansion among the constituents (Bi2223, Ag and Ag alloy

sheath) [1-15]. It has been known that such a compressive residual strain of Bi2223 filaments contributes largely to the tensile strain-tolerance of critical current of Bi2223/Ag/Ag alloy composite tape [1-28].

The compressive residual strain of Bi2223 filaments is raised by reinforcing the Bi2223/Ag/Ag alloy composite tape with materials having high modulus and low coefficient of thermal expansion [1-6]. It has been demonstrated that, when reinforced with stainless steel or molybdenum, the tensile strain tolerance of critical current, and the size of the strain tolerance window, defined as the axial strain range from compression through tension in which the critical current remains above 95% of its original level, and the strength of the composite tape are improved [1-6].

In the laminated tape, the residual strain of each constituent (Bi2223, Ag, Ag alloy and stainless steel) is composed of (a) the mechanically induced strain by lamination and (b) the thermally induced one by temperature change, due to the following mechanism.

(a)Mechanically induced strain by lamination: In the reinforcing process, the reinforcing material (strip) is solder-laminated on the insert Bi2223/Ag/Ag alloy composite tape at elevated temperatures and at selected pre-tension levels in the strips and the insert composite tape [1-4]. When the externally imposed pre-tension is removed after lamination, the mechanically coupled composite relaxes axially to equilibrium where the constituents are under residual axial stress but the net force is zero [1]. As the tensile pre-load applied on the strips is higher than that on the insert composite tape, compressive strain is given to Bi2223, Ag and Ag alloy in the insert tape after the load relaxation.

(b)Thermally induced strain by temperature change: The composite tape is exposed in the following temperature change. First the insert tape is cooled down from the heat treatment temperature to room temperature and then it is heated to the lamination temperature. After the lamination, the laminated composite is cooled down to room- and then cryogenic temperatures for test. After the test, it is heated to room temperature. Under such a temperature change, strain is induced in each constituent due to the difference in coefficient of thermal expansion among the constituents.

The total strain of the elastically deforming constituents (Bi2223, Ag alloy and stainless steel) is the sum of mechanically and thermally induced strains. Ag behaves elastically and plastically depending on the stress situation, since the yield strain is low

(0.02% [27]). Thus the total strain of Ag is not the sum. Such an elastic-plastic behavior shall be incorporated for estimation.

The aim of the present work is to describe the accumulation process of the mechanically and thermally induced strains of each constituent (Bi2223, Ag, Ag alloy and stainless steel) in the stainless steel-laminated composite tape by elastic-plastic mechanics and to discuss the effects of stainless steel lamination on the residual strain accumulation process and critical current at 77K. The present work has the following contents.

(1) The mechanically and thermally induced residual strain of Bi2223 at 77K in the laminated tape has been analyzed by Otto et al [1] and Voccio et al [6]. In their analysis, the elastic-plastic behavior of Ag has, however, not been incorporated. In the present work, their approach was extended as to express the thermo-mechanical behavior of the constituents by incorporating the elastic-plastic behavior of Ag, as will be shown in 4.3.1 and 4.3.2.

(2) The laminated composite tape fabricated by American Superconductor Corporation (AMSC), in which the high critical current type Bi2223/Ag/Ag alloy composite tape was used as the insert tape, was studied in the present work. The stress-strain behavior and residual strain accumulation process of the insert tape have been studied in the preceding work [27]. The obtained results for the insert tape were used in the analysis of the present work, as will be shown 4.3.2 and 4.3.4. Also the residual strain of Bi2223 in the laminated composite tape at room temperature was measured in the present work at SPring 8, Japan. The measured value was used to estimate the effectively acting pre-load on stainless steel in the lamination process, as will be shown in 4.3.3.

(3) From the comparison of the result on the residual strain change in the mechanical and thermal process for the laminated composite tape obtained in the present work with that for the insert tape obtained in the preceding work [27], the lamination effect on the residual strain accumulation behavior was extracted, as will be shown in 4.3.4.

(4) From the comparison of the critical current-applied tensile strain relation of the laminated tape at 77K with that of insert tape, the effect of lamination on the tensile strain tolerance and strain tolerance window of the critical current was discussed, as will be shown in 4.3.5.

4.2 Procedure for experiment and analysis

4.2.1 Samples

The stainless steel-laminated composite tape, consisting of insert tape, stainless steel and solder was supplied by AMSC. In this composite tape, a high I_C tape is used as the insert tape, whose residual strain accumulation process has been shown in our preceding work [27]. The polished cross-section is presented in figure 4.1. The measured cross-sectional areas of the insert tape, stainless steel and solder are listed in Table 4.1. The lamination temperature, at which the insert tape was laminated with stainless steel (SS), has been reported to be 453K [1]. The supplied composite tape had been cooled down from the heat-treatment temperature (TH) to room temperature, heated to lamination temperature (453K), cooled down to 77K through room temperature for pre-checking of the critical current and then heated to room temperature, as schematically shown in figure 4.2. Due to such a thermal history, the Ag had been yielded in compression at room temperature, as will be shown in 4.3.4.

4.2.2 Measurement of residual strain of Bi2223 filaments at room temperature

The residual strain in the length direction of Bi2223 filaments in the composite tape at room temperature was measured at the beam line 46XU of a synchrotron-radiation facility, SPring 8, Japan. The procedure is the same as that in our preceding work [27]. As a stress free- reference samples, the bare Bi2223 filaments, extracted from the composite tape by etching away the Ag and Ag alloy with a NH_4OH/H_2O_2 solution, was used. Tensile strain ε_c was given to the samples up to 0.1% in a step of around 0.03%. The peak positions of the (220) planes were measured for the strained Bi2223 filaments in the composite as well as for the strain-free extracted Bi2223 ones. From the difference in the peak position between the strained and strain-free Bi2223 filaments, the strain of Bi2223 filaments in the composite was obtained for two samples at each applied strain. Then, the residual strain of Bi2223 filaments $\varepsilon_{Bi,r}(RT)$ corresponding to $\varepsilon_{c,T}=0\%$, was estimated by applying the least

square method to the measured relation between the strain of Bi2223 filaments in the composite and applied strain on composite $\varepsilon_{c,T}$.

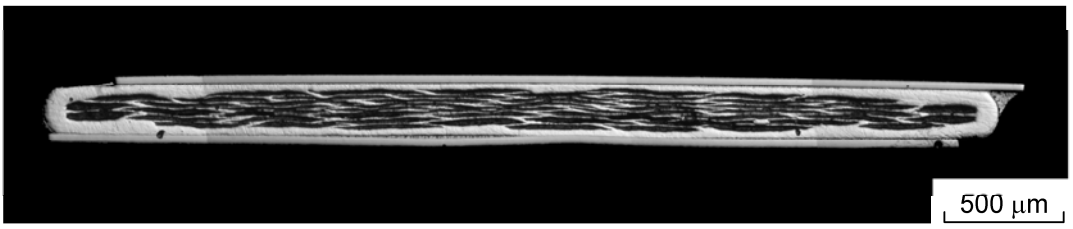

Figure 4.1. Polished cross-section of the supplied stainless steel-laminated composite tape.

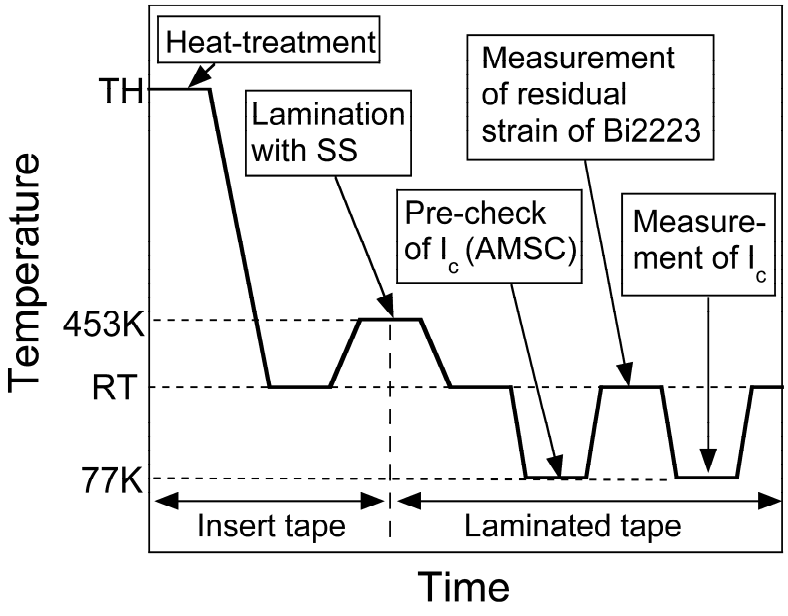

Figure 4.2. Thermal and mechanical history of the composite tape used in the present work.

Table 4.1. Measured and cited mechanical property values, which were input for analysis.

(a)	Cross-sectional area A_i (mm^2) (Measured in this work)	Laminated tape: A_{LT} Insert tape: A_{IT} Stainless steel: A_{SS} Solder: A_{Solder}	1.25 0.89 0.31 0.05
(b)	Volume fraction $V_{i,LT}$ of the constituents in laminated tape (Calculated from (a))	Insert tape: $V_{IT,LT}$ Stainless steel: $V_{SS,LT}$ Solder: $V_{Solder,LT}$	0.71 0.25 0.04
(c)	Young's modulus x volume fraction, $E_iV_{i,IT,}$ of the constituents in insert tape (GPa) (Ref.[27])	Ag: $E_{Ag}V_{Ag,IT}$ Ag alloy: $E_{Alloy}V_{Alloy,IT}$ Bi2223: $E_{Bi}V_{Bi,IT}$	22.9 22.1 40.7
(d)	Overall Young's modulus of insert tape in Regions I and II (GPa) (Ref.[27])	Region I: $E_{I,IT}$ Region II: $E_{II,IT}$	85.7 62.8
(e)	Young's modulus of stainless steel (GPa) (Ref.[1])	E_{SS}	193
(f)	Young's modulus x volume fraction, $E_iV_{i,LT}$, of the constituents in laminated tape (GPa) (Calculated from (b), (c) and (e) and E_{Solder}=24 GPa (Ref.[1]))	Ag: $E_{Ag}V_{Ag,LT}$ Ag alloy: $E_{Alloy}V_{Alloy,LT}$ Bi2223: $E_{Bi}V_{Bi,LT}$ Stainless steel: $E_{SS}V_{SS,LT}$ Solder: $E_{Solder}V_{Solder,LT}$	16.3 15.7 28.9 48.3 0.96
(g)	Overall Young's modulus of laminated tape in Regions I and II (GPa) (Calculated from (f))	Region I: $E_{I,LT}$ Region II: $E_{II,LT}$	110 93.9
(h)	Yield strain of Ag (%) (Ref.[27])	$\varepsilon_{Ag,y}$	0.02
(i)	Coefficient of thermal expansion of constituents α_i (i=Ag, Ag alloy, Bi2223, stainless steel and solder) (10^{-6}/K) (Refs.[1], [27])	Ag: α_{Ag} Ag alloy: α_{Alloy} Bi2223: α_{Bi} Stainless steel: α_{SS} Solder: α_{Solder}	17.1 17.1 11.0 16.0 23
(j)	Overall coefficient of thermal expansion of insert tape (10^{-6}/K) (Calculated from (c), (d) and (i))	Region I: $\alpha_{I,IT}$ Region II: $\alpha_{II,IT}$	14.2 13.1
(k)	Overall coefficient of thermal expansion of laminated tape (10^{-6}/K) (Calculated from (f), (g) and (i))	Region I: $\alpha_{I,LT}$ Region II: $\alpha_{II,LT}$	15.1 14.7

4.2.3 Key temperatures for analysis

The key temperatures in the thermo-mechanical history of the insert and laminated composite tapes are schematically shown in figure 4.3. The insert tape is heat-treated at TH and is cooled down to room temperature. During cooling, the strain accumulation starts practically at T0 since the residual strains are released by the creep behavior of Ag/Ag alloy at high temperature region. The T0-value of the insert tape has been estimated in our preceding work [27] to be 563K in terms of the property values of the constituents in the relevant temperature range.

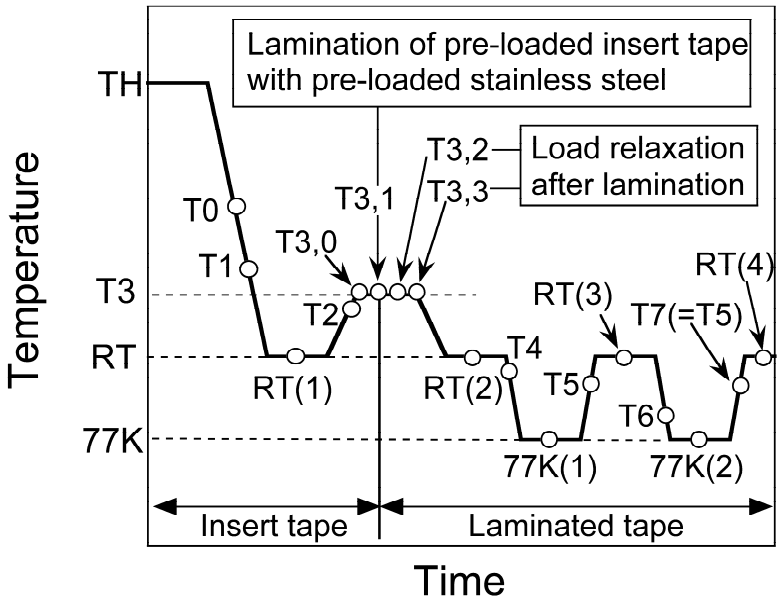

Figure 4.3. Key temperatures in the thermo-mechanical history of the insert and laminated composite tapes.

As Ag and Ag alloy have higher coefficient of thermal expansion than Bi2223, tensile strain is induced during cooling in Ag and Ag alloy and compressive one in Bi2223. As Ag in the present insert tape has a low yield strain (0.02% [27]), it is

yielded in tension and in compression during cooling and heating, respectively, when the exerted strain reaches the yield strain. In the insert tape, the change of zero strain to tensile (and compressive) yielding state is caused by the temperature difference 69K and the change of tensile to compressive (and vice versa) yielding by the temperature difference 138K, as will be shown in 4.3.2. Thus, during cooling from T0 (563K) to room temperature 293K (RT(1) in figure 4.3), Ag is yielded in tension at T1 (=563-69=494K) before the temperature reaches the room temperature. Thus at room temperature, Ag has been yielded in tension. Then, from the room temperature RT(1), the tape is heated to T3 for lamination. During heating, compressive stress is exerted on Ag, due to which Ag is yielded in compression at T2 (=293+138=431 K).

At the lamination temperature T3 (453K), Ag has been yielded in compression. Such a situation is noted as T3,0 in figure 4.3. The insert tape is pre-loaded in tension and is solder-laminated with the pre-loaded stainless steel (T3,1). In the pre-tensile loading of the insert tape, Ag, which has been yielded in compression at T3,0, deforms elastically and tensile strain is added, but the strain of Ag does not exceed the tensile yield strain due to the low pre-load on the insert tape (4.5N [1]), as will be shown later. After the lamination, the pre-loads are relaxed. In the load-relaxation process, the Ag is compressed first elastically until Ag is yielded in compression at T3,2. Then Ag deforms plastically in compression until the load is completely relaxed at T3,3.

After the load relaxation, the laminated tape is cooled down from T3,3 to room temperature RT(2) and then from RT(2) to 77K(1). On the way, Ag that has been yielded in compression at T3,3 is yielded in tension at T4. Such a change from tensile to compressive (and vice versa) yielding is caused by the temperature difference 200K in the laminated tape, as will be shown in 4.3.2. At 77K(1), Ag is in a tensile yielded state. The critical current of the tape was pre-checked at AMSC At 77K(1). Then the tape was heated from 77K(1) to room temperature RT(3). On the way, as compressive stress is exerted on Ag, Ag is yielded in compression at T5. Thus at RT(3), Ag is in a compressively yielded state, while at RT(2) before the cooling down to 77K, Ag is in a tensile yielded state. At room temperature RT(3), the residual strain of Bi2223 filaments was measured by X-ray diffraction, as shown later in 4.3.3. When the laminated tape is again cooled down from room temperature RT(3) to 77K(2) for measurement of critical current, the Ag, which has been yielded in compression at RT(3), is yielded in tension at T6. Thus at 77K(2), Ag is yielded in tension, which is

the same situation at 77K(1). When the tape is heated from 77K(2) to room temperature RT(4), Ag comes to be yielded in compression at T7 on the way. Thus Ag is in a compressively yielded state at RT(4), which is the same situation at RT(3), but not the same situation at RT(1) at which Ag is in tensile yielded state. As the stress state at RT(3) is the same as that at RT(4) and also the stress state at 77K(1) is the same as that at 77(K), T7 is equal to T5, as will be shown in 4.3.3 and 4.3.4.

The mechanical strain is induced through the application of pre-loads to insert tape and stainless steel, lamination and the subsequent load-relaxation. Taking the behavior at T3 (T3,0 to T3,3) stated above into consideration, the mechanically induced strain in each constituent (Bi2223, Ag, Ag ally and steel) will be formulated in 4.3.1, which will be used in 4.3.3 for estimation of effectively acted pre-load on stainless steel. The temperature change – induced thermal strain will be formulated in 4.3.2, which will be used in 4.3.4 for calculation of the change of residual strain of each constituent as a function of temperature.

4.2.4 Input values for analysis

For analysis of the strain accumulation in the constituents, the property values listed in Table 4.1 were used. As the strain is accumulated in the insert tape and laminated one before and after the lamination, respectively (figures 4.2 and 4.3), the property values for both insert and laminated tapes are included. They were obtained in the following manner.

(a) The cross-sectional area A_i (i=laminated tape, insert tape, stainless steel and solder) was measured from the SEM image of the cross-section shown in figure 4.1.

(b)The volume fraction $V_{i,LT}$ of the constituents in the laminated tape (i=insert tape, stainless steel and solder, and the subscript LT refers to the laminated tape) was calculated from the cross-sectional area obtained in (a).

(c) The term, Young's modulus x volume fraction, $E_iV_{i,IT,}$ of the constituents in the insert tape (i=Ag, Ag alloy and Bi2223, and IT refers to the insert tape) were taken from Ref.[27].

(d) The overall Young's moduli of the insert tape in Region I, where Ag, Ag alloy and Bi2223 deform elastically, and that in Region II, where Ag deforms plastically and

Ag alloy and Bi2223 deform elastically, were taken from Ref.[27].

(e)The Young's modulus of the stainless steel was taken from Ref.[1].

(f) The term, Young's modulus x volume fraction, $E_i V_{i,LT}$, of the constituents in the laminated tape (i=Ag, Ag alloy, Bi2223, stainless steel and solder) were calculated from (b), (c) and (e) and E_{Solder}=24 GPa (Ref.[1]).

(g) The overall Young's modulus of the laminated tape in Region I ($E_{I,LT}$) where all constituents (Bi2223, Ag, Ag alloy, stainless steel and solder) deform elastically and in Region II ($E_{II,LT}$), where Ag deform plastically and other constituents deform elastically, were calculated by the rule of mixtures as follows.

For Region I, the overall Young's modulus, $E_{I,LT}$ is given by

$$E_{I,LT}=E_{Ag}V_{Ag,LT}+E_{Alloy}V_{Alloy,LT}+E_{Bi}V_{Bi,LT}+E_{SS}V_{SS,LT}+E_{Solder}V_{Solder,LT} \quad \text{(Region I)} \quad (4.1)$$

$$E_{II,LT}=E_{Alloy}V_{Alloy,LT}+E_{Bi}V_{Bi,LT}+E_{SS}V_{SS,LT}+E_{solder}V_{Solder,LT} \quad \text{(Region II)} \quad (4.2)$$

Substituting the $E_i V_{i,LT}$(i=Ag, Ag alloy, Bi2223, stainless steel and solder)-values obtained in (f), the $E_{I,LT}$ and $E_{II,LT}$ were calculated.

(h) Yield strain of Ag was taken from Ref.[27].

(i) The coefficients of thermal expansion of Ag (α_{Ag}), Ag alloy (α_{Alloy}) and Bi2223 (α_{Bi}) were taken from Refs.[27]. The coefficient of the stainless steel (α_{SS}) was taken from Ref.[29].

(j) The overall coefficient of thermal expansion of insert tape was taken from Ref.[27].

(k) The overall coefficient of thermal expansion of laminated tape for Regions I ($\alpha_{I,LT}$) and II ($\alpha_{II,LT}$) were calculated by equations (4.17) and (4.18) shown later.

4.3 Results and Discussion

4.3.1 Formulation of mechanically induced residual strain in the lamination, followed by the load relaxation process

The residual strain of Bi2223 filaments at room temperature $\varepsilon_{Bi,r}(RT)$ in the stainless steel-laminated composite tape was measured by X-ray diffraction method at RT(3) in figure 4.3. It is given by the sum of the mechanical strain $\varepsilon_{Bi,M}$ arising from the lamination, followed by load relaxation, and the thermally accumulated strain at RT(3) $\varepsilon_{Bi,T}(RT)$ arising from the difference in thermal expansion among the constituents [1,6];

$$\varepsilon_{Bi,r}(RT)=\varepsilon_{Bi,M}+\varepsilon_{Bi,T}(RT). \quad (4.3)$$

In the present work, $\varepsilon_{Bi,M}$ and $\varepsilon_{Bi,T,}(RT)$ were derived as follows. The Bi2223, stainless steel and Ag alloy were treated as the elastic body. As Ag is soft [27], it was treated as an elastic- perfect plastic body with a yield strain $\varepsilon_{Ag,y}$=0.02%, as similarly as in our preceding work [27].

In this section, the change of mechanical strain of insert tape and stainless steel due to the lamination is analyzed. In the lamination process, the insert tape and stainless steel are heated to the lamination temperature T3 (453 K) and are pulled in tension up to the loads F_{IT}^{0} and F_{SS}^{0}, respectively. Under the pre-loaded condition, they are bonded together with solder. After the bonding, the total load $F_{SS}^{0}+F_{IT}^{0}$ is relaxed until the total load of the laminated tape reaches zero in the filament axis direction. The change of strain of the constituents is calculated by dividing the process into the following stages.

Stage 0 (T3,0 in figure 4.3):

The insert tape and stainless steel are heated to 453K (T3). As the yield strain of Ag is low (0.02%), Ag in the insert tape has been yielded in tension at room temperature (RT(1)) during cooling from the heat-treatment temperature [27]. When the insert tape is heated to 453K (T3), the Ag is yielded in compression on the way, as will be shown later in 4.3.2 and 4.3.4.

Stage 1 (T3,0→T3,1 in figure 4.3):

The insert tape and stainless steel are pulled in tension up to the loads F_{IT}^{0} and F_{SS}^{0}, respectively, and were bonded together with solder at 453K. As Ag in the insert tape is yielded in compression, it deforms elastically upon tensile loading. Thus the increment of the strain of the insert tape $\Delta\varepsilon_{1,IT}$ is given by

$$\Delta\varepsilon_{1,IT}=F_{IT}^{0}/(E_{I,IT}A_{IT}) \quad (4.4)$$

where $E_{I,IT}$ is the overall Young's modulus in Region I and A_{IT} is the cross-sectional area of the insert tape (Table 4.1). The F_{IT}^{0} has been reported to be 4.5N [1]. Substituting these values into equation (4.4), we have $\Delta\varepsilon_{1,IT}$=0.006 %, which is lower than the yield strain 0.02% of Ag. Thus Ag in the loaded insert tape is in the elastic range. The increment of strain $\Delta\varepsilon_{1,SS}$ of the stainless steel due to the applied load F_{SS}^{0} is given by

$$\Delta\varepsilon_{1,SS}= F_{SS}^{0}/(E_{SS}A_{SS}) \quad (4.5)$$

where E_{SS} and A_{SS} are the Young's modulus and cross-sectional area of the stainless steel, respectively (Table 4.1).

Stage 2 (T3,1→T3,2 in figure 4.3):

After the lamination, the total load $F_{SS}^{0}+ F_{IT}^{0}$ is relaxed. In the relaxation process, the stainless steel that is more strained by the higher tensile pre-load (71.4N as shown later) shrinks more than the insert tape that is less strained by the lower tensile pre-load (4.5N). Accordingly, the compressive and tensile loads are given to the insert tape and stainless stress, respectively, after the load relaxation. In the initial stage of relaxation, Ag in the insert tape, which is in the elastic state, deforms elastically until Ag is yielded in compression. The change of the elastic strain $\Delta\varepsilon_{2,IT}$ of the insert tape and that of stainless steel $\Delta\varepsilon_{2,SS,}$ corresponding to the strain range from elastic state to compressive yielding of Ag, are given by

$$\Delta\varepsilon_{2,IT}=\Delta\varepsilon_{2,SS}=-\Delta(F_{IT}^{0}+F_{SS}^{0})_{2}/(E_{I,LT}A_{LT}) \quad (4.6)$$

where $-\Delta(F_{IT}^{0}+F_{SS}^{0})_2$ is the change of the load. The strain range $\Delta\varepsilon_{2,IT}$ ($=\Delta\varepsilon_{2,SS}$) is equal to $-\Delta\varepsilon_{1,IT}$ ((Eq.(4)), which is expressed as

$$\Delta\varepsilon_{2,IT}(=\Delta\varepsilon_{2,SS})= -\Delta(F_{IT}^{0}+F_{SS}^{0})_2/(E_{I,LT}A_{LT})=-\Delta\varepsilon_{1.IT} \quad (4.7)$$

Substituting the known values of $E_{I,LT}$ and A_{LT} listed in Table 4.1 and $-\Delta\varepsilon_{1,IT}$ =-0.006 % mentioned above into equation (4.7), $-\Delta(F_{IT}^{0}+F_{SS}^{0})_2$ is calculated to be -8.04 N. This means that the total applied load $F_{IT}^{0}+F_{SS}^{0}$ is consumed by 8.04 N and the remaining load is $F_{IT}^{0}+F_{SS}^{0} - \Delta(F_{IT}^{0}+F_{SS}^{0})_2$.

Stage 3 (T3,2→T3,3 in figure 4.3).

After the stress of Ag reaches its compressive yield stress, Ag deforms plastically. The change of strain of the insert tape, $\Delta\varepsilon_{3,IT}$, and stainless steel, $\Delta\varepsilon_{3,SS}$ from the onset of the compressive yielding of Ag to the final stress state at which the stress reaches the equilibrium state (total load of the composite is zero) is given by

$$\Delta\varepsilon_{3,IT} =\Delta\varepsilon_{3,SS} = - \{(F_{IT}^{0}+F_{SS}^{0})-\Delta(F_{IT}^{0}+F_{SS}^{0})_2\}/(E_{II,LT}A_{LT}) \quad (4.8)$$

Thus, the mechanical strain of the insert tape $\varepsilon_{IT,M}$ and stainless steel $\varepsilon_{SS,M}$ induced by the lamination and subsequent stress relaxation is given by

$$\varepsilon_{IT,M}=\Delta\varepsilon_{1,IT}+ \Delta\varepsilon_{2,IT}+\Delta\varepsilon_{3,IT} =-[(F_{IT}^{0}+F_{SS}^{0})-\{\Delta(F_{IT}^{0}+F_{SS}^{0})_2\}]/(E_{II,LT}A_{LT}) \quad (4.9)$$

$$\varepsilon_{SS,M}=\Delta\varepsilon_{1,SS}+\Delta\varepsilon_{2,SS}+\Delta\varepsilon_{3,SS}$$
$$=F_{SS}^{0}/(E_{SS}A_{SS})-\Delta(F_{IT}^{0}+F_{SS}^{0})_2/(E_{I,LT}A_{LT})-[(F_{IT}^{0}+F_{SS}^{0})-\{\Delta(F_{IT}^{0}+F_{SS}^{0})_2\}]/(E_{II,LT}A_{LT}) \quad (4.10)$$

The mechanically induced strain in Bi2223, $\varepsilon_{Bi,M}$, and that in Ag alloy, $\varepsilon_{Alloy,M}$, are the same as that of $\varepsilon_{IT,M}$. As Ag is yielded in compression after the load relaxation, the elastic strain of Ag is $-\varepsilon_{Ag,y}$. The unknown value of F_{SS}^{0} will be obtained later in 4.3.3 from the comparison of the calculation result with the measured residual strain of Bi2223 with X ray.

4.3.2 Formulation of thermally induced strain during cooling and heating

The thermally induced residual strain of Bi2223 varies in the insert tape until it is laminated with stainless steel, and it varies also in the laminated tape during cooling from the lamination temperature (T3). Thus the thermal history of the insert tape until the lamination, and that of the laminated tape after the lamination (figure 4.3), shall be incorporated for calculation of the change of thermal strain.

The necessary formulae and parameters for thermal stress analysis for the insert and laminated tapes are given as follows.

(A) Formulation for calculation of thermally induced residual strain change before lamination

The thermal history and the change of thermally induced strain of Bi2223 in the insert tape have been studied in the preceding paper [27]. Using the result for the insert tape, the coefficient of the overall thermal expansion of the insert tape for Regions I (all constituents deform elastically) and II (Ag deforms plastically and the other constituents deform elastically) is given by

$$\alpha_{I,IT}=(\alpha_{Bi}E_{Bi}V_{Bi,IT}+\alpha_{Ag}E_{Ag}V_{Ag,IT}+\alpha_{Alloy}E_{Alloy}V_{Alloy,IT})/E_{I,IT} \quad \text{(Region I)} \quad (4.11)$$

$$\alpha_{II,IT}=(\alpha_{Bi}E_{Bi}V_{Bi,IT}+\alpha_{Alloy}E_{Alloy}V_{Alloy,IT})/E_{II,IT} \quad \text{(Region II)} \quad (4.12)$$

In Region I, the thermally induced elastic strain of the constituents for the change in temperature ΔT is given by

$$\Delta\varepsilon_{Bi,IT}=(\alpha_{I,IT}-\alpha_{Bi})\,\Delta T,\ \Delta\varepsilon_{Ag,IT}=(\alpha_{I,IT}-\alpha_{Ag})\,\Delta T,\ \Delta\varepsilon_{Alloy,IT}=(\alpha_{II,IT}-\alpha_{Alloy})\,\Delta T \quad (4.13)$$

In Region II, the thermally induced elastic strain of Bi2223 and Ag alloy are given by

$$\Delta\varepsilon_{Bi,IT}=(\alpha_{II,IT}-\alpha_{Bi})\Delta T,\ \Delta\varepsilon_{Alloy,IT}=(\alpha_{II,IT}-\alpha_{Alloy})\Delta T \quad (4.14)$$

The total strain of Ag under plastic deformation (Region II) is the sum of the elastic strain $\varepsilon_{Ag,elastic}$ and plastic one $\varepsilon_{Ag,plastic}$. Under the approximation of Ag as an elastic-

perfect plastic body, only the elastic strain is concerned with the stress carrying capacity of Ag, and the stress of Ag, σ_{Ag}, is given by $\varepsilon_{Ag,elastic}E_{Ag}$. The elastic component of residual strain of Ag, $\varepsilon_{Ag,IT,elastic}$, in Region II is given by [27]

$$\varepsilon_{Ag,IT,elastic}=+\varepsilon_{Ag,y} \text{ when Ag deforms plastically is tension} \quad (4.15)$$

$$\varepsilon_{Ag,IT,elastic}=-\varepsilon_{Ag,y} \text{ when Ag deforms plastically is compression} \quad (4.16)$$

(B) Formulation for calculation of thermally induced residual strain change after lamination

After lamination, Bi2223 filaments exist in the laminated tape. The Young's modulus of the laminated tape $E_{I,LT}$ for elastically deforming Ag (Region I) and $E_{II,LT}$ for plastically deforming Ag (Region II) are listed in Table 4.1. The coefficient of thermal expansion of the laminated tape is given by

$$\alpha_{I,LT}=(\alpha_{Bi}E_{Bi}V_{Bi,LT}+\alpha_{Ag}E_{Ag}V_{Ag,LT}+\alpha_{Alloy}E_{Alloy}V_{Alloy,LT}+\alpha_{SS}E_{SS}V_{SS,LT} +\alpha_{Soldeer}E_{Solder}V_{Solder,LT})/E_{I,LT} \quad \text{(Region I)} \quad (4.17)$$

$$\alpha_{II,LT}=(\alpha_{Bi}E_{Bi}V_{Bi,LT}+\alpha_{Alloy}E_{Alloy}V_{Alloy,LT}+\alpha_{SS}E_{SS}V_{SS,LT}+\alpha_{Soldeer}E_{Solder}V_{Solder,LT})/E_{II,LT} \quad \text{(Region II)} \quad (4.18)$$

In Region I, the thermally induced elastic strain change of Bi2223, Ag, Ag alloy and stainless steel for the temperature range ΔT is given by

$$\Delta\varepsilon_{Bi,LT}=(\alpha_{I,LT}-\alpha_{Bi})\Delta T, \quad \Delta\varepsilon_{Ag,LT}=(\alpha_{I,LT}-\alpha_{Ag})\Delta T,$$
$$\Delta\varepsilon_{Alloy,LT}=(\alpha_{I,LT}-\alpha_{Alloy})\Delta T, \quad \Delta\varepsilon_{SS,LT}=(\alpha_{I,LT}-\alpha_{SS})\Delta T \quad (4.19)$$

In Region II, the thermally induced elastic strain for Bi2223, Ag alloy and stainless steel is given by

$$\Delta\varepsilon_{Bi,LT}=(\alpha_{II,LT}-\alpha_{Bi})\Delta T, \Delta\varepsilon_{Alloy,LT}=(\alpha_{II,LT}-\alpha_{Alloy})\Delta T, \Delta\varepsilon_{SS,LT}=(\alpha_{II,LT}-\alpha_{SS})\Delta T \quad (4.20)$$

and the elastic component of residual strain of Ag, $\varepsilon_{Ag,LT,elastic}$ in Region II is given in a

similar manner to those for the insert tape.

$$\varepsilon_{Ag,LT,elastic}=+\varepsilon_{Ag,y} \text{ when Ag deforms plastically is tension} \quad (4.21)$$

$$\varepsilon_{Ag,LT,elastic}=-\varepsilon_{Ag,y} \text{ when Ag deforms plastically is compression} \quad (4.22)$$

(C) Calculation of thermally induced strain change

The thermally induced residual strain change of the constituents is calculated by equations (4.11) to (4.22) as a function of temperature, as follows. The necessary values for calculation are listed in Table 4.1.

Step 0

The thermal strain is practically accumulated in the insert tape below the temperature T0 (563K) in terms of the material property values in the relevant temperature range (77K-600K), as has been shown in the preceding paper [27].

Step 1 (T0→T1)

During cooling from T0 (563 K), Ag in the insert tape deforms elastically until the temperature reaches T1 and then plastically in the temperature range from T1 to room temperature (RT=293 K). T1 satisfies

$$(\alpha_{I,IT}-\alpha_{Ag})(T1-T0)=\varepsilon_{Ag,y} \quad (4.23)$$

The T1 was calculated to be 494 K. This means that the change from zero strain to yielding state of Ag is caused by the temperature difference 69 K. The change of strain of each constituent from T0 to T1, $\Delta\varepsilon_{i,T0\rightarrow T1}$ (i=Bi2223,Ag and Ag alloy) is calculated by equation (4.13). The strain of Ag varies from zero at T0 to $+\varepsilon_{Ag,y}$ at T1.

Step 2 (T1→RT(1))

Upon further cooling of the insert tape from T1 (495 K) to room temperature 293K (RT(1) in figure 4.3), Ag deforms plastically in tension. The change of strain of each constituent from T1 to RT, $\Delta\varepsilon_{i,T1\rightarrow RT}$ (i=Bi2223 and Ag alloy) is calculated by equation (4.14). The elastic strain of Ag does not change from T1 to RT(1), being equal to $+\varepsilon_{Ag,y}$.

Step 3 (RT(1)→T2)

Then the insert tape is heated to the lamination temperature (T3=453K) from RT(1). In this process, as the compressive thermal stress is imposed on Ag, Ag deforms first elastically up to the temperature T2 at which Ag is yielded in compression, and then deforms plastically in compression up to the lamination temperature T3. The temperature T2 satisfies

$$(\alpha_{I,IT}-\alpha_{Ag})\,(T2-RT)=-2\varepsilon_{Ag,y} \qquad (4.24)$$

T2 was calculated to be 431K. This means that the change of tensile to compressive yielding state (and also the change of compressive to tensile yielding state) of Ag is caused by the temperature difference 138K in the insert tape. The change of strain of each constituent from RT to T2, $\Delta\varepsilon_{i,RT\rightarrow T2}$ (i=Bi2223,Ag and Ag alloy), is calculated by equation (4.13). The elastic strain of Ag changes from $+\varepsilon_{Ag,y}$ at RT(1) to $-\varepsilon_{Ag,y}$ at T2.

Step 4 (T2→T3)

Upon further heating of the insert tape from T2 (431 K) to T3 (lamination temperature: 453K), Ag deforms plastically in compression. The change of strain of each constituent from T2 to T3, $\Delta\varepsilon_{i,T2\rightarrow T3}$ (i=Bi2223 and Ag alloy) is calculated by equation (4.14). The elastic strain of Ag remains to be $-\varepsilon_{Ag,y}$.

Step 5 (T3→RT(2))

At T3 (453 K), the insert tape and stainless steel are assembled. As will be shown in 4.3.3, Ag is yielded in compression after the load relaxation. Thus, upon cooling from T3, as tensile stress is thermally imposed on Ag, Ag behaves elastically until the temperature reaches T4 at which Ag is yielded in tension. The temperature T4 satisfies

$$(\alpha_{I,LT}-\alpha_{Ag})\,(T4-T3)=2\varepsilon_{Ag,y} \qquad (4.25)$$

T4 was calculated to be 253 K. This means that the change of compressive to tensile yielding state (and also the change of tensile to compressive yielding state) of Ag in the laminated tape is caused by the temperature difference 200 K, which is larger than 138

K in the insert tape. As RT(293K)>T4, Ag is in the elastic state at RT(2). The change of strain of each constituent from T3 to RT(2), $\Delta\varepsilon_{i,T3\rightarrow RT(2)}$ (i=Bi2223,Ag, Ag alloy and stainless steel) is calculated by equation (4.19). The elastic strain of Ag changes from $-\varepsilon_{Ag,y}$ at T3 to $-\varepsilon_{Ag,y}+\Delta\varepsilon_{Ag,T3\rightarrow RT(2)}$ at RT(2).

Step 6 (RT(2)→T4)

As shown in Step 5, T4 was 253 K. Upon further cooling of the laminated tape from RT(2) to T4, Ag deforms elastically in tension. The change of strain of each constituent from RT(2) to T4, $\Delta\varepsilon_{i,T4\rightarrow RT}$ (i=Bi2223, Ag, Ag alloy and stainless steel) is calculated by equation (4.19). The elastic strain of Ag becomes $+\varepsilon_{Ag,y}$ at T4.

Step 7 (T4→77K(1))

During further cooling of the laminated tape from T4 (253 K) to 77K(1), Ag deforms plastically in tension. The change of strain of each constituent from T4 to 77K, $\Delta\varepsilon_{i,RT\rightarrow 77K}$ (i=Bi2223, Ag alloy and stainless steel) is calculated by equation (4.20). The elastic strain of Ag remains to be $+\varepsilon_{Ag,y}$.

Step 8 (77K(1)→T5)

At 77K, Ag is yielded in tension. When the laminated tape is heated from 77K(1), compressive stress is imposed on Ag. Thus Ag behaves elastically up to T5 at which Ag is yielded in compression. The temperature T5, satisfying $(\alpha_{I,LT}-\alpha_{Ag})$ (T5-77K)$=-2\varepsilon_{Ag,y}$, was calculated to be 277 K. The change of strain of each constituent from 77K(1) to T5, $\Delta\varepsilon_{i,77K\rightarrow T5}$ (i=Bi2223,Ag, Ag alloy and stainless steel) is calculated by equation (4.19). The elastic strain of Ag changes from $+\varepsilon_{Ag,y}$ at 77K(1) to $-\varepsilon_{Ag,y}$ at T5.

Step 9 (T5→RT(3))

During further heating of the laminated tape from T5 (277 K) to RT(3), Ag deforms plastically in compression. The change of strain of each constituent from T5 to RT(3), $\Delta\varepsilon_{i,T5\rightarrow RT}$ (i=Bi2223, Ag alloy and stainless steel) is calculated by equation (4.20). The elastic strain of Ag remains to be $-\varepsilon_{Ag,y}$.

Step 10 (RT(3)→T6)

When the laminated tape is cooled down again to 77K, tensile stress is thermally imposed on Ag. Thus Ag behaves elastically until T6 at which Ag comes to be yielded in tension. The temperature T6 satisfying, $(\alpha_{I,LT}-\alpha_{Ag})$ (T6-RT)$=2\varepsilon_{Ag,y}$, was calculated to be 93 K. The change of strain of each constituent from RT(3) to T6, $\Delta\varepsilon_{i,RT\rightarrow T6}$ (i=Bi2223,Ag, Ag alloy and stainless steel) is calculated by equation (4.19). The elastic strain of Ag changes from $-\varepsilon_{Ag,y}$ at RT(3) to $+\varepsilon_{Ag,y}$ at T6.

Step 11 (T6→77K(2))

During further cooling of the laminated tape from T6 (93 K) to 77K, Ag deforms plastically in tension. The change of strain of each constituent from T6 to 77K, $\Delta\varepsilon_{i,T6\rightarrow 77K}$ (i=Bi2223, Ag alloy and stainless steel) is calculated by equation (4.20). The elastic strain of Ag remains to be $+\varepsilon_{Ag,y}$.

Step 12 (77K(2)→T7)

At 77K, Ag is yielded in tension. When the laminated tape is heated from 77K, compressive stress is thermally imposed on Ag. Thus Ag behaves elastically up to T7 (277K) at which Ag is yielded in compression, as in Step 8. The change of strain of each constituent from 77 to T7 is the same as $\Delta\varepsilon_{i,77K\rightarrow T5}$ (i=Bi2223,Ag, Ag alloy and stainless steel) in Step 8.

Step 13 (T7(=T5)→RT(4))

During further heating of the laminated tape from T7(=T5=177 K) to RT(4), Ag deforms plastically in compression, as in Step 9. Therefore, the change of strain of each constituent from T7 (=T5) to RT(4) is the same as $\Delta\varepsilon_{i,T5\rightarrow RT}$ (i=Bi2223, Ag alloy and stainless steel) in Step 9. The elastic strain of Ag remains to be $-\varepsilon_{Ag,y}$.

As stated above, the strain of each component varies in each stage/step in the thermo-mechanical process. The equations used for calculation of the change in elastic strain of Ag ($\Delta\varepsilon_{Ag}$), Ag alloy ($\Delta\varepsilon_{Alloy}$), Bi2223 ($\Delta\varepsilon_{Bi}$) and stainless steel ($\Delta\varepsilon_{SS}$) in the thermo-mechanical process are tabulated in Table 4.2.

Table 4.2. Equations used for calculation of the change in elastic strain of Ag ($\Delta\varepsilon_{Ag}$), Ag alloy ($\Delta\varepsilon_{Alloy}$), Bi2223 ($\Delta\varepsilon_{Bi}$) and stainless steel ($\Delta\varepsilon_{SS}$) in the thermo-mechanical process. –(*) and –(**) for $\Delta\varepsilon_{Ag}$ refer to plastic deformation in tension and in compression, respectively.

		$\Delta\varepsilon_{Ag}$	$\Delta\varepsilon_{Alloy}$	$\Delta\varepsilon_{Bi}$	$\Delta\varepsilon_{SS}$
Thermal process before lamination	T0 → T1	$(\alpha_{T,LT} - \alpha_{Ag})(T1-T0)$	$(\alpha_{T,LT} - \alpha_{Alloy})(T1-T0)$	$(\alpha_{T,T} - \alpha_{Bi})(T1-T0)$	-
	T1 → RT(1)	-(*)	$(\alpha_{R,LT} - \alpha_{Alloy})(RT-T1)$	$(\alpha_{R,LT} - \alpha_{Bi})(RT-T1)$	-
	RT(1) → T2	$(\alpha_{T,T} - \alpha_{Ag})(T2-RT)$	$(\alpha_{T,LT} - \alpha_{Alloy})(T2-RT)$	$(\alpha_{T,LT} - \alpha_{Bi})(T2-RT)$	-
	T2 → T3,0	-(**)	$(\alpha_{R,LT} - \alpha_{Alloy})(T3-T2)$	$(\alpha_{R,LT} - \alpha_{Bi})(T3-T2)$	-
Mechanical process during lamination	T3,0 → T3,1	$F_{LT}^0/(E_{LLT}A_{LT})$	$F_{LT}^0/(E_{LLT}A_{LT})$	$F_{LT}^0/(E_{LLT}A_{LT})$	$F_{SS}^0/(E_{SS}A_{SS})$
	T3,1 → T3,2	$-\Delta(F_{LT}^2+F_{SS}^0)_2/(F_{LLT}A_{LT})$ $(=-F_{LT}^0/(E_{LLT}A_{LT}))$	$-\Delta(F_{LT}^2+F_{SS}^0)_2/(F_{LLT}A_{LT})$ $(=-F_{LT}^0/(E_{LLT}A_{LT}))$	$-\Delta(F_{LT}^0+F_{SS}^0)_2/(F_{LLT}A_{LT})$ $(=-F_{LT}^0/(E_{LLT}A_{LT}))$	$-\Delta(F_{LT}^0+F_{SS}^2)_2/(F_{LLT}A_{LT})$ $(=-F_{LT}^0/(E_{LLT}A_{LT}))$
	T3,2 → T3,3	-(**)	$-\{(F_{LT}^0+F_{SS}^0)-\Delta(F_{LT}^0+F_{SS}^0)_2\}$ $/(E_{LLT}A_{LT})$	$-\{(F_{LT}^2+F_{SS}^0)-\Delta(F_{LT}^0+F_{SS}^0)_2\}$ $/(E_{LLT}A_{LT})$	$-\{(F_{LT}^0+F_{SS}^0)-\Delta(F_{LT}^0+F_{SS}^0)_2\}$ $/(E_{LLT}A_{LT})$
Thermal process after lamination	T3,3 → RT(2)	$(\alpha_{T,LT} - \alpha_{Ag})(RT-T3)$	$(\alpha_{T,LT} - \alpha_{Alloy})(RT-T3)$	$(\alpha_{T,LT} - \alpha_{Bi})(RT-T3)$	$(\alpha_{T,LT} - \alpha_{SS})(RT-T3)$
	RT(2) → T4	$(\alpha_{T,LT} - \alpha_{Ag})(T4-RT)$	$(\alpha_{T,LT} - \alpha_{Alloy})(T4-RT)$	$(\alpha_{T,LT} - \alpha_{Bi})(T4-RT)$	$(\alpha_{T,LT} - \alpha_{SS})(T4-RT)$
	T4 → 77K(1)	-(*)	$(\alpha_{T,LT} - \alpha_{Alloy})(77K-T4)$	$(\alpha_{T,LT} - \alpha_{Bi})(77K-T4)$	$(\alpha_{T,LT} - \alpha_{SS})(77K-T4)$
	77K(1) → T5	$(\alpha_{T,LT} - \alpha_{Ag})(T5-77K)$	$(\alpha_{T,LT} - \alpha_{Alloy})(T5-77K)$	$(\alpha_{T,LT} - \alpha_{Bi})(T5-77K)$	$(\alpha_{T,LT} - \alpha_{SS})(T5-77K)$
	T5 → RT(3)	-(**)	$(\alpha_{T,LT} - \alpha_{Alloy})(RT-T5)$	$(\alpha_{T,LT} - \alpha_{Bi})(RT-T5)$	$(\alpha_{T,LT} - \alpha_{SS})(RT-T5)$
	RT(3) → T6	$(\alpha_{T,LT} - \alpha_{Ag})(T6-RT)$	$(\alpha_{T,LT} - \alpha_{Alloy})(T6-RT)$	$(\alpha_{T,LT} - \alpha_{Bi})(T6-RT)$	$(\alpha_{T,LT} - \alpha_{SS})(T6-RT)$
	T6 → 77K(2)	-(*)	$(\alpha_{T,LT} - \alpha_{Alloy})(77K-T6)$	$(\alpha_{T,LT} - \alpha_{Bi})(77K-T6)$	$(\alpha_{T,LT} - \alpha_{SS})(77K-T6)$
	77K(2) → T7	$(\alpha_{T,LT} - \alpha_{Ag})(T7-77K)$	$(\alpha_{T,LT} - \alpha_{Alloy})(T7-77K)$	$(\alpha_{T,LT} - \alpha_{Bi})(T7-77K)$	$(\alpha_{T,LT} - \alpha_{SS})(T7-77K)$
	T7 → RT(4)	-(**)	$(\alpha_{T,LT} - \alpha_{Alloy})(RT-T7)$	$(\alpha_{T,LT} - \alpha_{Bi})(RT-T7)$	$(\alpha_{T,LT} - \alpha_{SS})(RT-T7)$

4.3.3 Estimation of effectively acted pre-load on stainless steel

Figure 4.4 shows the change of strain ε_{Bi} of Bi2223 filaments in the laminated composite tape at room temperature RT(3) under applied tensile strain $\varepsilon_{c,T}$, measured by the X-ray diffraction. From this result, the residual strain $\varepsilon_{Bi,r}$(RT) of Bi2223 at room temperature, corresponding to ε_c=0 %, was found to be –0.133 %.

The mechanical strain and the thermally induced strain of each constituent are calculated by the procedure stated above. The total strain of each constituent except Ag is the sum of the mechanical and thermal strains. The total strain of the Bi2223 was measured with X ray method at room temperature for the laminated tape with the thermal history TH→T0→T1→RT(1)→T2→T3→T4→RT(2)→77K→T5→RT(3) and mechanical history at the lamination temperature T3 (figure 4.3).

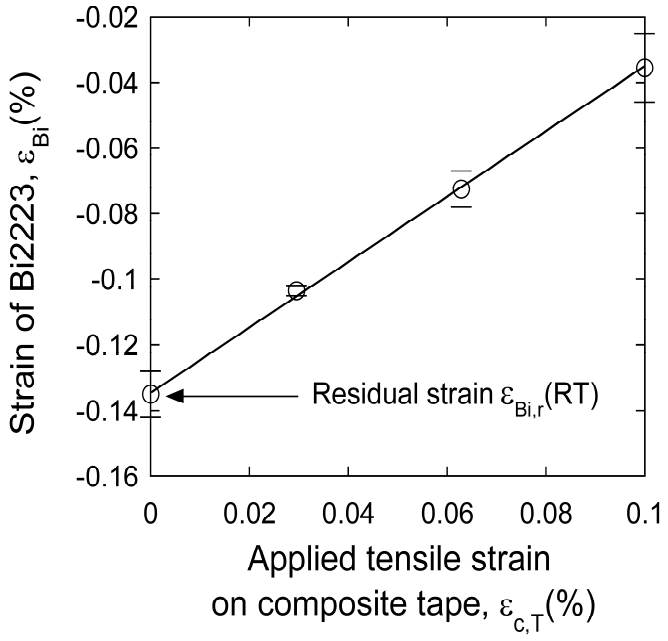

Figure 4.4. Change of strain of Bi2223 filaments in the laminated composite tape at room temperature RT(3) under applied tensile strain $\varepsilon_{c,T}$, measured by X-ray diffraction.

The thermal strain $\varepsilon_{Bi,T}(RT(3))$ of Bi2223 at RT(3) in the laminated tape with the thermal history mentioned above was calculated to be -0.075 % by

$$\varepsilon_{Bi,T}(RT) = \Delta\varepsilon_{Bi,T0\rightarrow T1}+\Delta\varepsilon_{Bi,T1\rightarrow RT(1)}+\Delta\varepsilon_{Bi,RT(1)\rightarrow T2}+\Delta\varepsilon_{Bi,T2\rightarrow T3}+\Delta\varepsilon_{Bi,T3\rightarrow RT(2)} +\Delta\varepsilon_{Bi,RT(2)\rightarrow T4}+\Delta\varepsilon_{Bi,T4\rightarrow 77K}+\Delta\varepsilon_{Bi,77K\rightarrow T5}+\Delta\varepsilon_{Bi,T5\rightarrow RT(3)} \quad (4.26)$$

Using the pre-load on the insert tape, F_{IT}^{0}=4.5N [1], equation (4.9) and $\Delta(F_{IT}^{0}+F_{SS}^{0})_2$=8.04N calculated in 4.3.1, the mechanical strain of Bi2223, $\varepsilon_{Bi,M}$, was calculated as a function of F_{SS}^{0} as shown in figure 4.5. The sum of the thermal and mechanical strains of Bi2223 as a function of F_{SS}^{0} is presented with the solid curve also in figure 4.5. As the measured residual strain of Bi2223 at RT(3) by X ray diffraction was -0.133%, the corresponding F_{SS}^{0} was read to be 71.4 N. Otto [1] has mentioned the value in the range of 45 to 98 N for F_{SS}^{0}. The present result F_{SS}^{0}=71.4 N is in such a range. The mechanical strain $\varepsilon_{Bi,M}$ of Bi2223 induced by the lamination, followed by load relaxation, for F_{IT}^{0}=4.5N and F_{SS}^{0} =71.4 N was calculated to be -0.058 %.

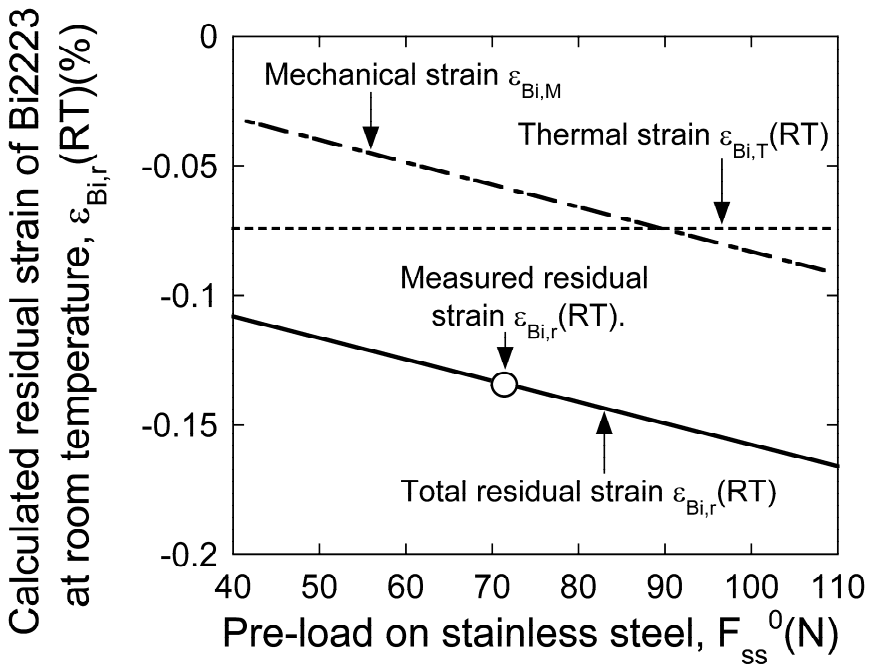

Figure 4.5. Calculated residual strain of Bi2223 at room temperature RT(3) as a function of pre-load on the stainless steel, together with the measured value by X-ray diffraction.

In this way, from the comparison of the measured residual strain of Bi2223 by X ray with the calculation result, the contributions of thermal and mechanical strains to the total residual strain at room temperature RT(3) were estimated to be -0.075 and -0.058 %, respectively.

4.3.4 Change of residual strain of each constituent as a function of temperature

The changes of elastic strain of Bi2223, Ag, Ag alloy and stainless steel in the thermo-mechanical history were calculated by adding the strain change in the order of Step 1 (T0→T1), Step 2 (T1→RT(1)), Step 3 (RT(1)→T2), Step 4 (T2→T3,0), Stage 1 (T3,0→T3,1), Stage 2 (T3,1→T3,2), Stage 3 (T3,2→T3,3), Step 5 (T3,3→T4), Step 6 (T4→RT(2)), Step 7 (RT(2)→77K(1)), Step 8 (77K(1)→T5), Step 9 (T5→RT(3)), Step 10 (RT(3)→T6), Step 11 (T6→77K(2)), Step 12 (77K(2)→T5) and Step 13 (T5→RT(4)). The strain of the stainless steel was calculated by adding the strain change from Stage 0 (T3,0) to Step 13 (T5→RT). For calculation, the estimated value of F_{SS}^{0}=71.4 N, T0=563K [27], the values listed in Table 4.1 and Equations listed in Table 4.2 were used. The calculation results for Ag, Ag alloy, stainless steel and Bi2223 are presented in figures 4.6 to 4.9, respectively. Following features are read.

(A) Ag (figure 4.6) deforms elastically and plastically in tension and compression, depending on the thermo-mechanical history, due to the low yield strain (0.02%). Such a variation of the strain state of Ag affects on the variation of the strain of other constituents as shown below. It is noted that, when the laminated composite tape is thermally cycled between RT and 77K, the elastic strain of Ag is cycled along RT(3)($-\varepsilon_{Ag,y}$) → T6($+\varepsilon_{Ag,y}$) → 77K(2)($+\varepsilon_{Ag,y}$) → T7($-\varepsilon_{Ag,y}$) → RT(4)($-\varepsilon_{Ag,y}$). The elastic strain of Ag at RT during thermal cycling is always $-\varepsilon_{Ag,y}$. On the other hand, in the case where the tape is cooled from the heat treatment temperature (TH) to RT, the elastic strain of Ag at RT(1) is $+\varepsilon_{Ag,y}$. In this way, the elastic strain of Ag is different even at the same temperature, being dependent on the thermal history.

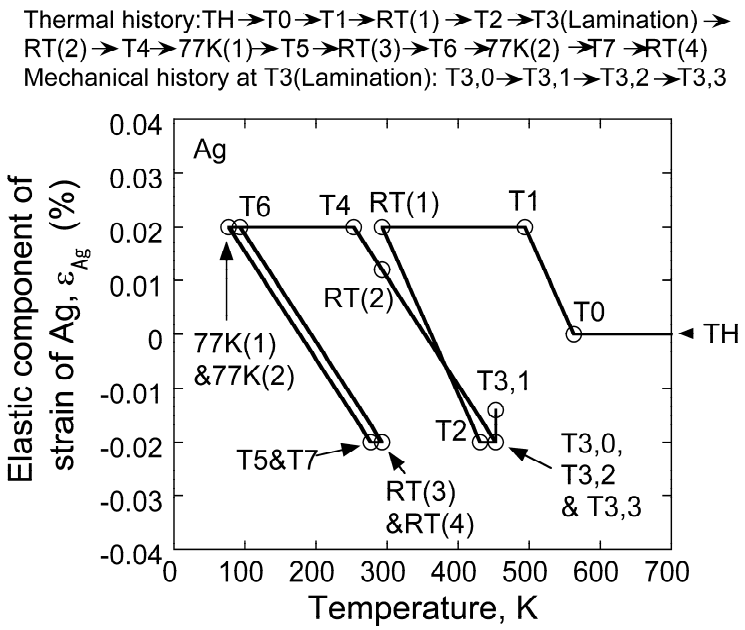

Figure 4.6. Change of elastic component of strain of Ag in the thermo-mechanical history.

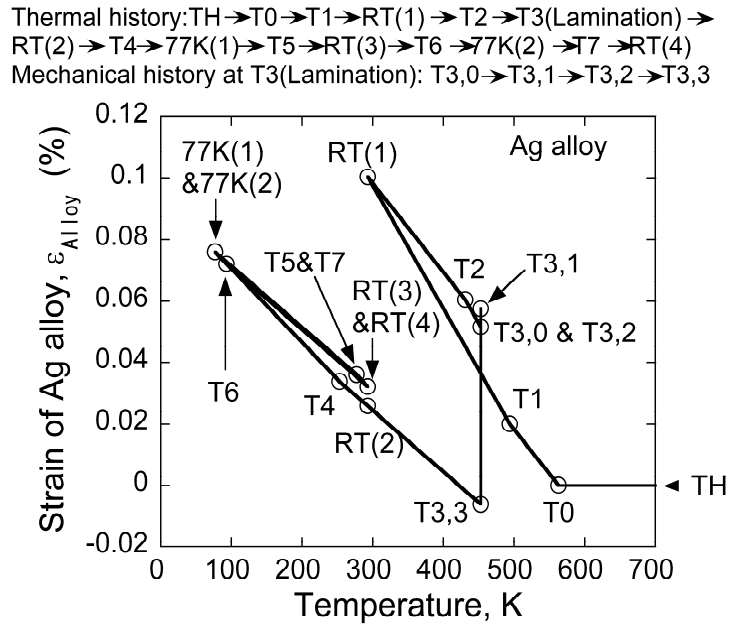

Figure 4.7. Change of strain of Ag alloy in the thermo-mechanical history.

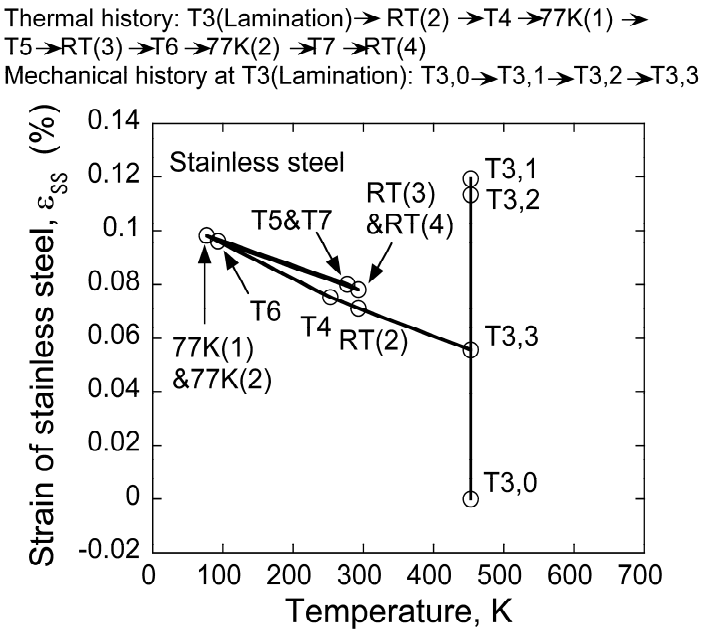

Figure 4.8. Change of strain of stainless steel in the thermo-mechanical history.

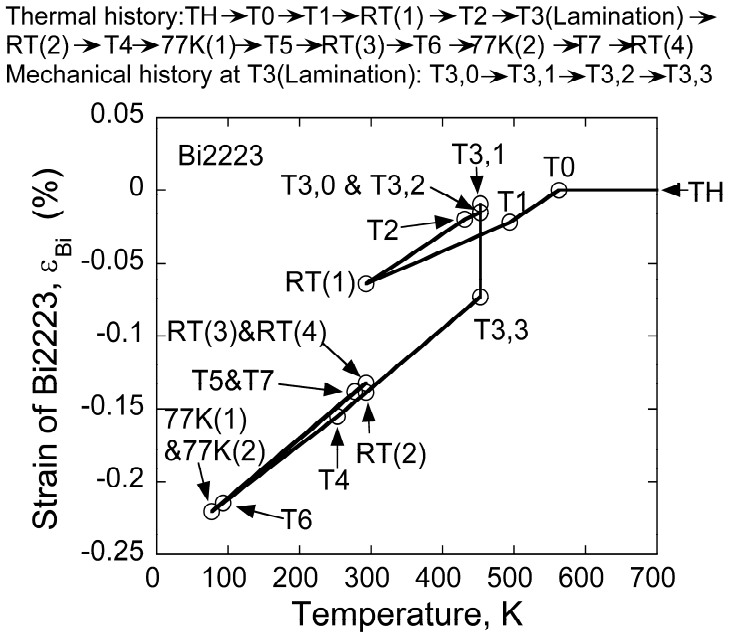

Figure 4.9. Change of residual strain of Bi2223 filaments in the thermo-mechanical history.

(B) The tensile strain is accumulated in Ag alloy in the insert tape with decreasing temperature (figure 4.7). At room temperature RT(1), the strain of Ag alloy becomes 0.100 % when cooled from the heat-treatment temperature. When the tape is heated to the lamination temperature (T3=453K), it decreases to 0.052%. At lamination, the strain becomes 0.058 % at T3,1 due to the applied tensile pre-load (4.5N). Then the strain decreases to -0.006 % at T3,3 due to the load relaxation. During cooling from the lamination temperature, also tensile strain is added due to the higher coefficient of thermal expansion than Bi2223 and stainless steel. The strain becomes 0.026 % at room temperature (RT(2)) and 0.076 % at 77K(1). It is noted that, when the sample is cooled down to 77K(1) and then is heated to RT(3), the strain 0.032% at RT(3) is different from 0.026% at RT(2). This is attributed to the difference in the state of Ag (yielded in tension and compression for the former and latter cases, respectively). When the tape is thermally cycled between RT and 77K, the strain hysteresis of Ag alloy (and also Bi2223 and stainless steel) becomes cyclic (77K(1)→T5→RT(3)→T6→77K(2)), due to the compressive and tensile yielding of Ag at T5 and T6, respectively (figure 4.6).

(C) The stainless steel (figure 4.8) is pulled in tension by 0.119 % for lamination, and it decreases to 0.056 % by the load relaxation after lamination. When the laminated tape is cooled down from the lamination temperature (T3), tensile stress is imposed and the strain at 77K becomes 0.098 %, which is similar to the applied strain 0.119% for lamination.

(D)The strain of Bi2223 (figure 4.9) is practically accumulated below the temperature T0 due to the difference in coefficient of thermal expansion among the constituents. Then the compressive strain increases with decreasing temperature. At room temperature RT(1), the strain of Bi2223 in the insert tape before lamination is -0.064%. When the tape is heated to the lamination temperature T3,0 (=453K), it becomes -0.015%. In advance of the lamination, it is pulled in tension, due to which the strain of Bi2223 becomes -0.009% at T3,1. In the load relaxation process after lamination, Ag deforms first elastically and then plastically in compression. Accordingly, the strain of Bi2223 varies first from T3,1 to T3,2 and then T3,2 to T3,3. It becomes -0.073% at T3,3 after load relaxation process. When the laminated tape is

cooled, the compressive strain increases. At room temperature RT(2), the strain of Bi2223 becomes -0.139 %. When the tape is cooled down to 77K(1) and then heated to room temperature RT(3), the strain of Bi2223 becomes -0.133 %, which is the measured value by the X ray diffraction. In this way, the residual strain varies due to the additional thermal cycle between room temperature and 77K. The reason for this stems from the difference in stress state of Ag (Ag is yielded in tension and in compression in the former and latter cases, respectively.)

Figures 4.10 and 4.11 show the comparison of the variation of the strain in the laminated tape with that in the insert tape alone for Ag alloy and Bi2223, respectively. In the case of bare insert tape, the residual strains of Ag alloy and Bi2223 vary along ABCDEFGHEFG (figure 4.10). In the case of laminated tape, they vary along ABCDIJKJLMNOPQROPQ (figure 4.11).

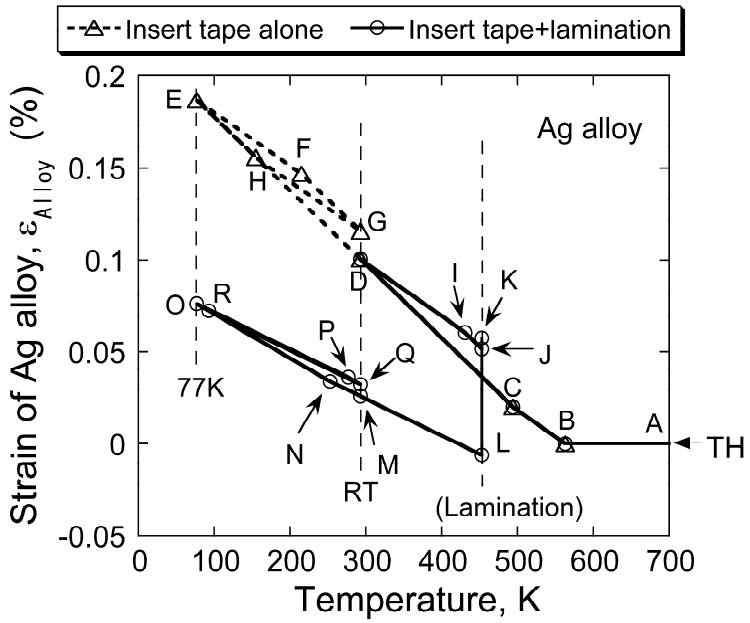

Figure 4.10. Comparison of the residual strain accumulation process of Ag alloy in the laminated tape with that in the insert tape alone.

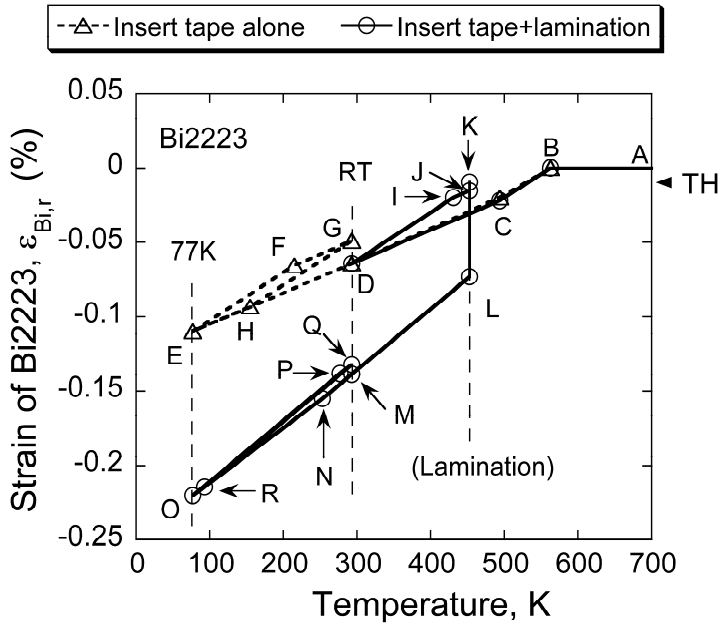

Figure 4.11. Comparison of the residual strain accumulation process of Bi2223 filaments in the laminated tape with that in the insert tape alone.

Three distinct features are found. (1) The residual strains of Ag alloy at room temperature and 77K in the laminated tape are lower than those in the insert tape. The stainless steel lamination acts to reduce the residual strain of Ag alloy. (2) The compressive residual strains of Bi2223 at room temperature and 77K in the laminated tape are higher than those in the insert tape. The stainless steel lamination acts to enhance the compressive residual strain of Bi2223, contributing the high tensile strain tolerance of critical current of the laminated tape. (3) The strain hysteresis of Bi2223 (and Ag alloy also) in the thermal cycling between room temperature and 77K in the laminated tape is smaller than that in the insert tape. The lamination of the insert tape with high modulus stainless steel acts to hide the influence of the change in stress state Ag on the strain of Bi2223 (Ag alloy), reducing the hysteresis.

4.3.5 Effect of lamination on the strain- tolerance of the critical current at 77K

Figure 4.12 shows the measured changes of the normalized critical current I_C/I_{C0} at 77K with applied tensile strain $\varepsilon_{c,T}$ in the insert and laminated tapes, where I_C is the critical current at arbitrary applied tensile strain and I_{C0} is the original current at $\varepsilon_{c,T}$=0. Based on the result shown in figure 4.12, the effect of lamination on the strain tolerance of critical current is to be discussed in this sub-section.

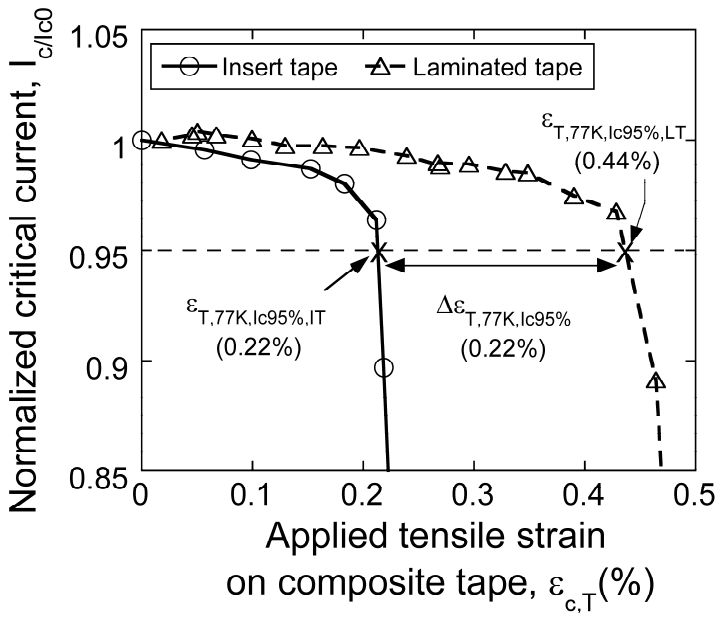

Figure 4.12. Change of normalized critical current I_c/I_{c0} with increasing applied tensile strain $\varepsilon_{c,T}$ at 77K in the insert and laminate tapes.

(A) Improvement of tensile strain tolerance of critical current by lamination.

We note the applied tensile strain on the tape in the early stage of fracture process, at which the critical current is reduced by 5% from the original value (= tensile strain at I_C/I_{C0} =0.95), as $\varepsilon_{T,77K,Ic95\%,IT}$ and $\varepsilon_{T,77K,Ic95\%,LT}$ for insert and laminated tapes, respectively. The measured values of $\varepsilon_{T,77K,Ic95\%,IT}$ and $\varepsilon_{T,77K,Ic95\%,LT}$ were 0.22 and 0.44%, respectively, as shown in figure 4.12. The increase in tensile strain tolerance at I_C/I_{C0} =0.95 by lamination, given by $\Delta\varepsilon_{T,77K,Ic95\%}$ (=$\varepsilon_{T,77K,Ic95\%,LT}$ - $\varepsilon_{T,77K,Ic95\%,IT}$), was

0.22%.

The $\varepsilon_{T,77K,Ic95\%,IT}$ and $\varepsilon_{T,77K,Ic95\%,LT}$ are expressed by [10,12,22,27,28]

$$\varepsilon_{T,77K,Ic95\%,IT} = \varepsilon_{Bi,f,T,77K,IT} - \varepsilon_{Bi,r,77K,IT} \quad \text{for insert tape} \quad (4.27)$$

$$\varepsilon_{T,77K,Ic95\%,LT} = \varepsilon_{Bi,f,T,77K,LT} - \varepsilon_{Bi,r,77K,LT} \quad \text{for laminated tape} \quad (4.28)$$

where $\varepsilon_{Bi,f,T,77K,IT}$ and $\varepsilon_{Bi,f,T,77K,LT}$ are the tensile fracture strains of Bi2223 filaments in the insert and laminated tapes at I_C/I_{C0} =0.95, respectively, and $\varepsilon_{Bi,r,77K,IT}$, (= -0.11% [27]) and $\varepsilon_{Bi,r,77K,LT}$,(=-0.22 % as has been estimated in this work) are the residual strains of Bi2223 filaments in the insert and laminated tape at 77K. The $\varepsilon_{Bi,f,T,77K,IT}$ is estimated to be 0.11% by substituting $\varepsilon_{T,77K,Ic95\%,IT}$= 0.22% and $\varepsilon_{Bi,r,77K,IT}$=-0.11%. If we assume that the tensile fracture strain of Bi2223 filaments in the laminated tape ($\varepsilon_{Bi,f,T,77K,LT}$) is equal to that of the insert one ($\varepsilon_{Bi,f,T,77K,LT}$=$\varepsilon_{Bi,f,T,77K,IT}$=0.11%), the strain tolerance of the laminated tape is calculated to be 0.33%. The calculated value 0f 0.33% is lower than the measured value of 0.44%. Also the lamination effect $\Delta\varepsilon_{T,77K,Ic95\%}$ is calculated to be 0.11%, which is lower than the measured value of 0.22%. This suggests that the increase in tensile strain tolerance of critical current by lamination is not accounted for solely by the increase in residual strain, and the assumption of $\varepsilon_{Bi,f,T,77K,LT}$=$\varepsilon_{Bi,f,T,77K,IT}$ is not valid.

Substituting $\varepsilon_{T,77K,Ic95\%,LT}$=0.44% and $\varepsilon_{Bi,r,77K,LT}$=-0.22% into equation (4.28), we have $\varepsilon_{Bi,f,T,77K,LT}$=0.22% for the laminated tape. The present result suggests that the improvement of tensile strain tolerance of the critical current by lamination, $\Delta\varepsilon_{T,77K,Ic95\%}$ (=$\varepsilon_{T,77K,Ic95\%,LT}$ - $\varepsilon_{T,77K,Ic95\%,IT}$)=0.22%, was caused by the sum of the increase in compressive residual strain ($|\varepsilon_{Bi,f,T,77K,LT} - \varepsilon_{Bi,f,T,77K,IT}|$=0.11%) and that of tensile fracture strain ($\varepsilon_{Bi,f,T,77K,LT} - \varepsilon_{Bi,f,T,77K,IT}$=0.11%). Such a difference in fracture strain of the filaments at I_C/I_{C0} =0.95 between the insert and laminate tapes is considered to be related to the increase in strain tolerance window by lamination reported by Otto et al [1], as follows.

(B) Improvement of strain tolerance window of critical current by lamination.

Otto et al [1] have shown that the strain tolerance window $\Delta\varepsilon_{w95\%Ic}$, defined as the axial strain range from compressive through tensile in which the critical current I_C

remains above 95% of its original level, is increased by lamination with high modulus reinforcing materials such as stainless steel, invar and molybdenum. They have derived an empirical equation for the strain tolerance window in the form [1],

$$\Delta\varepsilon_{w95\%Ic} = 0.0036 f_r E_r + 0.40\ (\%) \tag{4.29}$$

where f_r and E_r are the area fraction and Young's modulus (GPa) of the reinforcement, respectively. The present insert and stainless steel-laminated tapes correspond to f_rE_r=0 and 47.9 GPa, respectively.

Noting the compressive fracture strain of Bi2223 filaments in the insert tape as $\varepsilon_{Bi,f,C,77K,IT}$ and that in the laminated tape as $\varepsilon_{Bi,f,C,77K,LT}$, the strains $\Delta\varepsilon_{w95\%Ic}$ for the insert and laminated tapes are expressed by

$$\Delta\varepsilon_{w95\%Ic,IT} = \varepsilon_{Bi,f,T,77K,IT} - \varepsilon_{Bi,r,77K,IT} - (\varepsilon_{Bi,f,C,77K,IT} - \varepsilon_{Bi,r,77K,IT}) = \varepsilon_{Bi,f,T,77K,IT} - \varepsilon_{Bi,f,C,77K,IT} \tag{4.30}$$

$$\Delta\varepsilon_{w95\%Ic,LT} = \varepsilon_{Bi,f,T,77K,LT} - \varepsilon_{Bi,r,77K,LT} - (\varepsilon_{Bi,f,C,77K,LT} - \varepsilon_{Bi,r,77K,LT}) = \varepsilon_{Bi,f,T,77K,LT} - \varepsilon_{Bi,f,C,77K,LT} \tag{4.31}$$

Equations (4.30) and (4.31) contain no residual strain term. As shown in 4.3.5.1, the increase in compressive residual strain acts to raise the strain tolerance of critical current under applied tensile strain. On the other hand, it acts to reduce the strain tolerance under applied compressive strain. Namely, the positive contribution of the increased compressive residual strain under applied tensile strain is counterbalanced with the negative one under applied compressive strain. Thus, the experimentally observed increase in strain tolerance window in the laminated tape cannot be accounted for by the increase in compressive residual strain. Another mechanism is needed for explanation.

The strain windows $\Delta\varepsilon_{w95\%Ic\ IT}$ and $\Delta\varepsilon_{w95\%Ic,LT}$ for the insert and laminated tapes are calculated to be 0.40 and 0.57% by equation (4.29), respectively. Substituting $\Delta\varepsilon_{w95\%Ic,IT}$=0.40% and $\varepsilon_{Bi,f,T,77K,IT}$=0.11% into equation (4.32), we have $\varepsilon_{Bi,f,C,77K,IT}$=-0.29% for the insert tape, and substituting $\Delta\varepsilon_{w95\%Ic,LT}$=0.57% and $\varepsilon_{Bi,f,T,77K,IT}$=0.22% into equation (4.31), we have $\varepsilon_{Bi,f,C,77K,LT}$=-0.35% for the laminate tape. This result indicates that the lamination raises the tensile fracture strain of Bi2223 filaments from 0.11 to 0.22% and compressive one from -0.29 to -0.35%. In other

words, the lamination acts to suppress the fracture of the Bi2223 filaments under both applied tensile and compressive strains.

Concerning the increase in tensile and compressive fracture strains of the Bi2223 filaments at I_C/I_{C0} =0.95 by lamination, the mechanism is unknown within the present work but the following mechanism might be mentioned from the fracture mechanical viewpoint of the fiber-reinforced metal matrix composites [30,31]. When the weaker Bi2223 filaments are fractured, the stress concentration is induced in the neighboring filaments. Comparing the stress concentration in the neighboring filament intact to the fractured one in the insert tape with that in the laminated tape, the latter can be higher than the former due to the existence of the stainless steel with high modulus. Accordingly, the fracture of the neighboring filaments in the laminated tape tends to be suppressed. On the other hand, the fracture of the weaker filaments tends to induce the fracture of the neighboring filaments in the insert tape. Once the neighboring filaments are fractured in the insert tape, much higher stress concentration is induced on the next neighboring filaments, which causes the fracture of the next neighboring filaments. Due to such a difference in fracture mode of the filaments between the insert and laminated tapes, the more number of filaments that transport superconducting current can survive through in the laminated tape. Such a mechanism could account for the experimentally observed increase in the strain window by lamination from the viewpoint that the lamination acts to change the fracture mode as to retard the reduction in critical current. Such a mechanism is, however, one candidate. Further study is needed for full understanding.

4.4 Conclusions

(1) To describe the thermally induced axial strain changes of the constituents (Bi2223, Ag, Ag alloy and stainless steel) during heating and cooling and mechanically induced strain changes due to the lamination, followed by the stress relaxation, a calculation procedure based on the elastic-plastic mechanics was presented.

(2) The variation of the strain of each constituent in the lamination and

subsequent stress relaxation process and in the heating and cooling process in the stainless steel-laminated Bi2223/Ag/Ag alloy superconducting composite tape, fabricated at American Superconductor Corporation, was calculated by inputting the mechanical property values of the constituents and the residual strain of Bi2223 in the laminated composite at room temperature measured by the X ray diffraction method. It was shown that the stainless steel lamination acts to reduce the residual strain of Ag alloy, to enhance the compressive residual strain of Bi2223 and to retard the fracture of the filaments, contributing the high tensile strain tolerance of critical current of the laminated tape. Also it was shown that the lamination acts to reduce the strain hysteresis of Bi2223 and Ag alloy in the thermal cycling between room temperature and 77K.

References

[1] A.Otto, E. J. Harley, R. Marson, Supercond. Sci. Technol., **18** (2005) S308.

[2] L. J. Masur, D. Buczek, E. Harley, T. Kodenkandath, X. Li, J. Lynch, N. Nguyen, M. Rupich, U. Schoop, J. Scudiere, E. Siegal, C. Thieme, D. Verebelyi, W. Zhang, J. Kellers, Physica C, **392-396** (2003) 989.

[3] M. Buczek, L. J. Masur, P. K. Miles, F. Sivo, D. Marlowe, E. R. Podtburg, D. I. Parker, J. D. Scudiere, P. Metra, M. Nassi, M. Rahman, D. W. Von Dollen, IEEE Trans. Appl. Supercond., **7** (1997) 2196.

[4] A. Salazar, J. K. Pastor, J. Llorca IEEE Trans. Appl. Supercond., **14** (2004) 1941.

[5] C. G. King, D. A. Grey, A. Mantone, K. Herd, E. T. Laskaris, IEEE Trans. Appl. Supercond., **7** (1997) 2046.

[6] J. P. Voccio, O. O. Ige, S. J. Young, C. C. Duchaine, IEEE Trans. Appl. Supercond., **11** (2001) 3070.

[7] S. Ochiai, K. Hayashi, K. Osamura, Cryogenics, **33** (1993) 976.

[8] S. Ochiai, K. Hayashi, K. Osamura, Cryogenics, **32** (1992) 799.

[9] S. Ochiai, T. Ishida, D. Doko, K. Morishita, H. Okuda, S. S. Oh, D. W. Ha, M. Hojo, M. Tanaka, M. Sugano, K. Osamura, Supercond. Sci. Technol., **18** (2005) S232.

[10] S. Ochiai, T. Nagai, H. Okuda, S. S. Oh, M. Hojo, M. Tanaka, M. Sugano, K. Osamura, Supercond. Sci. Technol., **16** (2003) 988.

[11] W. R. Blumenthal, R. A. Moore, J. Y. Coulter, J. F. Bingert, K. V. Salazar, J. Electron. Mater., **24** (1995) 1805.

[12] K. Osamura, M. Sugano, K. Matsumoto, Supercond. Sci. Technol., **16** (2003) 971.

[13] A. Nyilas, K. Osamura, M. Sugano, Supercond. Sci. Technol., **16** (2003) 1036.

[14] H. Okuda, K. Morishita, S. Ochiai, D. Doko, M. Matsui, H. Fujimoto, M. Sato, Physica C, **411** (2004) 114.

[15] M. Hojo, M. Nakamura, T. Matsuoka, M. Tanaka, S. Ochiai, M. Sugano, K. Osamura, Supercond. Sci. Technol., **16** (2003) 1043.

[16] J. W. Ekin, D. K. Finnemore, Q. Li, J. Tenbrink, W. L. Carter, Appl Phys Lett., **61** (1992) 858.

[17] B. Ullmann, A. Babler, M. Quilitz, W. Goldacker, IEEE Trans. Appl. Supercond., **7** (1997) 2042.

[18] S. Salib, C. Vipulananandan, Metr. Res. Bull., **32** (1997) 1333.

[19] B. ten Haken, A. Beuink, H. ten Kate, IEEE Trans. Appl. Supercond., **7** (1999) 2043.

[20] H. Kitaguchi, K. Itoh, H. Kumakura, T. Takeuchi, K. Togano, W. Wada, IEEE Trans. Appl. Supercond., **11** (2001) 3058.

[21] R. T. Aloysius, A. Sobha, P. Guruswamy, U. Samaprasad, Supercond. Sci. Technol., **14** (2001) 85.

[22] R. Passerini, M. Dhallé, E. Giannini, G. Witz, B. Seeber, R. Flükiger, Physica C, **371** (2002) 173.

[23] S. J. Sun, W. Liu, X. P. Chen, M. Y. Li, Z. Han, Supercond. Sci. Technol., **16** (2003) 984.

[24] K. Katagiri, H. S. Shin, K. Kasaba, T. Tsukinokizawa, K. Hiroi, T. Kuroda, K. Itoh, H. Wada, Supercond. Sci. Technol., **16** (2003) 995.

[25] H. S. Shin, K. Katagiri, Supercond. Sci. Technol., **16** (2003) 1012.

[26] H. J. N. van Eck, D. C. van der Laan, M. Dhallé, B. ten Haken, H. H. J. ten Kate, Supercond. Sci. Technol., **16** (2003) 1026.

[27] S. Ochiai, H. Rokkaku, K. Morishita, J. K. Shin, S. Iwamoto, H. Okuda, M. Hojo, K. Osamura, M. Sato, A. Otto, J. Harley, A. Malozemoff, Supercond. Sci. Technol., **20** (2007) 202.

[28] S. Ochiai, T. Matsuoka, J. K. Shin, H. Okuda, M. Sugano, M. Hojo, K. Osamura, Supercond. Sci. Technol., **20** (2007) 1076.

[29] Metals Handbook 8^{th} edition, 1961 Vol.1, Properties and Selection of Metals, American Society for Metals, Metals Park, Ohio, 1961, p423.

[30] J. L. Houpert , S. L. Phoenix, R. Raj, Acta Metall. Mater., **42** (1994) 4177.

[31] S. Ochiai, M. Hojo, J. Mater. Sci., **31** (1996) 3861.

Chapter 5

Local and overall critical current of Bi2223-composite tape under applied tensile and bending strains

5.1 Introduction

The high temperature superconductor composite tapes have been studied extensively for application to the power cables, linear motor cars and so on. The fracture strain of Bi2223 filaments, which are the path of superconducting current transportation are, however, around 0.1~0.2% [1-5], being much lower than that of Nb_3Sn (0.5-1.2%) [6,7] and Nb_3Al (0.6-1.0%) [8]. For industrial application, the study on the fracture behavior and its relation to superconducting property is needed.

It is well known that the critical current decreases beyond an irreversible strain under tensile, compressive and bending strains due to the damage evolution in the filaments [1-17]. It is noted that the strength of the Bi2223 filaments embedded in the composite are different to each other; namely the composite is inhomogeneous from the mechanical viewpoint. Actually, the damage takes place non-uniformly within a sample, due to which the critical current value is different from position to position within the sample [2,4,18]. In the present work, the variation of local critical current I_C and n-value along the sample length and its relation to the overall I_C and n-value under tensile and bending strains were studied.

5.2 Experimental procedure

The multifilamentary Bi2223 composite tape consisting of Bi2223 filaments, Ag and Ag-alloy, fabricated at Korea Electrotechnology Research Institute, were used for tests. It contained 55 Bi2223 filaments. The composite tape had a thickness of 0.23mm and a width of 4.9mm. The volume fractions of Bi2223, Ag, and Ag-alloy were 0.38, 0.32 and 0.30, respectively.

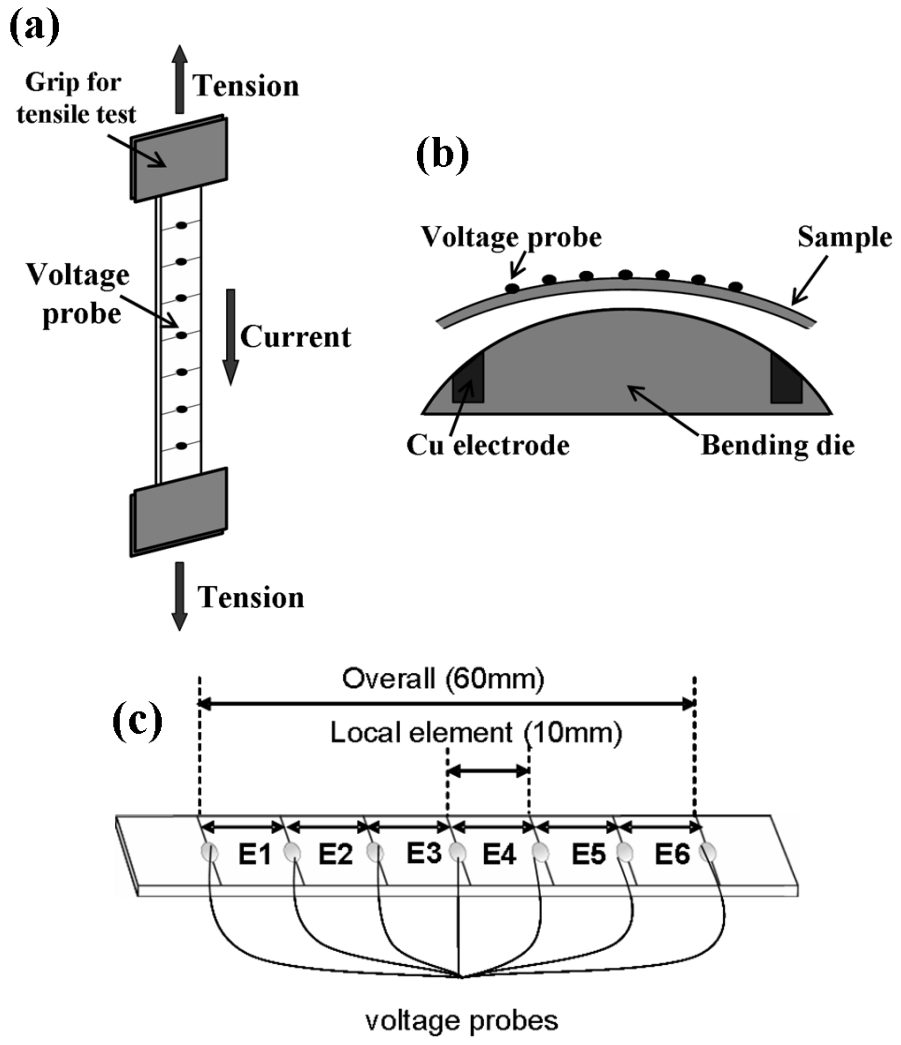

Figure 5.1. Schematic illustrations of critical current I_C measurement (a) sample set in tensile method, (b) sample set in bending method and (c) variations of local elements (1cm) and overall (6cm) of I_C (and n-value) along the sample length.

Tensile test (schematically illustration as shown figure 5.1(a)) in was carried out with an Instron type tensile testing machine (NMB TCM-500) at liquid nitrogen temperature, 77K. The indium plates were attached to both ends of the tape for preventing from breakage in the grips. The strain was measured with a couple Nyilas type extensometer [17], which was directly attached to the sample with a 25mm gauge length. On the other hand, the bending strain was applied to the sample at room temperature by the bending dies (schematically illustration as shown figure 5.1(b)) with different curvatures (R=∞(straight dies), 61.6, 34.0, 22.3, 17.3 and 13.8mm, corresponding to the bending strain 0, 0.19, 0.34, 0.52, 0.66 and 0.83%, respectively). The assembly of the sample and the bending dies was cooled to 77K, and the I_C –measurement was carried in the bent state.

The I_C and n-value were measured at 77K in a self magnetic field. It is noted again that the sample was damaged at 77K under the tensile strain and it was damaged at room temperature under bending strain. In order to detect the local variation of I_C and n-value along the length and its relation to overall I_C and n-value, the voltage probes were attached in a step of 10mm on an overall sample with a 60 mm length, as shown in figure 5.1(c). The critical current was estimated with a criterion of 1μV/cm. The relation of voltage (V) and current (I) near the critical point was approximately by

$$V=A\cdot I^n \tag{5.1}$$

The n-value, referring to the sharpness of the transition from superconductor to normal conducting state, was estimated for the range of V=0.1 to 10μV/cm.

5.3 Results and discussion

5.3.1 Estimation of the irreversible strain and critical current determining factor “fracture strain (ε_f)–residual strain (ε_r)” along the sample length for tensile and bending strains

In the tensile test result, the normalized I_C/I_{C0} values, where I_{C0} is the critical current at ε_T=0%, decreased slightly with increasing strain even below the irreversible strain. Such a strain dependence of the critical current below the irreversible strain has been observed also for other fabrication route-Bi2223 composite tape and has been

attributed to the intrinsic strain effect [19]. The relation of I_C/I_{C0} to the tensile strain ε_T in the non-damaged region was expressed by I_C/I_{C0}=1-0.09·ε_T(%) empirically. After the damage of filament arose, the I_C/I_{C0} values were significantly reduced with increasing strain. In the present work, the relation of the measured I_C/I_{C0}-ε_B relation was expressed by the two order polynomial and the irreversible strain $\varepsilon_{T,irr}$ under tensile strain was estimated to the 0.27% as the strain at which the measured I_C/I_{C0} became lower by 0.01 than the value of I_C/I_{C0}=1-0.09·ε_T(%), as shown in figure 5.2(a). It is noted that the irreversible strain under the tensile strain is given by ε_f–ε_r where ε_f is the intrinsic tensile fracture strain of Bi2223 filament and ε_r is the residual strain of Bi2223 in the current transportation direction [2,4,5]. The variation of ε_f–ε_r of the local elements under tensile strain is presented in figure 5.3(a). The variation of ε_f–ε_r under bending strain was estimated as follows.

The bending strain ε_B (defined by the strain of the outer surface of the composite tape in the tensile side) was given by

$$\varepsilon_B = t / (2R) \tag{5.2}$$

where R is the radius of the die and t is the thickness of the sample(0.23mm). In order to describe the relation of critical current to bending strain, the model proposed in our former work [5] was applied. According to this model, the normalized critical current I_C/I_{C0} is given as a function of ε_B as follows.

(a) $\varepsilon_B < \varepsilon_{B,irr}$, where $\varepsilon_{B,irr}$ is the irreversible bending strain. The $\varepsilon_{B,irr}$ is given by $(\varepsilon_f-\varepsilon_r)/V_{SC}$ [5], where V_{SC} is the volume fraction of the current-transporting core given by the sum of the volume fraction of Bi2223 filaments (0.38) and Ag (0.32) in the present sample. In this range, as no damage arises, the I_C/I_{C0} is unity.

(b) $\varepsilon_B > \varepsilon_{B,irr}$. The I_C/I_{C0} decreases with increasing ε_B. When the damages occur only in tensile side, I_C/I_{C0} is given by [5]

$$I_C/I_{C0} = (1/2)[1+\{(\varepsilon_f-\varepsilon_r)/(\varepsilon_B V_{SC})\}] \tag{5.3}$$

If the damages occur in both tensile and compressive side, other expression is given [5], but it is not the present case. Then, the ε_f-ε_r was estimated as to fit the experimentally observed overall critical current–bending strain curve for ε_B>0.34% where damage took place. The best fit value of ε_f-ε_r was 0.21% from which the $\varepsilon_{B,irr}$(=$(\varepsilon_f-\varepsilon_r)/V_{SC}$) was estimated to be 0.30%. With this value, the measured I_C/I_{C0}-ε_B relation of the overall

sample was described well as shown in figure 5.2(b). The variation of ε_f–ε_r of the local elements under bending strain is presented in figure 5.3(b). The ε_f-ε_r values are also different among the local elements as well as those under tensile strain.

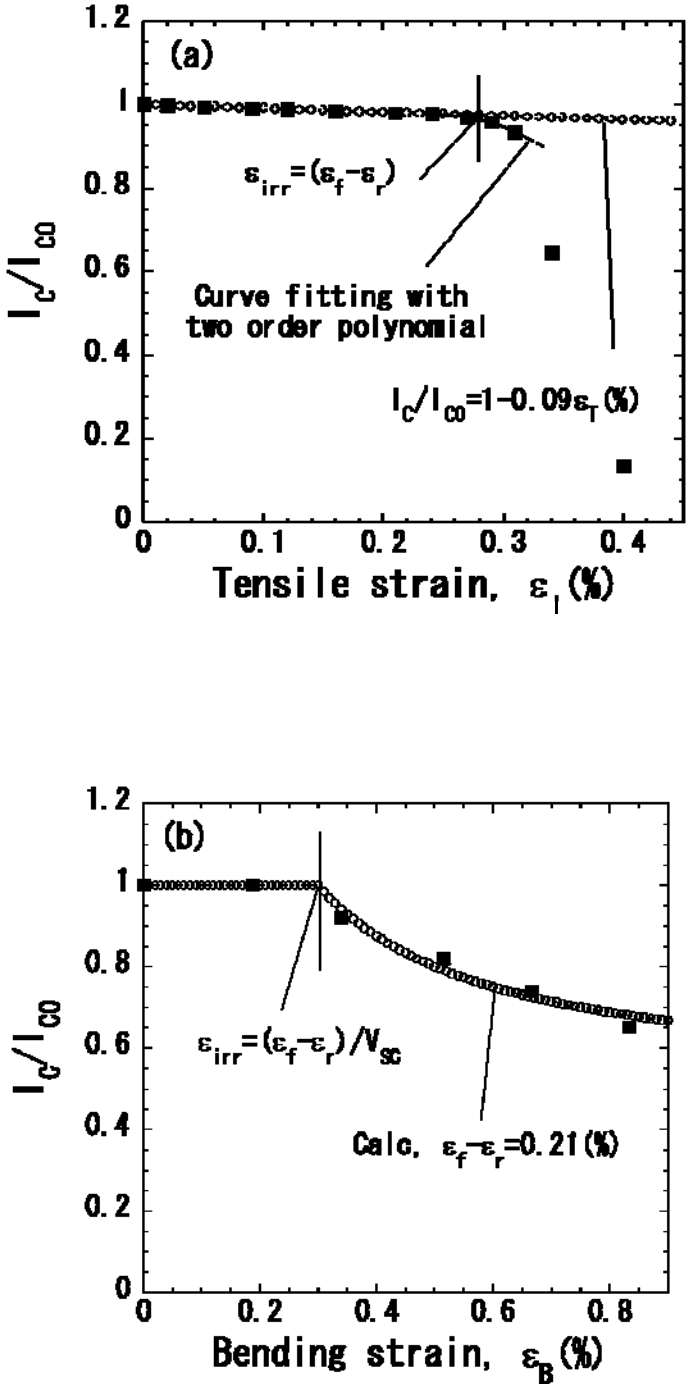

Figure 5.2. Estimation of the irreversible strain under (a) tensile and (b) bending strains.

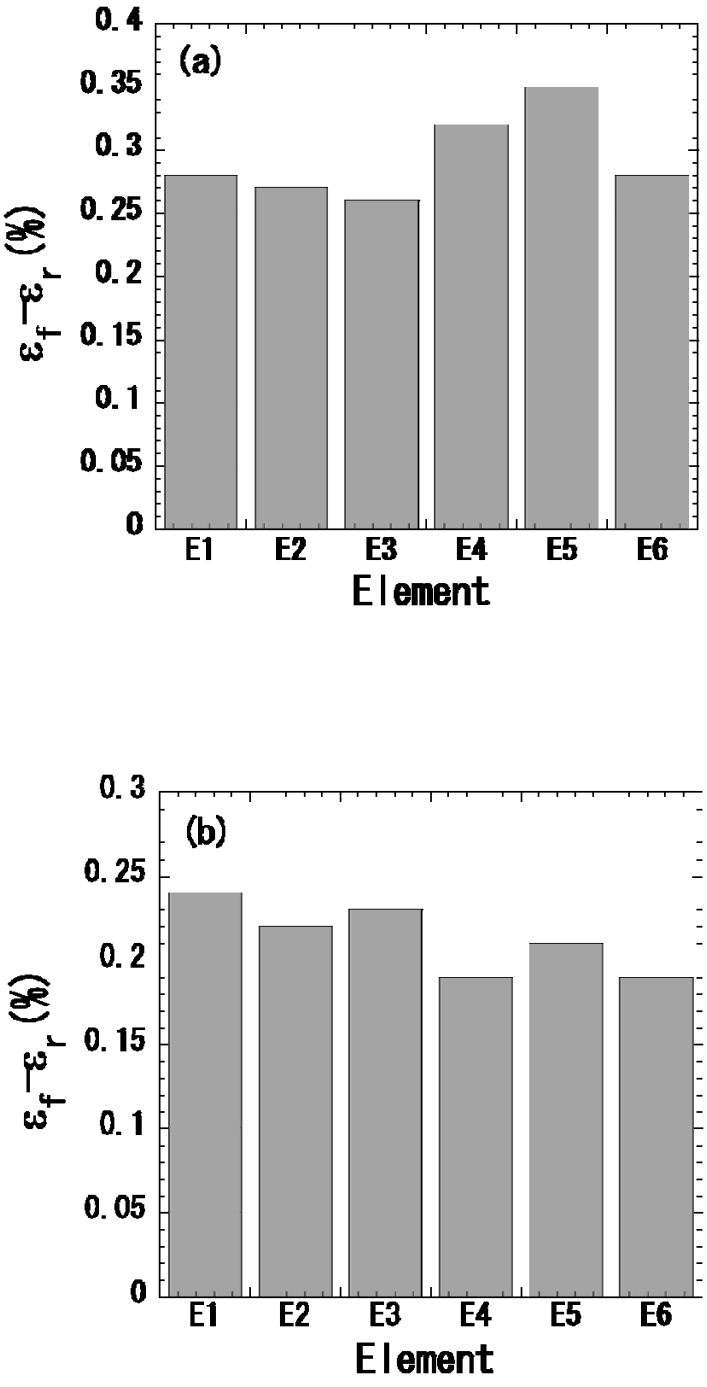

Figure 5.3. Variation of the irreversible strain along the sample length under (a) tensile and (b) bending strains.

5.3.2 Comparison of the *V-I* curve of tensile-strained sample with that of bending-strained one

Figures 5.4 and 5.5 show examples of the voltage(V)-current(I) curve of the overall sample and each element near the transition from superconductor to normal conductor under tensile (ε_T) and bending (ε_B) strains, respectively. Before the application of strain (ε_T=0% (figure 5.4(a)) and ε_B=0% (figure 5.5(a))), the difference in *V-I* curve among the local elements was small for both strains. The voltage of each element contributed almost evenly to the overall voltage in the original state. However, once damage took place, the difference in generated voltage and critical current among the local elements became large, as shown below. The extent of such a difference under tensile strain was larger than that under bending strain.

As described in 5.3.1, the irreversible strain of overall sample under tensile strain ($\varepsilon_{T,irr}$) was 0.27% and that under bending one ($\varepsilon_{B,irr}$) was 0.30%. The *V-I* curves at a tensile strain 0.34%, which is by 0.07% higher than the irreversible strain 0.27%, is shown in figure 5.4(b). Some elements showed severe reduction in critical current. Such elements generated higher voltage than other elements retaining the original critical currents. In this way, the difference in critical current among the local elements was very large under tensile strain. The *V-I* curves of the elements at the bending strain 0.83%, which is by 0.53% higher than the irreversible strain 0.30%, is shown in figure 5.5(b). The *V-I* curve for overall sample and each element shift to the lower critical current region in a similar manner. Namely, the difference in critical current among the local elements was small, implying the small difference in damage extent among the elements under bending strain.

5.3.3 Features of variation of I_C and n-value of local elements as a function of applied tensile and bending strains

Figures 5.6(a) and 5.6(b) show the change of local and overall critical currents with increasing (a) tensile and (b) bending strains, respectively. The local I_C values (and n-values) were not so much different to each other at 0% strain as shown in figures 5.4 to 5.6. Such a situation continued up to the onset strain of the damage (irreversible strain). Beyond the irreversible strain, the change of I_C with increasing applied tensile strain was quite different from that under bending as follows.

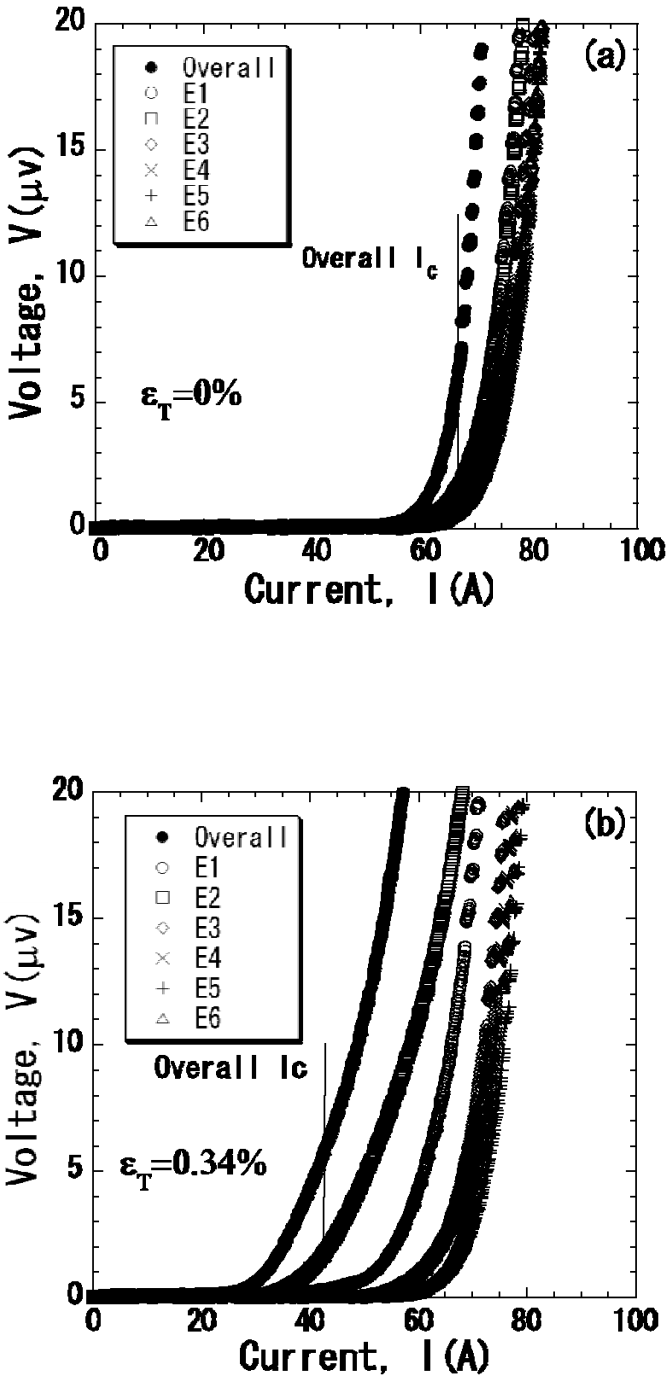

Figure 5.4. Measured *V-I* curves for the overall sample and local elements under tensile strain, ε_T (a) 0% and (b) 0.34%.

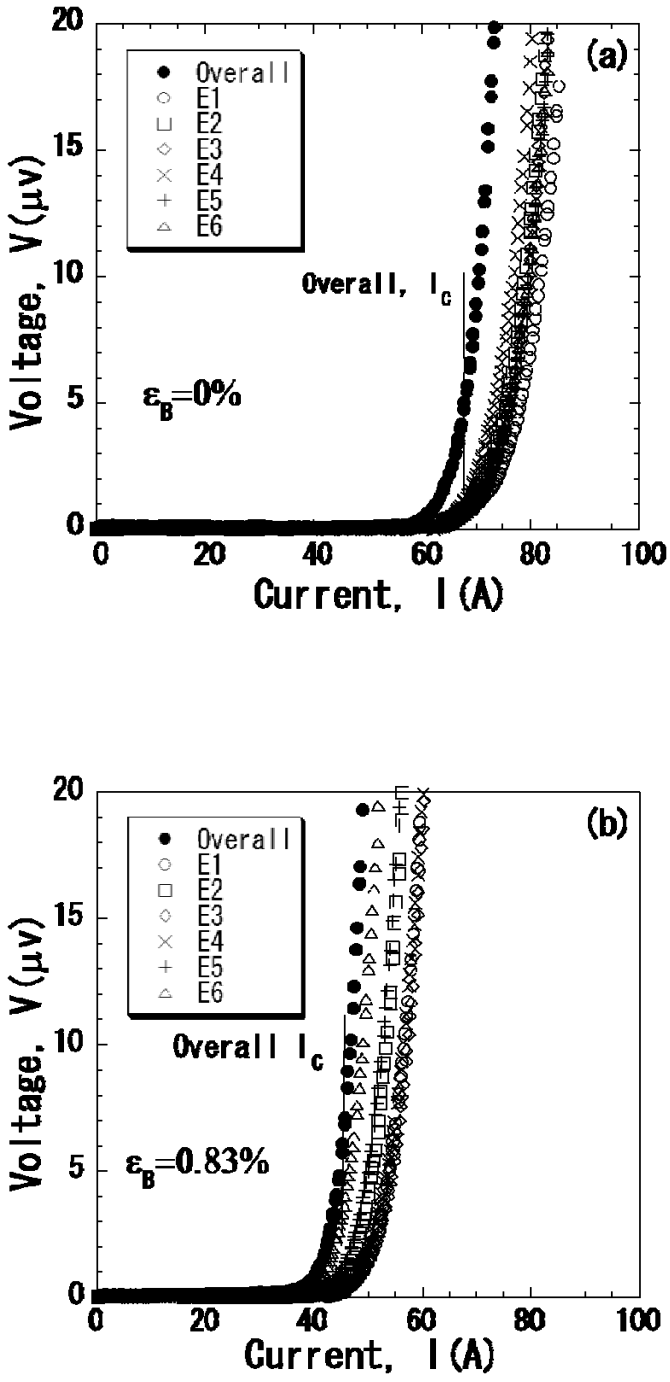

Figure 5.5. Measured *V-I* curves for the overall sample and local elements under bending strain, ε_B (a) 0% and (b) 0.83%.

In the case of tensile strain (figure 5.6(a)), the overall critical current beyond the irreversible strain was reduced seriously (from 64.7A at ε_T=0.27% to 9.0A at ε_T=0.4%). In this process, the critical current was not reduced in some local elements (E3, E4, E5 and E6) but was reduced seriously in other local elements (E1 and E2) at ε_T=0.34%, suggesting the big difference in damage among the local elements. With further increase in applied strain, the elements that had survived at 0.34% were also damaged but the local elements E5 and E6 had still high critical current level even at ε_T=0.4%. In this way, the more and less damaged local elements co-existed up to high strain in the case of tensile strain.

On the other hand, under the bending strain (figure 5.6(b)), the critical current beyond the irreversible strain 0.30% decreased rather gradually with increasing strain in all elements and also in overall sample in comparison with that under tensile strain. With further increasing bending strain, critical currents decreased more but gradually up to 0.83%. On this way, the difference in critical current among the elements under bending strain was much smaller than that under tensile one.

5.3.4 Description of the overall I_C and n-value from the distributed I_C- and n-values of the local elements

As the overall sample can be regarded to be composed of a series circuit of local elements (figure 5.1(c)), the overall voltage can be expressed by the sum of the voltage of the constituting local elements. Applying a simple voltage summation approach [2], the overall voltage V(overall) is expressed as

$$V(\text{overall}) = \Sigma\{(I/I_C(\text{i})\}^{n(\text{i})} \qquad (5.4)$$

Setting V(overall) =6μV, and substituting the measured values of I_C(i) and n(i) of each element into equation (5.4), the overall I_C(overall) for 1μV/cm criterion was calculated. Also, n(overall) was estimated by fitting the curve $\Sigma\{I/I_C(\text{i})\}^{n(\text{i})}$ to A(overall)$I^{n(\text{overall})}$ in the range of V=0.6 to 60 μV.

The calculation results are superimposed in figure 5.6. The measured and calculated overall values were in good agreement. In this way, the measured overall critical currents and n-value were described well with voltage summation model for both tensile and bending strains, despite the difference in damage process.

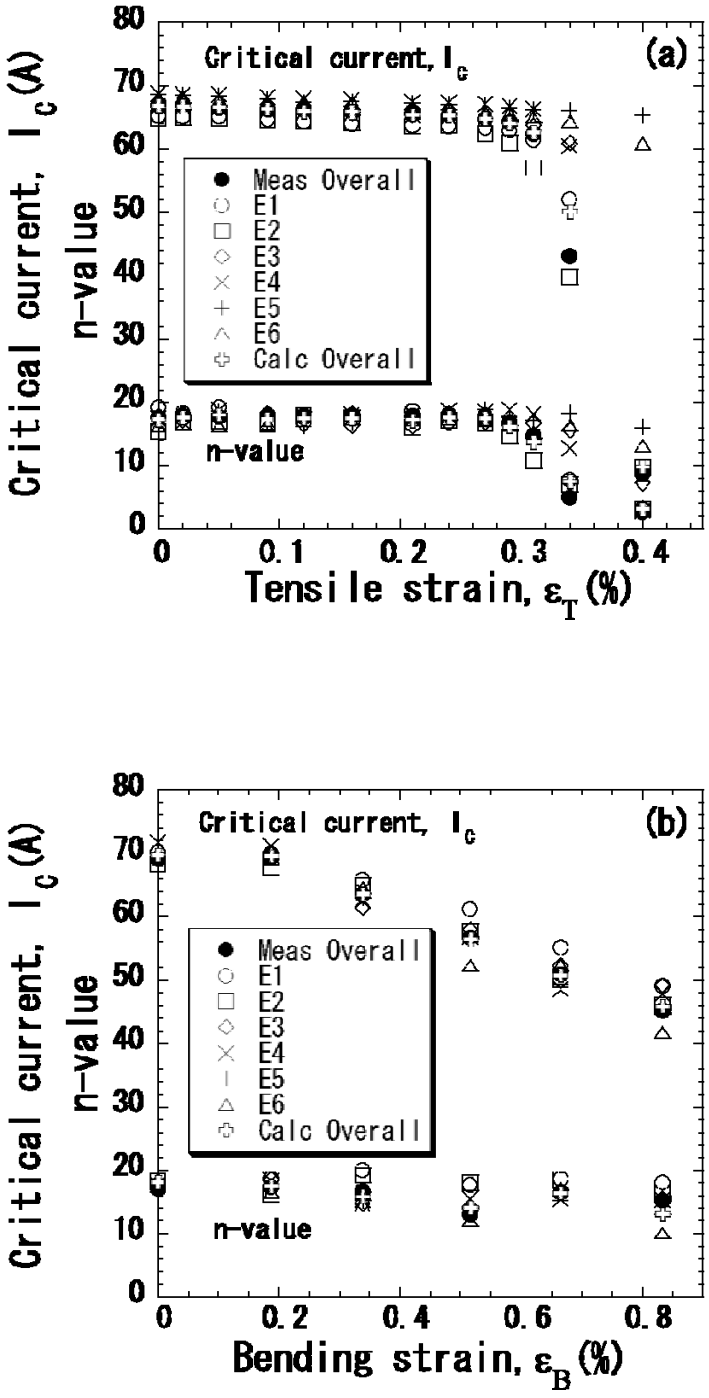

Figure 5.6. Variation in critical current and n-value of overall sample and local elements under (a) tensile and (b) bending strains.

5.3.5 Description of the variation of the I_C/I_{C0}-ε_B curve of the bent overall sample from the ε_f–ε_r value by the tensile test

As shown above, the (ε_f-ε_r) values estimated from the change of I_C/I_{C0} with applied tensile and bending strain were 0.27% and 0.21%, respectively. There is a difference by 0.06% between them. Such a difference is attributed to the difference in temperature at which damage was given as follows. In the present work, the bending strain was given at room temperature, while the tensile strain was given at 77K. Thus, the temperature to cause damage is different between the tensile- and bending-strained samples.

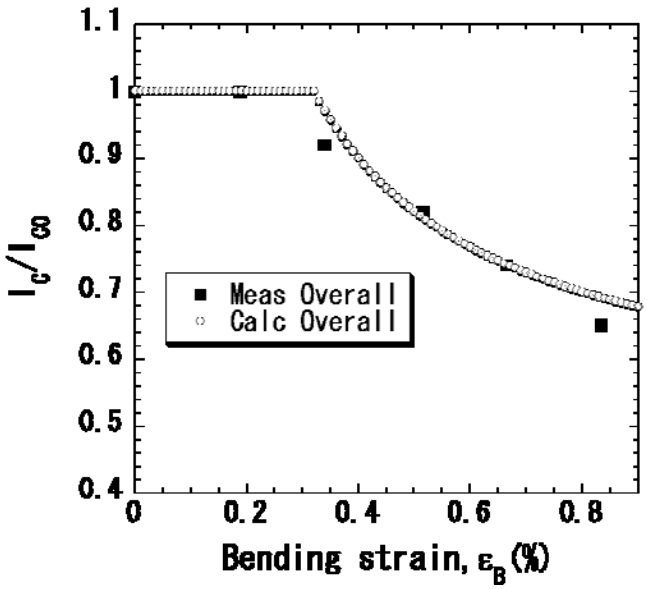

Figure 5.7 Measured and simulated variation of I_C/I_{C0} for the overall sample with increasing bending strain.

The difference in residual strain of Bi2223, $\Delta\varepsilon_r$, for the temperature difference ΔT is evaluated by $\Delta\varepsilon_r=(\alpha_c-\alpha_{Bi})\Delta T$, where α_c and α_{Bi} are the coefficient of thermal expansion of the composite as a whole and Bi2223 filament, respectively [4]. Substituting α_c= 13.4*10^{-6}K^{-1} [4], α_{Bi}=11.0*10^{-6}K^{-1} [4] and ΔT= -221K (from 298K (room temperature) to 77K), we have ε_r= -0.05%. This means that the ε_r value at room temperature is equal to "ε_r at 77K +0.05%". This calculation result accounts well for the

experimentally observed difference (0.06%) of the ε_f-ε_r value between the tensile- and bending- strained samples. This result implies that the variation of I_C/I_{C0}-ε_B relation of the sample damaged by bending at room temperature can be predicted by converting the ε_f–ε_r value at 77K under tensile strain to that at room temperature.

The ε_f-ε_r value at room temperature was calculated by subtracting 0.05% from the ε_f-ε_r value at 77K (0.27%) of the tensile strained sample. The irreversible bending strain, $\varepsilon_{B,irr}$, was calculated to be 0.31% being close to the measured value 0.30%. Then taking I_C/I_{C0} = 1 for $\varepsilon_B<\varepsilon_{B,irr}$, and calculating I_C/I_{C0} by equation (5.3) for $\varepsilon_B>\varepsilon_{B,irr}$, we had the I_C/I_{C0}-ε_B relation, as shown in figure 5.7. The experimentally measured I_C/I_{C0}-ε_B relation is described satisfactorily.

5.4 Conclusions

(1) The local I_C and n-value varied along the length of the overall sample under both tensile- and bending-strains. The damage extent was quite different between the tensile and bending strains.

(2) The overall current and n-value under both tensile- and bending- strains were described well with a voltage summation model from those of the short constituting elements, although the damage behavior under tensile strain was different from that under bending one.

(3) The critical current determining parameter "fracture strain (ε_f) – residual strain (ε_r)" of the local elements and overall sample was estimated for the tensile- and bending-strained samples. Corresponding to the coexistence of no damaged and severely damaged local elements within the overall sample, the parameter value was different from element to element under both tensile and bending strains.

(4) It was attempted to describe the critical current- bending strain relation of the sample damaged at room temperature from the critical current– tensile strain relation of the sample damaged at 77K. The experimentally measured critical current- bending strain relation was described satisfactorily.

References

[1] J. W. Ekin, D. K. Finnermore, Q. Li, J. Tenbrink, W. Carter, Appl. Phys. Lett., **61** (1992) 858.

[2] S. Ochiai, K. Hayashi, K. Osamura, Cryogenics, **33** (1993) 976.

[3] M. Suenaga, Y. Fukumoto, P. Haldar, T. R. Thurston, U. Wildgruber, Appl. Phys. Lett., **67** (1995) 3025.

[4] S. Ochiai, T. Nagai, H. Okuda, S. S. Oh, M. Hojo, M. Tanaka, M. Sugano, K. Osamura, Supercond. Sci. Technol., **16** (2003) 988.

[5] S. Ochiai, N. Miyazaki, D. Doko, T. Nagai, M. Nakamura, H. Okuda, S. S. Oh, M. Hojo, M. Tanaka, K. Osamura, J. Nuclear Mater., **329-333** (2004) 1585.

[6] M. Hojo, M. Nakamura, T. Matsuoka, M. Tanaka, S. Ochiai, M. Sugano, K. Osamura, Supercond. Sci. Technol., **16** (2003) 1043.

[7] S. Ochiai, K. Osamura, K. Watanabe, J. Appl. Phys., 74 (1993) 440.

[8] S. Ochiai, S. Nishino, M. Hojo, K. Watanabe, Supercond. Sci. Technol., **8** (1995) 863.

[9] S. Ochiai, T. Sawada, S. Nishino, H. Sekino, M. Hojo, Y. Yamada, K. Hayashi, N. Ayai, M. Koganeya, M. Ono, J. Mater. Sci. Lett., **18** (1999) 137.

[10] H. J. N van Eck, D. C. van der Laan, M. Dhalle, B ten Haken, H. H. J. ten Kate, Supercond. Sci. Technol., **16** (2003) 1026.

[11] H. S. Shin, K. Katagiri, Supercond. Sci. Technol., **16** (2003) 1012.

[12] A. Otto, L. J. Masur, J. Gannon, E. Podtburg, D. Daly, G. J. Yurek, A.P. Malozemoff, IEEE Trans. Appl. Supercond., **3** (1993) 915.

[13] B. ten Haken, A. Beuink, H.H.J. ten Kate, IEEE Trans. Appl. Supercond., **7** (1997) 2034.

[14] S. L. Bray, J. W. Ekin, C. C. Clicker, J. Appl. Phys., **88** (2000) 1178.

[15] R.L. Holtz, IEEE Trans. Appl. Supercond., **11** (2001) 3238.

[16] R. Passerini, M. Dhalle', E. Giannini, G. Witz, B. Seeber, R. Flükiger, Physica C, **371** (2002) 173.

[17] A. Nyilas, K. Osamura, M. Sugano, Supercond. Sci. Technol., **16** (2003) 1036.

[18] S. Ochiai, D. Doko, H. Okuda, S.S. Oh, D.K. Ha, Supercond. Sci. Technol., **19** (2006) 1097.

[19] K. Osamura, M. Sugano, K. Mtaumoto, Supercond. Sci. Technol., **16** (2003) 971.

Chapter 6

Direct measurement of difference in local deformation and its influence on critical current in Bi2223/Ag/Ag alloy composite tape

6.1 Introduction

During fabrication and application, the superconductor composite materials are subjected to mechanical and electromagnetic stresses, leading to the degradation of the superconducting property. It is well known that critical current (hereafter notes as I_C) at cryogenic temperatures such as 4.2K and 77K is reduced irreversibly for the fracture of filaments beyond the irreversible strain [1-4]. As has been reported [5,6], the strength of the superconducting filaments is scattered from sample to sample. This means that, under the applied strain, the I_C in the local portions are also different to each other. The I_C of the overall sample consisting of local portions is affected by such a local behavior. It is important to understand the difference in damage evolution and local I_C among the local portions in order to deign and fabricate the superconducting materials.

It has been reported the location-dependent variations in I_C under tensile and bending strains [7-9]. The bending strain can be applied uniformly with the sample holder up to high strain level [7-10]. However, in the case of tensile strain experiment, the strain of the sample is not uniform along the sample length direction, while the stress is constant at each cross-section. Experimentally, the measured strain is the average value within the coverage range by the strain measurement apparatus [11]. Therefore, it has not been precisely found the strain variance of short sample and its

relation to that of overall sample consisting of short local portions, beyond the irreversible strain. In the present work, the variation of local I_C under localized strain along the sample length and its relation to the overall I_C under applied strain were studied.

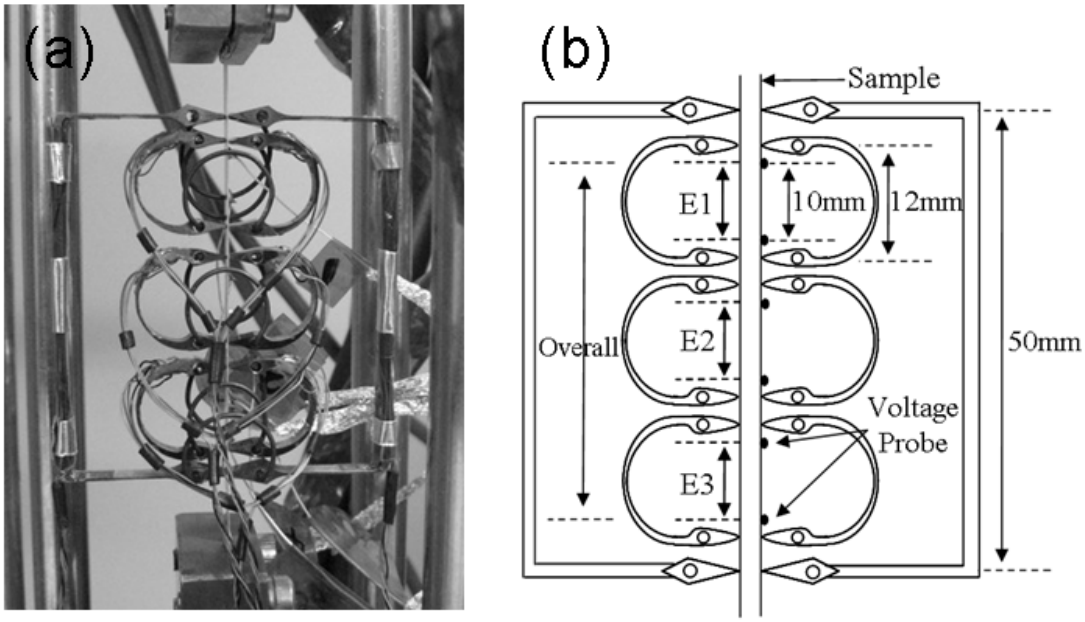

Figure 6.1. Illustration of the strain extensometers under applied tensile strain
(a) sample set in tensile testing apparatus and (b) measurement of local and overall I_C.

6.2 Experimental procedure

The 55 multi-filamentary Bi2223 filaments/Ag/Ag alloy composite tape fabricated by power-in-tube method at Korea Electrotechnology Research Institute (KERI) was used for tests. The composite tape sample of KERI had a thickness and width of 0.23mm and 4.9mm, respectively.

Tensile test was carried out using an Instron type tensile testing machine (NMB TCM-500) at 77K. To reduce the stress concentration at the grips, the indium plates were inserted between the tape and grips. In order to clarify the local strain and its influence to the overall strain, four couples of very light Nyilas type extensometers,

which was newly designed for the present work, were attached directly to the sample with small (12mm) and large (50mm) gauge length as shown in figure 6.1(a). The weight of the small extensometer to measure the local strain was 0.5gram and that of the large one to measure the overall sample was 1.6gram. The I_C was measured at 77K in a self magnetic field. In order to detect the local and overall variation of I_C along the length, the voltage probes were attached in a step of 10mm on an overall sample with a 40 mm length, as shown in figure 6.1(b). The I_C was estimated with a criterion of $1\mu V$/cm.

6.3 Results and discussion

6.3.1 Distribution of strain of each portion with increasing applied stress

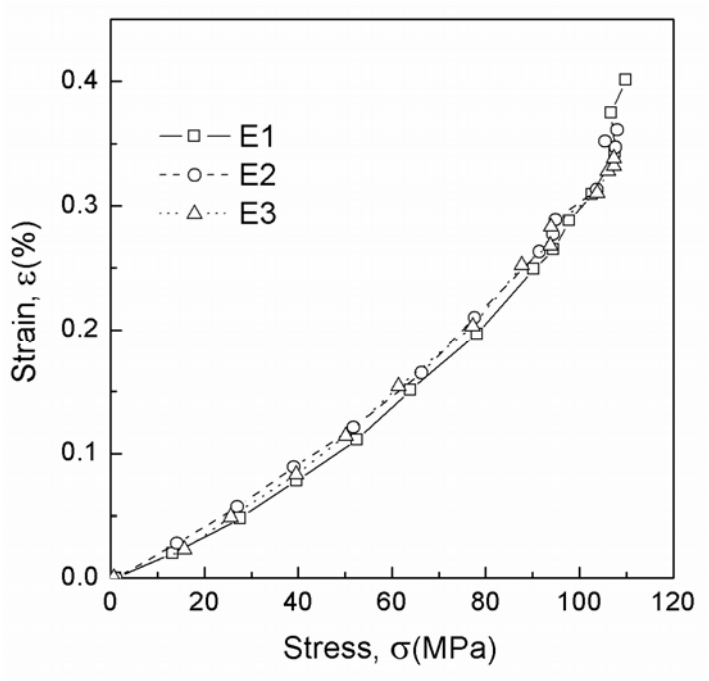

Figure 6.2. Distribution of strain of each portion with increasing applied stress at 77K, assuming the constant stress at each cross-section.

Figure 6.2 shows the distribution of strain of each portion with increasing tensile stress at 77K by using the newly designed apparatus. Under the tensile strain experiment, it is noted that the strain of the small portions is not uniform along the sample length direction, while the stress is constant at each cross-section. Before the applied stress was reached to 100MPa, the strain of each portion increased with the similar manner among portions. Accordingly, the difference of the measured strain of each portion was relatively small (±0.007%) within this stress level. However, beyond 100MPa which is assumed to be onset point of the fracture in Bi2223 filaments, the difference in the measured strain of each portion became large. As a result, in the measured relation of strain to the applied stress, while the strain in E1 showed 0.401% in final step, those in E2 and E3 were 0.361 and 0.338%, respectively, implying the large difference in damage extent among portions under tensile stress.

6.3.2 Comparison of the *V-I* curve of the local portions

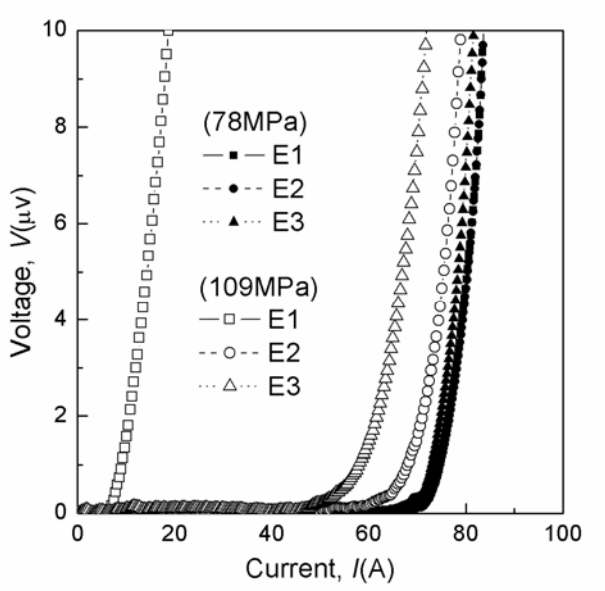

Figure 6.3. Measured *V–I* curves for local portions under tensile stresses at 78 and 109MPa.

The damage in local portions is responsible for degradation of superconducting transport current in the portions. Figure 6.3 shows the voltage (*V*)-current (*I*) curves of the each portion at the applied tensile stress 78 and 109MPa. Before the occurrence of

damage in the sample, the difference in *V-I* curves among portions was small. However, once damage took place, in the *V-I* curve at a tensile stress 109MPa which is higher than the fracture stress 100MPa, the difference in generated voltage among the local portions became large. Thus, the difference in local I_C among the portions was very large.

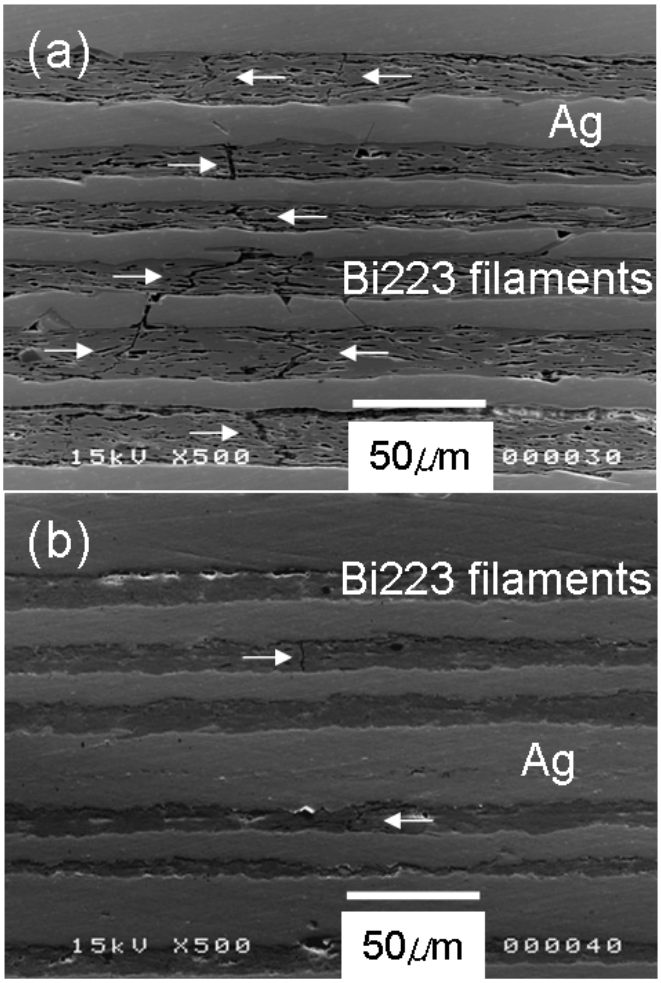

Figure 6.4. SEM images of the fracture morphology in the filaments. The arrows indicate fractures in the Bi2223 filaments: (a) a series of fractures transverse to neighboring filaments in E1 and (b) small damage amount in E2.

With this respect, the damage of filaments first took place in the restricted portion. Beyond the fracture stress in the weakest portion, the fracture occurs in weakest filaments. Once the fracture occurs in one filament, the stress concentration arises in the neighboring filaments, according to which the neighboring filaments are more easily fractured than any other place [12]. Such a process is repeated until almost all neighboring filaments are fractured. Figure 6.4(a) shows the polished fracture morphology of weakest portion E1. The other portions retain the original I_C or slightly lower. Figure 6.4(b) shows the polished fracture morphology of E2. Despite the given stress was common to that of E1, the damage amount is very small in E2. This result accounts for well small change of I_C in E2.

6.3.3 Features of the variation of critical current of local portions as a function of applied tensile strain

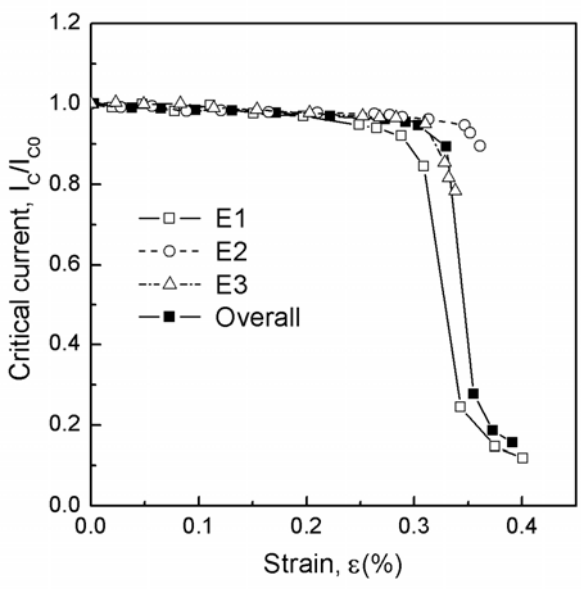

Figure 6.5. Change of the local and overall I_C against initial value (I_C/I_{C0}) with increasing applied tensile strain for the local (1cm) and the overall sample (4cm).

Generally, once the damage occurred in filaments, the I_C of the samples decreased significantly. The more and less damaged portions co-existed within the

overall sample length. This means the strain might be subjected differently from portion to portion since the damage extent is different. However, it was not perfectly understood how the damaged region affect on I_C–applied strain relation. Detailed information regarding the effect of local fracture on the I_C is obtained by the dependence of I_C on the applied tensile strain at 77K. Figure 6.5 show the change of local and overall I_C against each initial value (I_C/I_{C0}) with increasing applied tensile strains. Even though same load was applied in the sample, the strain of each portion was different, suggesting different damage extents among the portion as shown in figure 6.4(a) and 6.4(b). Significant reduction of I_C/I_{C0} in one portion was observed.

The E1 which was the weakest one among local portions showed severe reduction in the I_C–applied strain relation. In this process, the I_C was reduced in E1 at 0.24% (which was expected to the irreversible strain of E1), but the I_C was not reduced in E2 and E3. At this strain level, the I_C of overall was not influenced by the E1 yet. With further increase of applied tensile strain, the damage progress in E1 became more, but the E2 and E3 had still high I_C level. In the measured relation of I_C to the applied strain, while the subjected strain in E1 showed 0.401% in final step, those in E2 and E3 were 0.361 and 0.338%, respectively. From this result, it is emphasized that (i) first, the damage in the Bi2223 filaments occurred locally in the limited region and (ii) the applied strain in the weakest region was representative. Accordingly, the filaments damage in the early stage (up to 0.3%) was localized in the weakest portion.

As the filaments were embedded in Ag and Ag alloy sheath to form the composite tape, it is suggested for variation of the filament strain with position. In the present work, as a long length composite, the average fracture strain combining the strain distribution from position to position at 77K was evaluated to be 0.3% under the applied tensile strain. As shown in the I_C–strain of each portion relation, the average fracture strain 0.3% is rather large value, since the weakest portion was already fractured before reaching this strain value, resulting in showing the multiple fractures due to the induced fractures of neighboring filaments, however other portions were survived.

6.4 Conclusions

We have investigated the strain dependence of change of I_C in Bi2223 composite tapes with the newly designed strain extensometers. From the I_C–applied

local strain relation, the variation of the damage extents in short portions can be clearly detected experimentally. The fracture initiation in which I_C reduces is not the same between portions. The present measurements proved that it is useful to reveal the change of the I_C in the coexistence of no damaged and severely damaged local portions within the overall sample, resulting in local strain distribution in long sample.

References

[1] J. W. Ekin, D. K. Finnermore, Q. Li, J. Tenbrink, W. Carter, Appl. Phys. Lett., **61** (1992) 858.

[2] M. Suenaga, Y. Fukumoto, P. Haldar, T. R. Thurston, U. Wildgruber, Appl. Phys. Lett., **67** (1995) 3025.

[3] D. C. van der Laan, J. W. Ekin, H. J. N. van Eck, M. Dhalle, B. ten Haken, M. W. Davidson, J. Schwartz, Appl. Phys. Lett., **88** (2006) 022511.

[4] B. ten Haken, A. Beuink, H. H. J. ten Kate, IEEE Trans. Appl. Supercond., **7** (1997) 2034.

[5] S. Ochiai, K. Osamura, W. Watanabe, J. Appl. Phys., **74** (1993) 440.

[6] S. Ochiai, K. Hayashi, K. Osamura, Metall. Mater. Trans. A, **25** (1994) 349.

[7] K. Katagiri, H. S. Shin, K. Kasaba, T. Tsukinokizawa, K. Hiroi, T. Kuroda, K. Itoh, H. Wada, Supercond. Sci, Technol., **16** (2003) 995.

[8] S. Ochiai, D. Doko, H. Okuda, S. S. Oh, D. W. Ha, Supercond. Sci, Technol., **19** (2007) 1097.

[9] S. Ochiai, M. Fujimoto, H. Okuda, S. S. Oh, D. W. Ha, Supercond. Sci, Technol., **20** (2007) 800.

[10] D. C. van der Laan, J. W. Ekin, Appl. Phys. Lett., **90** (2007) 052506.

[11] A. Nyilas, K. Osamura, M. Sugano, Supercond. Sci. Technol., **16** (2003) 1036.

[12] S. Ochiai, Mechanical Propertied of Metallic Composites (New York: Deckker) (1993) 473.

Chapter 7

Voltage and current distribution by cracking of Bi2223 filament under applied tensile strain

7.1 Introduction

The $Bi_2Sr_2Ca_2Cu_3O_x$ (Bi2223) superconductor composite tape has been one of the most promising high temperature superconductors that are commercially applicable materials with long lengths and high current density. Up to now, Bi2223 composite tapes have been fabricated by the powder-in-tube method. The Bi223 filaments are embedded in Ag and the assembly is reinforced with Ag alloy sheath to give high mechanical strength withstanding the mechanical and electromagnetic stresses [1-3]. Nevertheless, under the applied strain, the superconducting current-transport Bi2223 filaments are cracked, resulting in the loss of superconductivity. It is the electro-mechanical properties, such as the relation of critical current variation with strains under the applied tensile and bending strains has been reported [4-9], and requested to describe the fracture behavior of Bi2223 composite tape under applied strain and its relation to the critical current for tape design and fabrication.

The current sharing in the interface between filaments and Ag near cracked filaments has been observed with the magneto-optical imaging (MOI) [10,11]. The numerical analysis of current and voltage distribution in Ag/Bi2223 composites was predicted by one-dimensionally distributed resistance model based on the resistivity of Ag (ρ_{Ag}), interfacial resistivity (ρ_i) and geometric parameters [12,13]. According to the model of Fang et al [12,13], before the initiation of cracking of the filaments, the current

is assumed to be carried fully by the superconducting filaments. However, after the cracking of the filaments, the current is shared by Ag. Namely, the transport current is shunted into Ag along the crack and return to the filaments. In this way, voltage generation along the interface between filaments and Ag takes place, and the critical current is reduced consequently. In the present work, the influence of the filament cracking on the voltage-current relation was investigated by modifying the Fang's model and the calculated ratio of the crack length under the applied tensile strain.

7.2 Model and Experimental procedure

7.2.1 Measurement of critical current under tensile strain at 77K

The multi-filamentary Bi2223 composite tape fabricated at Korea Electrotechnology Research Institute was used for present work as shown in figure 7.1. The thickness and width of composite tape containing 55 filaments were 0.23 and 4.9mm, respectively.

The change of critical current with increasing applied tensile strain (ε_c) was measured at 77K with an Instron type testing maching (NMB TCM-500). The critical current was defined with a criterion of 1μV/cm in a self-magnetic field. The distance of the voltage probes was 10mm. The strain of the sample at 77K was measured with the very lightweight Nyilas type extensometers [14], which was directly attached to the sample.

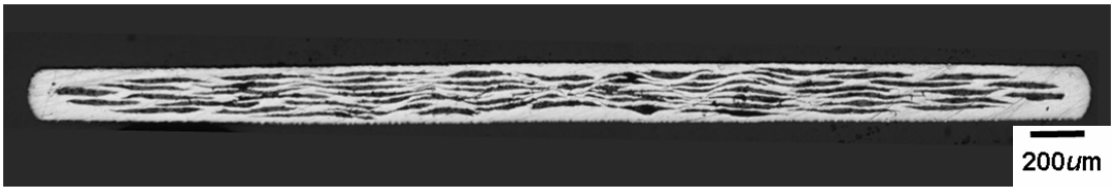

Figure 7.1. Transverse cross section of the Bi2223 composite tape.

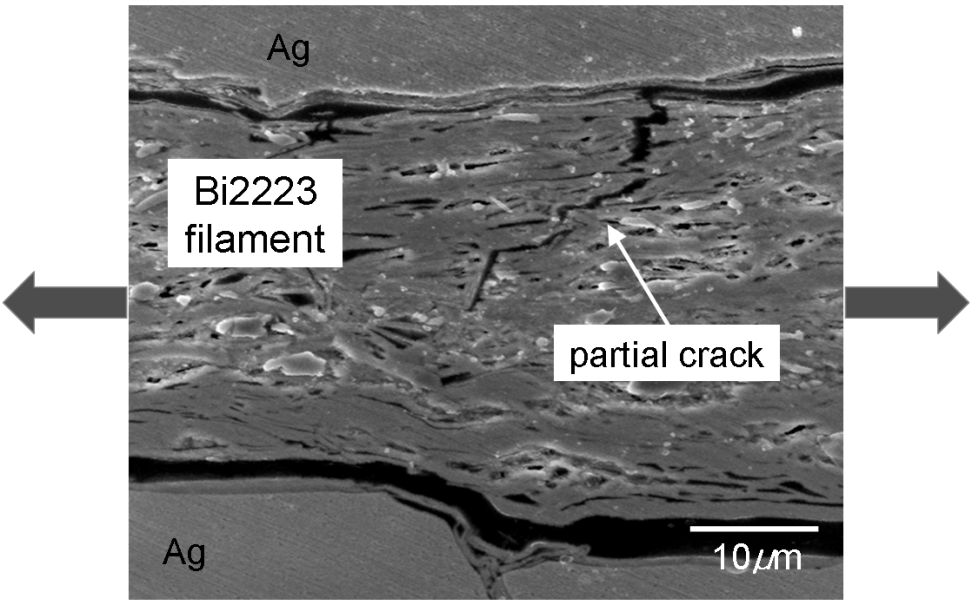

Figure 7.2. Polished longitudinal section of the damaged portion of the Bi2223 filament. Black arrows indicate the tensile axis.

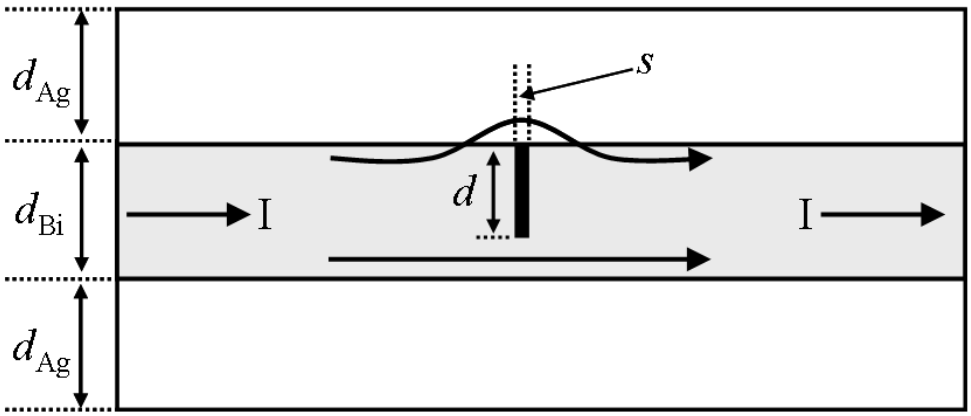

Figure 7.3. Schematic illustration of Bi2223 filament/Ag with the crack in the filament.

7.2.2 Modeling and input values for generated voltage calculation

Figure 7.2 shows the example of the polished longitudinal section of the damaged portion with a scanning electron microscope (SEM). In the Bi2223 filament, the partial crack before reaching fully crack under applied strain was observed. Actually, in the cracking process of the Bi2223 filament, the transverse (perpendicular to the tensile axis) and longitudinal (parallel to the tensile axis) damages take place alternatively, resulting in zigzag pattern [8]. In the present work, to simplify the current path and its distribution in the composite tape, the Bi2223 filament and Ag layers are regarded as plate shape, which are the series of multi layers of Bi2223 filament and Ag one after the other. Let us consider the voltage generation occurring from the transverse partial crack in the single filament. Figure 7.3 shows the schematic illustration of the filament/Ag with one transverse crack in the filament. Due to the cracking of the continuous Bi2223 filament, the current near the crack will flow through Ag and therefore, the generated voltage in Ag along the crack is satisfied by the Ohm's law. At the Bi2223 filament-Ag interface, the potential is subjected to the boundary satisfying the ohmic relationship between current and voltage across the Bi2223 filaments/Ag interface. In order to describe the relation of the current and the voltage under the crack formation, the one-dimensionally distributed resistance model proposed by Fang et al [13] was used. The Bi2223 filaments/Ag with a length L, width w, the filament thickness d_{Bi}, the Ag thickness d_{Ag}, the partial crack of width s and the partial crack length d is modeled. In order to calculate the effective resistance due to the crack in the Bi2223 filament, the parameters such as thickness of Bi2223 filament, Ag and the width of Bi2223 filament/Ag interface were taken to be d_{Bi}=15μm, d_{Ag}=20μm and w=0.05cm, respectively. Here, we use the ρ_{Ag} =2.9*10^{-7}Ωcm and ρ_i = 10^{-11}Ωcm^2 at 77K [15]. The effective resistance value R_e ($=\frac{1}{w}\sqrt{\frac{\rho_{Ag}\cdot\rho_i}{d_{Ag}}}$) was calculated to be 0.76$\mu\Omega$.

7.3 Results and discussion

7.3.1 Feature of variation of I_C with increasing applied tensile strain

Figure 7.4 shows the change of the critical current value (I_C/I_{C0}) with increasing applied tensile strain (ε_c) at 77K, where I_{C0} is the critical current at ε_c=0%.

The critical current decreased slightly with increasing applied tensile strain below the strain which filaments damage occurred, so called at the irreversible strain. Within non-damaged region, the relation to the critical current value (I_C/I_{C0}) under applied tensile strain (ε_c) was expressed by $I_C/I_{C0}=1–0.09\varepsilon_c(\%)$ empirically. With further increasing applied strain, the significant reduction of critical current was occurred due to the damage in filaments.

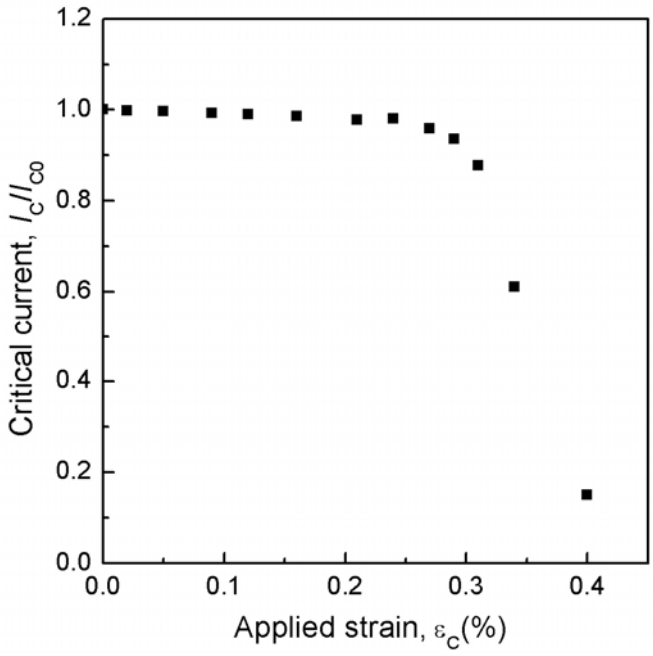

Figure 7.4. Change of the critical current (I_C/I_{C0}) with increasing applied tensile strain (ε_c) at 77K.

In order to confirm the relation of critical current reduction and increasing applied tensile strain, the voltage (*V*)-current (*I*) curve was monitored. Figure 7.5 shows the measured voltage (*V*)-current (*I*) curve of the Bi2223 composite tape with increasing applied tensile strains. Below the irreversible strain, the difference among *V-I* curves was small, which is retaining the original state. However, once damage took place in the filaments, the difference in generated voltage became large. Namely, beyond the irreversible strain, as the applied strain was increased, the higher voltage was generated, resulting in the *V-I* curves shift to the lower critical current region. It is noted that the

degradation of critical current is mainly due to the cracking of the Bi2223 filaments. In the present work, in order to describe the relation of the current and the voltage under the crack formation, the one-dimensionally distributed resistance model proposed by Fang et al [13] was used.

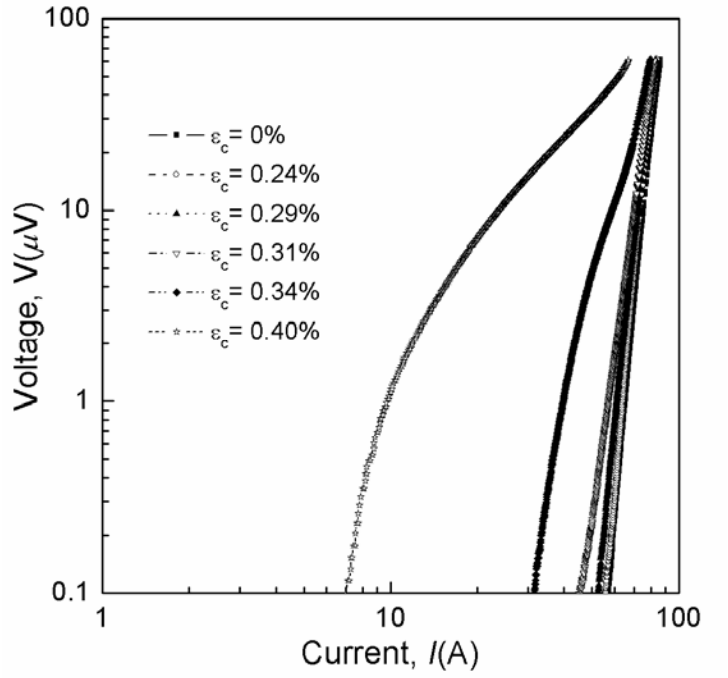

Figure 7.5. Measured voltage (V)-current (I) curve of the Bi2223 composite sample with increasing applied tensile strains.

7.3.2 Crack effect on voltage and current distribution

In the literature [13], the relation of generated voltage due to current shunting to Ag with 1μV/cm criterion was determined in the following form;

(a) Crack region: $V(s) = s(\frac{I_{Bi}}{I_C(s)})^n$ (7.1)

$$I = I_{C0}(1-\frac{d}{d_{Bi}})\left[\frac{V(s)}{s}\right]^{\frac{1}{n}} + \frac{V(s)}{R_e} \tag{7.2}$$

where n refers to an exponent in the power law, V(s) is the generated voltage, I_{Bi} is the current in filament, I_C(s) is the critical current in crack region and I_{C0} is the critical current at the applied tensile strain ε_c=0%, respectively. The d_{Bi} is the thickness of filament, d is the crack length, s is the crack width and R_e is the effective resistance at 77K, respectively.

(b) Non-crack region: $V(L-s) = (L-s)(\frac{I}{I_{C0}})^n$. (7.3)

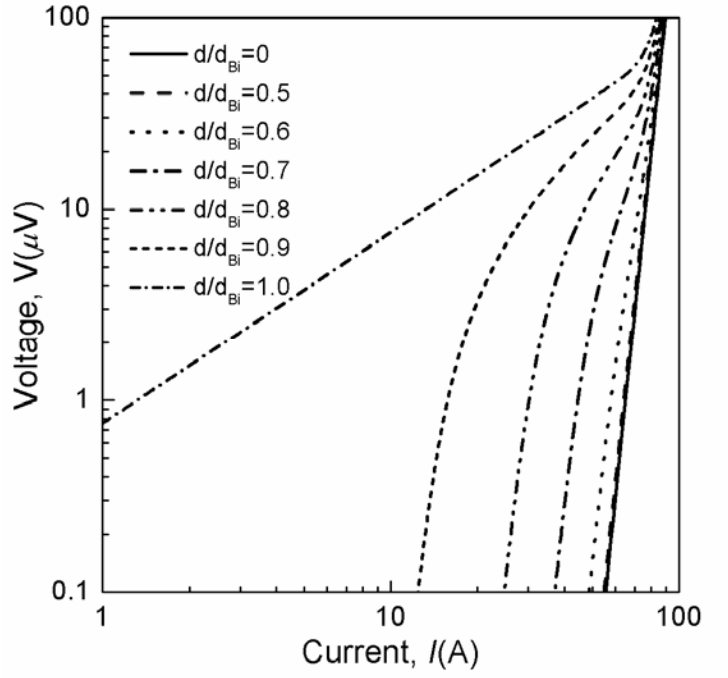

Figure 7.6. Calculated voltage (V)-current (I) curve at 77K containing one crack with increasing ratio of crack length d/d_{Bi} at 77K.

Therefore, total voltage V_t is given by the sum of the voltage of cracked $V(s)$ and non cracked region $V(L\text{-}s)$, which is expressed by

$$V_t = V(L\text{-}s) + V(s) \approx V(L) + V(s). \quad (7.4)$$

Due to the difficulty to form $V(s)$ as a function of transport current I as shown in equation (7.2), the total generated voltage was obtained by numerical method in the present work. Figure 7.6 shows the calculated voltage (V)-current (I) curve containing one crack with increasing ratio of crack length d/d_{Bi} for I_{C0}=65.12A, n=14.5, L=1cm, s=0.1μm, d_{Bi}=15μm, d_{Ag}=20μm, w=0.05cm and R_e =0.76$\mu\Omega$ at 77K. From the calculated V-I curves, as the crack length is increased, the V-I curves are shifted to the direction of degradation in critical current and the higher voltage was generated. In this way, it is suggested that the crack length d is increased with increasing applied tensile strain. In order to calculate the strain dependence of the propagative crack length, the ratio of crack length d/d_{Bi} was estimated as to fit the experimentally observed V-I curves (as shown in figure 7.5) where damage took place. The best fit value of d/d_{Bi} with increasing applied tensile strain was presented in figure 7.7.

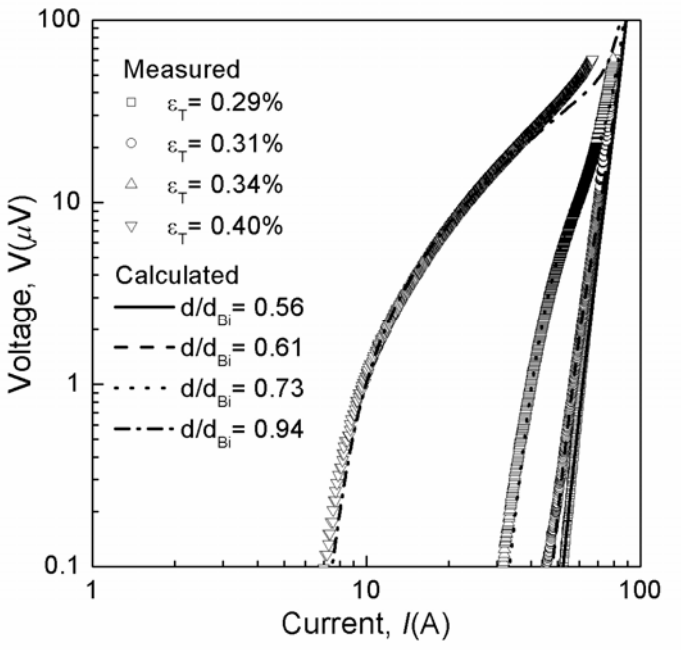

Figure 7.7. Estimation of the ratio of crack length d/d_{Bi} with increasing applied tensile strain (ε_c).

From this result, the boundary condition is assumed to be d/d_{Bi}=0, at $\varepsilon_c = \varepsilon_{min}$ and d/d_{Bi}=1, at ε_c = infinite. In order to make the relation of d/d_{Bi}-applied tensile strain as a form, we assume the relation of the estimated d/d_{Bi} and applied tensile strain was expressed by exponential function. With this respect, the ratio of crack length $F(=d/d_{Bi})$ under applied tensile strain is given by

$$F = 1 - \exp\left[-((\varepsilon_c - \varepsilon_{min}) / \varepsilon_0)^{m}\right] \quad (7.5)$$

where ε_c is irreversible strain given by $\varepsilon_f - \varepsilon_r$ where ε_f and ε_r are the intrinsic fracture strain and the residual strain of the Bi2223 filaments, respectively, ε_{min} is the minimum irreversible strain given by $\varepsilon_{f,min} - \varepsilon_r$ where $\varepsilon_{f,min}$ and ε_r are the minimum intrinsic fracture strain and the residual strain of the Bi2223 filaments, respectively, ε_0 is the scale parameter, m is the shape parameter. Accordingly, the relation ($\varepsilon_c - \varepsilon_{min}$) is expressed by $\varepsilon_f - \varepsilon_{f,min}$. Below $\varepsilon_{f,min}$, there is no crack in filaments. From the analysis of regression curve based on the relation of ln ln$(1-F)^{-1}$ and ln($\varepsilon_c - \varepsilon_{min}$), the unknown parameters such as m, ε_{min} and ε_0 can be obtained. Figure 7.8 shows the plot of ln ln$(1-F)^{-1}$ as a function of ln($\varepsilon_c - \varepsilon_{min}$). Based on this result, it was found that m=0.951, ε_{min}=0.245 and ε_0 =0.063, respectively.

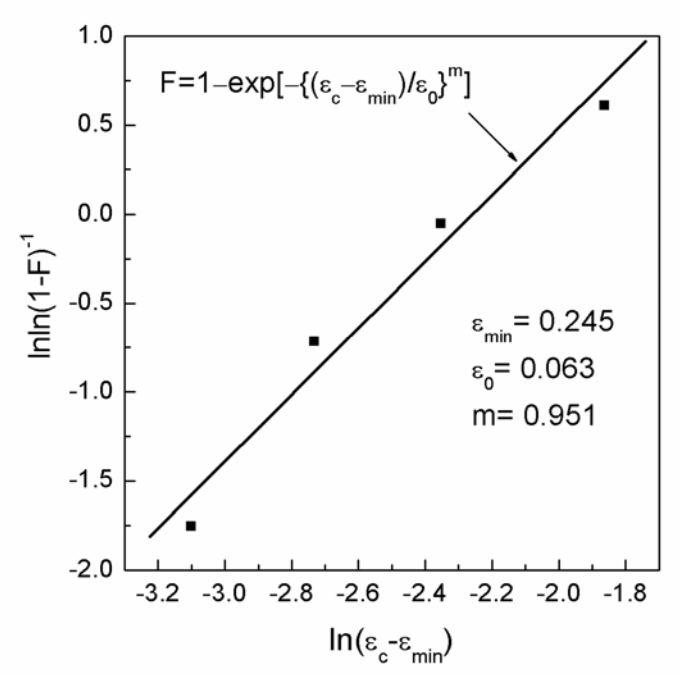

Figure 7.8. Plot of ln ln$(1-F)^{-1}$ against ln($\varepsilon_c - \varepsilon_{min}$).

7.3.3 Description of the variation of (I_C/I_{C0}) with increasing applied tensile strain

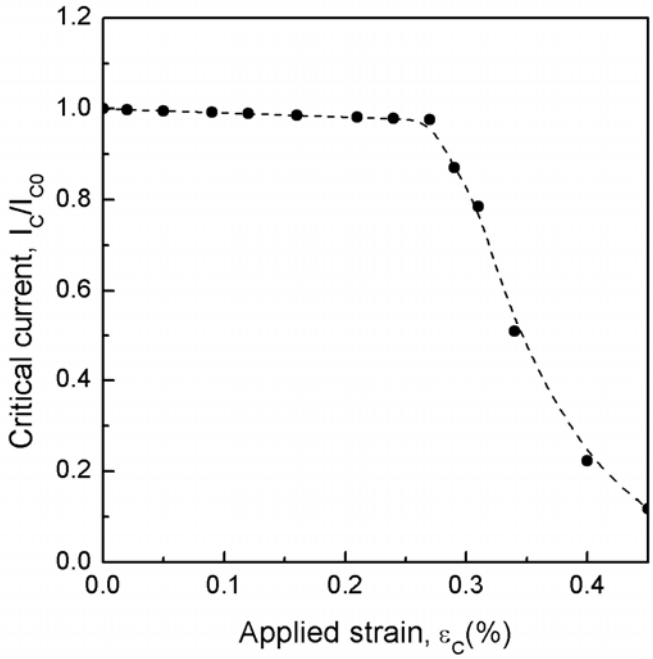

Figure 7.9. Calculated change of critical current (I_C/I_{C0}) with increasing applied tensile strain (ε_c) at 77K.

Actually, within non-damage region, the measured change of critical current value was given as $I_C/I_{C0}(\varepsilon_c)=1–0.09\varepsilon_c$ empirically. The voltage in non-cracked region was modified as a function of applied strain as follows,

$$V = [I / \{I_{C0}(1–0.09\varepsilon_c)\}]^n . \quad (7.6)$$

In addition, the ratio of crack length d/d_{Bi} was estimated as a function of applied tensile strain ε_c. With this respect, the voltage V(s) in cracked region was modified as follows,

$$I = I_{C0}(1-0.09\varepsilon_c)\cdot\exp\left(-\left(\frac{\varepsilon_c-\varepsilon_{min}}{\varepsilon_0}\right)^m\right)\left[\frac{V(s)}{s}\right]^{\frac{1}{n}}+\frac{V(s)}{R_e}. \quad (7.7)$$

Therefore, by combining equations (7.6) and (7.7), the V-I relation containing cracked

and non cracked region under the applied tensile strain can be written as follows,

$$V_t = \left(\frac{I}{I_{C0}(1 - 0.09\varepsilon_c)} \right)^n + V(s) . \qquad (7.8)$$

Figure 7.9 shows the calculated change of critical current as a function of applied strain. From the result, the influence of the filament cracking on the voltage-current relation and critical current reduction could be described well by the present approach. This implies that the combination of current sharing between superconducting filaments and Ag near the crack and the ratio of crack length as a function of applied tensile strain is useful for description of the measured strain tolerance of the critical current at 77K with Bi2223 composite tape.

7.4 Conclusions

The strain dependence of critical current of Bi2223 composite tape was studied under applied tensile strain at 77K. Beyond the irreversible strain, due to the cracking of Bi2223 filament, voltage generation along the interface between filament and Ag takes place, and the critical current is reduced consequently. To reveal the influence of filament cracking on critical current variation, the effect of the partial cracking of filament on the voltage-current relation were investigated with the ratio of the crack length and effective resistance due to the damage in filament. From the analytical result, the experimentally measured change of critical current-applied tensile strain relation was described well.

References

[1] P. Vase, R. Flukiger, M. Leghissa, B. Glowacki, Supercond. Sci. Technol., **13** (2000) R71.

[2] B. Fischer, T. Arndt, J. Gierl, H. Krauth, M. Munz, A. Szulczyk, M. Leghissa, H. W. Neumuller, IEEE Trans. Appl. Supercond., **11** (2001) 3261.

[3] K. Hayashi, T. Hikata, T. Kaneko, M. Ueyama, A. Mikumo, N. Ayai, S. Kobayashi, H. Takei, K. Sato, IEEE Trans. Appl. Supercond., **11** (2001) 3281.

[4] J.W. Ekin, D.K. Finnermore, Q. Li, J. Tenbrink, W. Carter, Appl. Phys. Lett., **61** (1992) 858.

[5] S. Ochiai, K. Hayashi, K. Osamura, Cryogenics, **32** (1992) 799.

[6] S. Ochiai, K. Hayashi, K. Osamura, Cryogenics, **33** (1993) 976.

[7] M. Suenaga, Y. Fukumoto, P. Haldar, T. R. Thurston, U. Wildgruber, Appl. Phys. Lett., **67** (1995) 3025.

[8] S. Ochiai, T. Nagai, H. Okuda, S. S. Oh, M. Hojo, M. Tanaka, M. Sugano, K. Osamura, Supercond. Sci. Technol., **16** (2003) 988.

[9] S. Ochiai, N. Miyazaki, D. Doko, T. Nagai, M. Nakamura, H. Okuda, S. S. Oh, M. Hojo, M. Tanaka, K. Osamura, J. Nuclear Mater., **329-333** (2004) 1585.

[10] T. B. Peterson, U. Welp, G. W. Crabtree, N. Vasanthamohan, J. P. Singh, M. T. Lanagan, V. K. Vlasko-Vlasov, V. I. Nikitenko, Appl. Phys. Lett., **71** (1997) 134.

[11] D. C. van der Laan, J. W. Ekin, H. J. N. van Eck, M. Dhalle, B. ten Haken, M. W. Davidson, J. Schwartz, Appl. Phys. Lett., **88** (2006) 022511.

[12] Y. Fang, S. Danyluk, Y. S. Cha, M. T. Lanagan, J. Appl. Phys., **79** (1996) 947.

[13] Y. Fang, S. Danyluk, M. T. Lanagan, Cryogenics, **36** (1996) 957.

[14] A. Nyilas, Supercond. Sci.Technol., **18** (2005) S409.

[15] Y. Fang, S. Danyluk, M. T. Lanagan, C. A. Youngdahl, X. Xu, K. Numata, Physica C, **252** (1995) 389.

Chapter 8

Conclusions

For practical use of high temperature superconductors, further improvement of current carrying capabilities and production techniques as well as understanding of the mechanical properties such as strength and reliability of superconducting composite materials. In the present thesis, the effects of the applied strain and the thermally induced residual strain during the fabrication/winding process, and their influences on the critical currents at 77K have been studied with the electro-mechanical view point. The results clearly showed the mechanical behavior and its relation to superconducting property of the Bi-system high temperature superconductors.

Chapter 2: Analysis of residual strain change of Bi2212, Ag alloy and Ag during heating and cooling process in Bi2212/Ag/Ag alloy composite wire

The residual strain change of Bi2212 and Ag during cooling and heating process in the Bi2212/Ag/Ag alloy composite superconductor was studied. First, the residual strain of Bi2212 filaments at room temperature was measured by the X-ray diffraction method. Then, the Young's moduli of the constituents (Bi2212 filaments, Ag and Ag alloy) and yield strains of Ag and Ag alloy were estimated from the analysis of the measured stress-strain curve, based on the rule of mixtures. Also the coefficient of thermal expansion of the Bi2212 filaments was estimated from the analysis of the measured thermal expansion curve of the composite wire. From the modeling analysis using the estimated property values such as Young's modulus of Bi2212, Ag and Ag alloy (66.3, 71.4 and 81.1GPa, respectively), residual strain of Bi2212 filaments at RT (-0.14%), intrinsic fracture strain of Bi2212 filaments (0.11~0.13%) and yield strains of Ag and Ag alloy (0.019% and 0.370%, respectively), the changes of residual strain of Bi2212, Ag alloy and Ag with temperature during cooling/heating process were revealed.

Chapter 3: Thermally induced residual strain accumulation in Bi2223/Ag/Ag alloy composite superconductor

A method to estimate the thermally induced residual strain accumulation under varying temperature in a Bi2223/Ag/Ag alloy composite superconductor was presented, in which the mechanical property values measured from the stress–strain curves of the samples with different residual strain states, the residual strain value of Bi2223 filaments in the composite tape at room temperature measured by X-ray diffraction and the reported coefficients of thermal expansion of the constituents (Bi2223, Ag and Ag alloy) in the relevant temperature range (77–600K) were incorporated. This method was applied to estimate the change of the residual strain of all constituents of the high critical current type composite tape fabricated by American Superconductor Corporation as a function of temperature. The residual strain value at 77 K (−0.11%) estimated by this method and the reported fracture strain of Bi2223 filaments (0.1%) accounted well for the measured strain tolerance of the critical current at 77 K (0.21%).

Chapter 4: Thermally and mechanically induced residual strain and strain tolerance of critical current in stainless steel-laminated Bi2223/Ag/Ag alloy composite superconductor

The thermally and mechanically induced residual strain accumulation process of the stainless steel-laminated Bi2223/Ag/Ag alloy superconducting composite tape fabricated at American Superconductor Corporation was studied. For description of the strain change of the constituents (Bi2223, Ag, Ag alloy and stainless steel) during cooling and heating, and during lamination, followed by the stress relaxation, a calculation procedure based on the elastic-plastic mechanics was presented. As the input values, the mechanical property values of the constituents and the residual strain of Bi2223 filaments in the laminated composite tape at room temperature, measured with X ray, were used. Such an approach revealed the change of residual strain of each constituent in the thermal- and mechanical- process in the laminated composite tape. Then, from the comparison of the residual strain accumulation in the laminated tape with that in the insert tape, it was shown that the stainless steel lamination acts to reduce the residual strain of Ag alloy, to enhance the compressive residual strain of Bi2223 and to retard the fracture of the filaments, contributing the high tensile strain tolerance of critical current of the laminated tape. Also it was shown that the lamination acts to reduce the strain hysteresis of Bi2223 and Ag alloy in the thermal cycling between room temperature and 77K.

Chapter 5: Local and overall critical current of Bi2223-composite tape under applied tensile and bending strains

Local and overall transport critical current I_C and n-value at 77K of multi-filamentary Bi2223-composite tape were studied under applied tensile and bending strains. The I_C and n-value of the local elements constituting of the overall sample and those of the overall sample were measured for the voltage probe distances 10 and 60 mm, respectively. The local I_C as well as n-value varied along the sample length under both tensile and bending strains, while the critical current reduction process under the tensile strain was quite different from that under bending one; a big difference in damage among the local elements was found under tensile strain but not under bending one. While the damage process was different between the tensile and bending strains, the relation of overall I_C and n-value to the local ones was described comprehensively by the voltage summation model. From the analysis of the experimentally observed critical current-applied strain relation of the local elements, the variation of the critical current determining factor "fracture strain – residual strain" along the sample length was revealed.

Chapter 6: Direct measurement of difference in local deformation and its influence on critical current in Bi2223/Ag/Ag alloy composite tape

A special device for simultaneous measurement of plural strains of local elements and overall sample was designed to study the sample location dependence of critical current I_C-applied tensile strain relation at 77K of multi-filamentary Bi2223 composite tape. The I_C values of the local elements and overall sample were measured for the voltage probe distances 10 and 40mm, respectively. The local strain of each element and overall strain of the sample were measured with using the newly designed couples of 12mm and 50mm extensometers. With this method, under a common applied stress, the difference in critical current I_C-tensile strain relation among the local elements was clearly detected. The difference in critical current I_C-applied strain relation among the local elements was attributed to the difference in damage evolution of the Bi2223 filaments from the observation with the scanning electron microscope. The local I_C varied along the sample length under applied tensile strain. From the experimentally measured difference in change of critical current reduction among elements, a big difference in damage extents among the local elements was found.

Chapter 7: Voltage and current distribution by cracking of Bi2223 filament under applied tensile strain

The critical current at 77K of multi-filamentary Bi2223 composite tape was

studied under applied tensile strain experimentally and analytically. Beyond the irreversible strain, the critical currents (I_C) were significantly reduced under the applied tensile strain (ε_c), due to the cracking of the Bi2223 filaments. The voltage generation in the voltage-current relation was calculated by the current share model in which the transport current is shared by Bi2223 filament and Ag near the cracked portion. Then the critical current was estimated with a 1μV/cm criterion. By the application of such a model to the experimental result, the effective crack length responsible for the reduced critical current was estimated from which the change of critical current as a function of applied strain could be described in quantitative manner.

In conclusion, the correlation between mechanical properties (intrinsic fracture strain of filaments, yield strain of Ag and Ag alloy and thermally induced residual strains) and macroscopic transport properties (critical current distributions, *V-I* relations and n-value) of Bi-system composite materials has been investigated and clarified. The author hoped that the present study will be useful for the understanding electro-mechanical properties of high temperature superconducting materials and the reliability and safety design in practical application.

Publication List

2006

1. **“In situ synchrotron-radiation measurements of axial strain in laminated Bi2223 superconducting composite tapes at room temperature”**, H. Okuda, H. Rokkaku, K. Morishita, J. K. Shin, S. Iwamoto, S. Ochiai, M. Sato, K. Osamura, A. Otto, E. J. Harley, A. Malozemoff, *Scripta Materialia*, **55** (2006) 691.

2007

2. **“Local and overall critical current of Bi2223-composite tape under applied tensile and bending strains”**, J. K. Shin, M. Fujimoto, H. Okuda, S. Ochiai, S. S. Oh, *Physica* C, **463-465** (2007) 876.

3. **“Correlation between local and overall critical current of bent multi-filamentary Bi2223/Ag tape”**, M. Fujimoto, D. Doko, J. K. Shin, H. Nakajima, S. Ochiai, H. Okuda, S. S. Oh, K. Osamura, *Physica* C, **463-465** (2007) 871.

4. **“Statistical analysis of scatter in critical current of bent superconducting Bi2223 composite tape”**, S. Ochiai, M. Fujimoto, J. K. Shin, H. Okuda, M. Hojo, T. Kurota, K. Itoh, H. Wada, *Physica* C, **463-465** (2007) 885.

5. **“Modeling analysis of the critical current of bent Bi2223 composite tape based on the damage strain parameter and the shape of the core”,** S. Ochiai, T. Matsuoka, J. K. Shin, H. Okuda, M. Sugano, M. Hojo, K. Osamura, *Supercond. Sci. Technol*., **20** (2007) 1076.

6. **“Thermally induced residual strain accumulation in Bi2223/Ag/Ag alloy composite superconductor”**, S. Ochiai, H. Rokkaku, K. Morishita, J. K. Shin, S. Iwamoto, H. Okuda, M. Hojo, K. Osamura, M. Sato, A. Otto, E. Harley, A. Malozemoff, *Supercond. Sci. Technol.*, **20** (2007) 202.

7. **“Estimation of critical current of bent Bi2223 composite tape by application of superconducting core shape-incorporated model”**, S. Ochiai, J. K. Shin, H. Okuda, S. S. Oh, D.W. Ha, *J. Japan Inst. Metals*, **71** (2007) 977.

2008

8. **“Analysis of residual strain change of Bi2212 and Ag during heating and cooling process in Bi2212/Ag/Ag alloy composite wire”**, J. K. Shin, S. Ochiai, M. Sugano, H. Okuda, Y. Mukai, M. Sato, S. S. Oh, D. W. Ha, S. C. Kim, *Supercond. Sci. Technol.*, **21** (2008) 075018.

9. **“Assessment of strain of Bi2223 laments in bent Ag-sheathed superconducting composites by synchrotron radiation”**, H. Okuda, J. K. Shin, S. Iwamoto, K. Morishita, Y. Mukai, H. Matsubayashi, S. Ochiai, A. Otto, E. J. Harley, A. P. Malozemo, M. Sato, *Scripta Materialia*, **58** (2008) 687.

10. **“Direct measurement of difference in local deformation and its influence on critical current in Bi2223/Ag/Ag alloy composite tape”**, J. K. Shin, S. Ochiai, M. Sugano, H. Okuda, A. Nyilas, S. S. Oh, *Scripta Materialia*, **59** (2008) 448.

11. **“Analysis of the distribution of critical current of bent Bi2223 composite tape based on a unifying parameter approach”**, S. Ochiai, J. K. Shin, H. Okuda, M. Sugano, M. Hojo, K. Osamura, T. Kuroda, K. Itoh, H.. Wada, *Supercond. Sci. Technol.*, **21** (2008) 054002.

12. **“Thermally and mechanically induced residual strain and strain tolerance of critical current in stainless steel-laminated Bi2223/Ag/Ag alloy composite superconductor”**, S. Ochiai, H. Rokkaku, J. K. Shin, S. Iwamoto, H. Okuda, K. Osamura, M. Sato, A. and A. P. Malozemoff, *Supercond. Sci. Technol.*, **21** (2008) 075009.

13. **“Estimation of young’s modulus, residual strain and intrinsic fracture strain of Bi2212 filaments in Bi2212/Ag/Ag alloy composite wire”**, J. K. Shin, S. Ochiai, H. Okuda, Y. Mukai, H. Matsubayashi, S. S. Oh, D. W. Ha, S. C. Kim, M. Sato, *Physica* C, (2008) (in press).

14. **“The influence of tensile strain on critical current of Bi2223 composite tape”**, Y. Mukai, J. K. Shin, S. Ochiai, H. Okuda, M. Sugano, K. Osamura, *Physica* C, (2008) (in press).

15. **“An attempt to estimate the distribution of irreversible bending strain for critical current in the Bi2223 composite tape by a core shape-incorporated model”**, S. Ochiai, J. K. Shin, Y. Mukai, H. Matsubayashi, H. Okuda, M. Sugano, M. Hojo, K. Osamura, T. Kuroda, K. Itoh, H. Wada, *Physica* C, (2008) (in press).

16. **“Dependence of critical current on sample length analyzed by the variation of local critical current of bent BSCCO superconducting composite Tape”**, H. Matsubayashi, Y. Mukai, J. K. Shin, S. Ochiai, H. Okuda, K. Osamura, A. Otto, A. Malozemoff, *Physica* C, (2008) (in press).

17. **“Voltage and current distribution by cracking of Bi2223 filament under applied tensile strain”**, J. K. Shin, S. Ochiai, H. Okuda, M. Sugano, S. S. Oh, *Supercond. Sci. Technol*., (submitted).

Acknowledgement

First of all, I would like to express my deep gratitude to my advisor, Professor Shojiro Ochiai of Kyoto University, for his help and appropriate guidance for three years. I owe all my works to his continuous support and the long-term discussions with him. I deeply appreciate affectionate encouragement and support in many ways, completing this thesis and study at Kyoto University possible.

I would like to thank Associate Professor Hiroshi Okuda of Kyoto University for his helpful suggestions, guidances and discussions of my research from the beginning. I would like to thank Professors Jun Kawai of Kyoto University for helpful suggestions during reviewing this thesis.

I am grateful to Assistance Professor Michinaka Sugano for his advises and assistances for many experiments, especially tensile tests at low temperature. I think this work could not be completed without his helping on research activities.

I also would like to express my sincere appreciation to Professor Soo-Woo NAM at Korea Advanced Institute of Science and Technology for his encouragement for studying in Japan.

I am grateful to all of the members of Professor Ochiai Laboratory for their various assistances.

I would like to express my appreciation for the Monbusho Scholarship from Ministry of Education, Culture, Sports, Science and Technology (MEXT), Japan.

Finally, I would like to thank to my parents, brothers and wife (Jung-Kyung JANG) for their countless support and hearty encouragement to have opportunity to study. I wish to thank again from my heart.